2012

Implementation and preliminary study of low temperature combustion with assorted biofuels in a Ford diesel engine

Tongyang Gao
University of Windsor

IMPLEMENTATION AND PRELIMINARY STUDY OF LOW TEMPERATURE COMBUSTION WITH ASSORTED BIOFUELS IN A FORD DIESEL ENGINE

by

Tongyang Gao

A Thesis
Submitted to the Faculty of Graduate Studies
through the Department of Mechanical, Automotive, and Materials Engineering
in Partial Fulfillment of the Requirements for
the Degree of Master of Applied Science at the
University of Windsor

Windsor, Ontario, Canada

2011

Implementation and Preliminary Study of Low Temperature Combustion with Assorted Biofuels in a Ford Diesel Engine

by

Tongyang Gao

APPROVED BY:

_____
Dr. Xiaohong Xu, Outside Department Reader
Department of Civil and Environmental Engineering

_____
Dr. Jimi S-Y Tjong, Department Reader
Department of Mechanical, Automotive and Materials Engineering

_____
Dr. Graham T. Reader, Advisor
Faculty of Engineering

_____
Dr. Ming Zheng, Advisor
Department of Mechanical, Automotive and Materials Engineering

_____
Dr. Hongfa Hu, Chair of Defense
Department of Mechanical, Automotive and Materials Engineering

December 07th, 2011

DECLARATION OF ORIGINALITY

I hereby certify that I am the sole author of this thesis and that the detailed technical core of this thesis has not been published or submitted for publication.

I certify that, to the best of my knowledge, my thesis does not infringe upon anyone's copyright nor violate any proprietary rights and that any ideas, techniques, quotations, or any other material from the work of other people included in my thesis, published or otherwise, are fully acknowledged in accordance with the standard referencing practices. Furthermore, to the extent that I have included copyrighted material that surpasses the bounds of fair dealing within the meaning of the Canada Copyright Act, I certify that I have obtained a written permission from the copyright owner(s) to include such material(s) in my thesis and have included copies of such copyright clearances to my appendix.

I declare that this is a true copy of my thesis, including any final revisions, as approved by my thesis committee and the Graduate Studies office, and that this thesis has not been submitted for a higher degree to any other University or Institution.

ABSTRACT

Biofuels have drawn increased attention from the public and the engine researchers during the past decades. The biofuel uses may benefit in reducing engine emissions and greenhouse gas production. In this work, a new engine platform with a modern Ford diesel engine was prepared to perform experiments on low temperature combustion (LTC) with diesel and biofuels. A detailed documentation of the engine platform implementation was recorded.

Engine experiments were performed to verify the platform preparation and to collect information for diesel baseline tests and ethanol port fuel injection (PFI) experiments. The ethanol PFI results were promising in suppressing the emissions of nitrogen oxides (NOx) and smoke. It was observed that both NOx and smoke emissions from PFI ethanol ignited by diesel direct injection (DI) were lower than those from diesel combustions. The combustion phasing of diesel-ethanol combustion was under the control of diesel injection timing and exhaust gas recirculation (EGR).

DEDICATION

This thesis is dedicated to my beloved:

Wife: Shanshan Luan,

For her continuous love and support

Through my entire Master's degree study

Father: Buyun Gao

Mother: Shaojie Sun

For their unconditional encouragement and support,

Without which this degree and thesis could never happen.

ACKNOWLEDGEMENTS

It is a great pleasure to express the sincere gratitude to my advisers: Dr. Ming Zheng and Dr. Graham T. Reader, for their valuable enlightening guidance and encouragement throughout my whole master's program and thesis work.

I would also like to thank my committee members, Dr. Xiaohong Xu and Dr. Jimi Tjong, for their precious time and wisdom of offering the advice and guidance to my thesis.

I would take the opportunity to thank my colleagues in Clean Diesel Engine Laboratory at the University of Windsor: Dr. Meiping Wang, Dr. Shui Yu, Dr. Usman Asad, Xiaoye Han, Kelvin Xie, Marko Jeftic, Arturo Mendoza, Xiaoxi Zhang and Prasad Divekar. They helped so much in my entire research process.

I would like to warmly thank our technologist Bruce Durfy for the technical support. During the platform setup process, he provided important assistance in the part components machining and welding.

I am grateful to the Ford Motor Company Powertrain Engineering Research and Development Center for their abundant support in the engine dynamometer preparation.

My research projects have received financial support from the Canada Research Chair Program, Canada Foundation of Innovation (CFI), Ontario Innovation Trust (OIT), Natural Sciences and Engineering Research Council of Canada (NSERC), Ford Motor Company of Canada, other non-disclosed OEMs, AUTO21 Network Centers of Excellence and the University of Windsor.

Finally, I am deeply grateful to my beloved wife for her continuous accompanying during the full my master's study and my parents for their countless support, encouragement and understanding. Without any member of my family, my master's degree and this thesis would never have happened.

Tongyang Gao

TABLE OF CONTENTS

LIST OF TABLES

LIST OF FIGURES

NOMENCLATURE

AC	Alternating Current
AIO	Analog Input/Output
ATDC	After Top Dead Center
abs	Absolute
BDC	Bottom Dead Center
BNC	Bayonet Neill–Concelman
BTDC	Before Top Dead Center
CA	Crank Angle
CA50	Crank Angle of 50% Heat Released
CAI	California Analytical Instruments
CI	Compression Ignition
CN	Cetane Number
CNG	Compressed Natural Gas
CO	Carbon Monoxide
CO_2	Carbon Dioxide
DxEy	Diesel IMEP x bar and ethanol IMEP y bar
DAQ	Data Acquisition
DC	Direct Current
DI	Direct Injection
DIO	Digital Input/Output
DOC	Diesel Oxidation Catalyst
ECU	Engine Control Unit
EGR	Exhaust Gas Recirculation
FPGA	Field Programmable Gate Array
GHG	Greenhouse Gas
GND	Ground
GPH	Gallon per Hour
HCCI	Homogenous Charge Compression Ignition
HRR	Heat Release Rate

HTC	High Temperature Combustion
ICE	Internal Combustion Engine
ID	Ignition Delay
IMEP	Indicated Mean Effective Pressure
I/O	Input / Output
L	Liter
LHV	Lower Heating Value
LPG	Liquefied Petroleum Gas
LTC	Low Temperature Combustion
MAF	Mass Air Flow Rate
m_f	Mass Fuel Flow
NI	National Instruments
NO_x	Nitrogen Oxides
NPT	National Pipe Thread
PFI	Port Fuel Injection
PM	Particulate Matter
p_{int}	Intake Pressure (bar)
p_{max}	Maximum Cylinder Pressure (bar)
PWM	Pulse Width Modulation
rpm	Revolutions per Minute
RT	Real-time
SOC	Start of Combustion
SOI	Start of Injection
TDC	Top Dead Center
T_{int}	Intake Temperature
THC	Total Hydrocarbon
TTL	Transistor-transistor Logic
VCV	Volume-control Valve
λ	Excess Air Fuel Ratio
ϕ	Equivalence Ratio
θ	Crank Angle (°CA)
η_{ind}	Indicated Thermal Efficiency (%)

LIST OF PUBLICATIONS

Refereed Conference Proceedings:

1. Shui Yu, Kelvin Xie, Xiaoye Han, Marko Jeftic, **Tongyang Gao**, and Ming Zheng, "A Preliminary Study of the Spark Characteristics for Unconventional Cylinder Charge with Strong Air Movement", ASME 2011 Internal Combustion Engine Division Fall Technical Conference, Morgantown, West Virginia, October 2-5, 2011.

Non-refereed Conference Proceedings:

1. Xiaoye Han, **Tongyang Gao**, Ming Zheng and Jimi Tjong (2010), "Fuel Injection Strategies to Enable Low Temperature Combustion in a Light-Duty Diesel Engine", Global Powertrain Congress, Troy, Michigan, November 3-4, 2010.

CHAPTER I

INTRODUCTION

1.1 The Diesel Engine

Internal combustion engines can be classified, by fuel uses, into gasoline engines, diesel engines, gaseous-fuel engines, and multi-fuel engines [1]. Diesel engines are considered to be highly efficient due to the combustion with relatively high compression ratios. The major diesel engines employed in modern vehicles are four-stroke engines. Therefore, only four-stroke engines are covered in the scope of this thesis work.

The four strokes of a diesel engine cycle are intake stroke, compression stroke, power stroke and exhaust stroke. Only fresh air is introduced into the cylinder while the piston moving down to the bottom dead center (BDC) during the intake stroke. Diesel fuel is injected into the cylinder directly at a controlled timing near the top dead center (TDC). The fuel starts to mix with the already compressed air inside the cylinder at high temperature and pressure. The physical and chemical preparations before the combustion are within several crank angles. This preparation time for conventional diesel engines is often short because of the high compression temperature and the high reactivity of diesel fuel. The in-cylinder air fuel ratio is defined as the mass fraction of air and fuel. If there is excess air in the cylinder, the mixture is lean; otherwise it is stoichiometric or rich.

The air fuel mixtures in diesel engines are typically overall lean but locally rich. In-cylinder combustion is initialized at the regions where the air fuel mixtures are near stoichiometric. The combustion flames expand over the whole combustion chamber at a low speed. Typical diesel combustion includes two steps: premixed dominated combustion and diffusion dominated combustion. The premixed combustion is detonation-like combustion and it is the main source of engine combustion noise. The diffusion combustion relies on the flame propagation inside the cylinder. Energy in the fuel is released to the cylinder charge and it heats and pressurizes the mixture inside the combustion chamber. The pressurized cylinder charge drives the piston and rotates the crankshaft. This rotation is eventually converted to the motion to move the vehicles. The

final stroke of a diesel engine cycle is the exhaust stroke, to get rid of the products of combustion and to prepare the cylinder for the next cycle. All the critical emissions are released to the atmosphere in this stroke.

The whole combustion process inside the cylinder of a diesel engine is often within several milliseconds, even on high loads of an automotive engine. With the high temperature (over 1800K) during the diesel combustion and the presence of oxygen and nitrogen, nitrogen oxides can be formed, which are harmful to humans and regulated by the stringent emission standards all over the world [2].

The diesel fuel direct injection normally occurs when the piston is near TDC. At that time, the cylinder charge is at high temperature and high pressure. Because of the auto-ignition tendency and the low volatility of diesel fuel, the fuel cannot be fully mixed with air before ignition. Therefore, the homogeneity of the cylinder air fuel charge is poor. The regions near the fuel spray, the cylinder wall and piston surfaces are much richer than other areas. The particulate matter (PM) is produced in these regions. The total hydrocarbon (THC) and carbon monoxide (CO) are also generated from the same regions because of the incomplete combustion (lack of oxygen, lower combustion temperature).

The carbon dioxide (CO_2) is the fully oxidized product of hydrocarbon fuels, which is one of the major emissions from diesel engines. CO_2 has not been considered as harmful emissions for decades. However, it has attracted increasing attention from the public, due to its strong impact on the global climate change. CO_2 is considered as the major greenhouse gas (GHG) and is highly probable to be regulated in the near future. There are two major measures to reduce CO_2 emissions, either by the alternative fuel uses to reduce the burning of carbon or by fuel efficiency improvement to generate more energy from the same amount of carbon fuel.

1.2 Low Temperature Combustion in Diesel Engines

To reduce the critical emissions, especially NOx and PM, previous researchers have been struggling for decades and many strategies and methodologies have been developed and studied, such as in-cylinder combustion control and exhaust after-treatment. Among all

these methods, low temperature combustion (LTC) in diesel engines is one of the most effective ways to simultaneously suppress the production of NOx and PM [3~6].

As discussed in the previous section, NOx is produced in the lean or stoichiometric regions with high flame temperature, while the PM is generated in the incomplete rich burning zone. This causes the emission trade-off between NOx and PM in conventional diesel engines. In order to reduce the production of NO_x and PM simultaneously, burning the fuel in a well-mixed lean cylinder charge at a low temperature is one of the effective methods.

For lower emissions, it is critical to extend the air fuel mixing time to form the homogeneous charge for approaching LTC zone. The time between the start of fuel injection and the initiation of combustion is defined as ignition delay (ID). From the definition of ID, a longer ID gives a longer time for air fuel mixing preparation. There are certain measures to prolong the ID, such as port fuel injection, early or multiple in-cylinder injections and excess use of EGR. The combustion with a homogeneous cylinder charge is premixed dominated and the temperature inside the cylinder is much lower compared with that of the conventional high temperature combustion. The introduction of EGR increases the concentration of CO_2 inside the cylinder charge, which helps reduce the temperature further because of the high heat capacity of CO_2. However, the use of EGR reduces the availability of oxygen inside the cylinder, thus limiting the engine load levels. Therefore higher intake boost is required to bring in more oxygen, which also consumes more energy from the engine.

Figure 1-1 demonstrates the typical pathway to enable LTC with diesel single injection by the heavy use of EGR. The emission of soot was the indication of the combustion mode switching. When it achieved the soot emission deceasing slope, within a narrow window of EGR increase, the sharply reduced soot emission and the already ultra-low emission of NO_x differentiated the LTC combustion from the classical high temperature combustion (HTC). However, the HC and CO emissions rose significantly, which could reach up to 5% penalty of the total fuel energy.

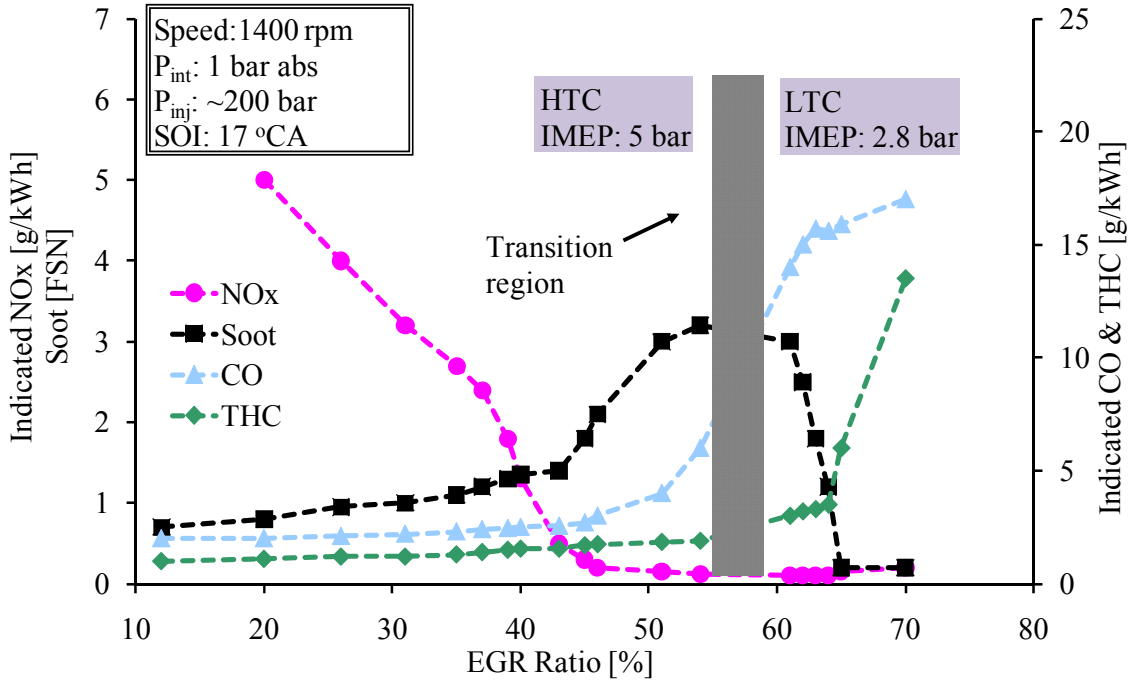

Figure 1-1 Typical Pathway of EGR Enabled LTC Cycles [7]

1.3 Alternative Energy Sources for Vehicles

The research of powering vehicles with a variety of energy sources has been carried on for more than one century. In the recent decades, due to the increased attention on energy security and impacts on global environment, the study has been performed on replacing conventional petroleum based fuels with alternative fuels, such as biofuels (ethanol, biodiesel) and gaseous fuels (hydrogen, compressed natural gas and liquefied petroleum gas). To utilize the energy from gaseous fuels, costly modifications are required, not only to the engines, but to the fuel storage, fuel delivery systems, and the whole vehicle layout. However, the use of biofuels does not require many modifications to the vehicle because of the similarity to the conventional petroleum fuels.

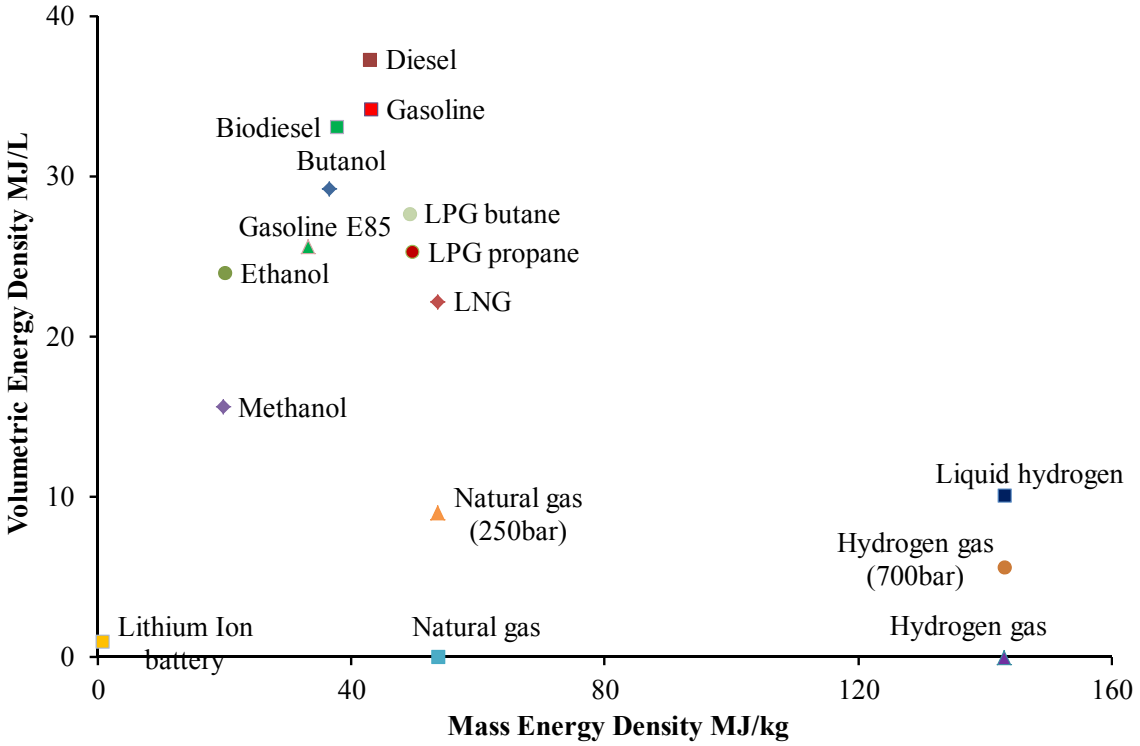

Figure 1-2 Volumetric and Mass Densities of Selected Energy Sources for Vehicles [8]

Figure 1-2 illustrates the energy densities of the selected potential fuel sources for vehicles based on both the volume and the mass. All the hydrocarbon fuels have comparable mass energy densities, while hydrogen carries extremely high mass based energy due to its low molar mass. However, when considering volumetric energy density, conventional gasoline and diesel, along with biodiesel, butanol, ethanol and LPG benefit much in the fuel storage and delivery aspects. A larger storage space will be occupied if a gaseous fuel is utilized even if it is pressurized to extremely high pressure (700 bar for hydrogen). The lithium ion battery has lower energy density in both volume and mass, which leads to a significant increase in weight and volume of energy storage when it is used in a vehicle.

1.4 Biofuels in Diesel Engines

Biofuels are generally produced from renewable bio-related materials. They are more attractive than the other potential energy sources mainly because of the lower environmental impact [9] and the advantages mentioned in Section 1.3. There are various sources for biofuel productions. In the world fuel market, ethanol and biodiesel have the

largest production and consumption rate. As shown in Figure 1-3, ethanol can be generated from food stocks, such as corn (the majority production of US), sugarcane (the production of Brazil), barley, plant residuals and wood chips. The bio-ethanol is typically blended with gasoline as E10 (a fuel mixture of 10% anhydrous ethanol and 90% gasoline) in North America and E25 in Brazil to partly reduce the consumption of petroleum based gasoline. Modern engines can run E10 without any modifications, while some engines in the flexible fuel vehicles can run up to E85. Biodiesel can be produced from vegetable oils and animal fats. In North America, a large portion of biodiesel is made from the soybean oil. Recently, the micro algae, due to its high production rate of biodiesel, has attracted increased attention from researchers [10~12].

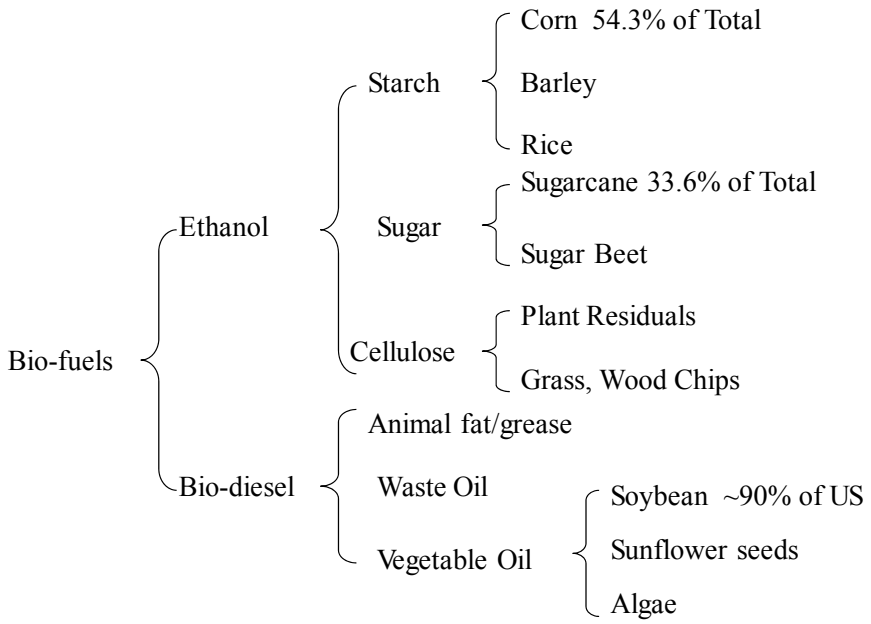

Figure 1-3 Major Biofuels and Production Resources

The fuel composition and the properties of biofuels differ significantly from the conventional diesel and gasoline (Table 1-1). The oxygen composition, the cetane number, the volatility and aromatic contents of the fuel are the main impact factors to the engine performance [17~21]. All these properties also affect the engine fuel storage and fuel management thus affecting the air fuel mixture formation, engine emissions and efficiency. These properties will be discussed in the following sections in details.

Table 1-1 Fuel Properties of Diesel, Gasoline and Ethanol [14~16]

Property	Diesel	Ethanol	Gasoline
Formula	C8~C25	C_2H_5OH	C4~C12
Molecular weight	~200	46.07	100~105
Composition, Weight %			
Carbon (%)	~87	52.2	85~88
Hydrogen (%)	~13	13.1	12~15
Oxygen (%)	0	34.7	0
Density	0.835	0.79	0.72~0.78
Boiling temperature (°C)	180~340	78	27~225
Aromatics (Volume %)	32-35	0	30~33
Viscosity @ 40°C (mPa s)	1.3~4.1	1.19	0.37~0.44
LHV (kJ/g)	43	29	43
Autoignition temperature (°C)	315	423	257
Cetane number	40~55	8~10	5~20
Octane number	-	92	80~88
Water tolerance	Negligible	Complete miscible	Negligible
Stoichiometric Air/fuel ratio	14.6	9	14.7

1.4.1 Oxygen Composition inside Biofuels

Oxygen is present in many of the commonly used biofuels along with the carbon and the hydrogen. Equation (1-1) demonstrates the reactions of typical biofuel combustion. λ is the excess air ratio, which is defined in Equation (1-2) [13]. Compared with conventional hydrocarbon fuels, the oxygen content in biofuels helps reduce the combustion demand on oxygen in the fresh air. Therefore, with the same mass of fuel injection, the biofuel mixture is leaner than the conventional hydrocarbon fuel mixture and the fuel borne oxygen is helpful in the reduction of soot, THC and CO emissions. At the same time, due to the presence of oxygen, the mass fraction of hydrocarbon inside the fuel is decreased. The lower heating value (LHV) of biofuels is often lower than that of diesel fuels. So a higher flow rate of biofuel is necessary to maintain the same engine load level. This requires reconsideration on the fuel delivery and injection control systems.

$$\begin{aligned} &C_\alpha H_\beta O_\gamma + \lambda\left(\alpha+\frac{\beta}{4}-\frac{\gamma}{2}\right)\left(3.76N_2+O_2\right)\rightarrow \\ &\alpha CO_2+\frac{\beta}{2}H_2O+\lambda\left(\alpha+\frac{\beta}{4}-\frac{\gamma}{2}\right)3.76N_2+\left(\lambda-1\right)\left(\alpha+\frac{\beta}{4}-\frac{\gamma}{2}\right)O_2 \end{aligned} \tag{1-1}$$

$$\lambda = \frac{MAF / m_f}{\lambda_{stoichiometric}} \tag{1-2}$$

Where: *MAF*: *Mass air flow rate* [g/s]

m_f: *Mass fuel flow rate* [g/s]

$\lambda_{stoichiometric}$: *Stoichiometric air fuel ratio*

The oxygen existence in biofuels makes the fuel more unstable than the diesel or gasoline fuels. Biofuels are degradable when they are in contact with air or water. The biofuels also can decay by themselves under the sunlight or when being heated-up. Thus it is not recommended to store biofuels inside the engine for a long period. There is also a higher requirement for the biofuel storage of sealing from air and water. The fuel line and filters may be blocked by the product from the degradation of biofuels. The rubber components, such as the gaskets, seals, and low pressure fuel lines, can have decomposition reactions due to the use of biofuels [22]. All these discussed aspects have to be considered for the new biofuel delivery system during the engine platform setup.

1.4.2 Cetane Number of Biofuels

Cetane number (CN) is a parameter describing the ignition ability of a fuel by compression ignition. The conventional CN measurement is defined in ASTM D613 procedure. The CN measurement is a time consuming and costly series test. The ignition delay time can be calculated from the precisely controlled fuel injection timing (with known injector opening delay) and cylinder pressure treatment (to decide the start of combustion) A larger CN indicates a shorter time of ignition delay, which means the specific fuel is easier to get auto-ignited. In order to approach LTC which can suppress NOx and PM simultaneously, longer ignition delay is often desirable.

Biodiesel has a higher cetane number compared with commercial diesel. The time of fuel physical and chemical preparation before combustion is shorter. Therefore, the combustion of biodiesel tends to be high temperature detonation-like combustion, which produces more NOx emissions than that of diesel combustion. On the other hand, due to its higher ignition ability, the emissions of THC and CO are almost negligible and the PM

emissions are also low [14]. Because of this nature of biodiesel, to reduce the NOx emissions together with PM, UHC and CO emissions, the control timeline is much shorter and the complexity is higher. Either a fast response control system is required and/or additional methods to withhold biodiesel from auto-ignition have to be taken (more EGR or a pilot injection).

Ethanol has a high auto-ignition temperature and very low cetane number. Thus it is difficult to be ignited by compressed ignition, while it could be ignited by external ignition sources, such as a spark igniter and a diesel pilot. The introduction of ethanol into the cylinder can improve the overall fuel cetane number and extend the ignition delay. Therefore, the utilization of ethanol will ease the control difficulties and requires a lower EGR level to enter LTC. Ethanol has been used as an octane number improver to be added into gasoline due to its anti-auto-ignition feature.

1.4.3 Volatility Impact of Biofuel Utilization

A minor change in the volatility of a fuel will affect the cylinder charge preparation and the fuel spray penetration if the in-cylinder direct injection is utilized. Therefore, when a new type of biofuel is applied to the engine, engine experiments are necessary to study and optimize the injection timing and injection pressure.

The boiling temperature of ethanol is 78°C. The volatility of ethanol is much different from that of the conventional diesel or biodiesel. Due to this high volatility, the low pressure port fuel injection to inject ethanol into the intake manifold is sufficient for the fuel preparation. This kind of fuel injection strategy can provide an extremely long fuel mixing timing by Injecting fuel near the BDC in the intake stroke. The homogeneity of the PFI intake mixture is much better than that of diesel direct injection. The combustion with well-mixed cylinder charge is typically premixed dominated. Low amount of soot is generated from premixed combustion. Because of the highly homogenous charge of air and ethanol fuel, the THC and CO produced from fuel quenching and incomplete combustion could increase largely. Ethanol fuel has a relatively high latent heat. The evaporation of ethanol lowers the overall intake temperature at the first stage and helps to

eventually reduce the combustion peak temperature. This lowered flame temperature can further suppress the NOx production.

The high fuel volatility helps ethanol mixing with air. The entire air preparation process is fast. The combustion phasing of neat ethanol is not determined by the fuel injection timing, but the kinetics of the fuel chemical reactions. The controllability on combustion phasing of this type of combustion might be one of the major difficulties [17]. When to ignite the fuel mixture, how much diesel pilot to be applied, and how to slow down the combustion process with EGR, need to be tested on a well-controlled and monitored engine test platform. Normally there is no PFI system equipped on diesel engines, therefore how to prepare a new fuel delivery and injection system for PFI is also discussed in this thesis.

1.4.4 Aromatics Effects

The aromatic hydrocarbons are the common contents inside the petroleum based diesel and gasoline fuels. It is agreed that these contents will affect the combustion characteristics and exhaust emissions [14,17,18,19]. The total quantity of aromatic is regulated and the test standard for aromatics is defined in ASTM D5186 [23]. Higher aromatic contents increase the flame temperature and potentially produce more NOx emissions. Because the aromatics are the precursors of the soot production [25], the soot production is not reduced, though the combustion temperature is high.

The aromatic contents are the fuel borne compositions from the fuel production process for conventional diesel fuels and most of biodiesel fuels, which provide a better lubricity to the high pressure fuel pump and injectors. However, there are no aromatics in the neat alcohol fuels from the bio-process production. When using alcohol fuels, the fuel lubricity needs to be reviewed and lubricity improvers are recommended to be added if necessary. At the same time, the effect from aromatics on the exhaust emissions and combustion characteristics can be avoided by the utilization of alcohol fuels. Due to the change in fuel properties, the classical engine control and optimization mechanism to diesel does not fit the new fuels. Further experiments and analysis are essential.

1.5 The Challenges and Objectives

Diesel LTC has been studied in CDEL and has been proved feasible to generate ultra-low soot and NOx simultaneously. The LTC combustion can be achieved by the use of EGR to dilute the cylinder air fuel mixture and lower the flame temperature inside the combustion chamber, or with the early and multiple fuel injections to modulate the HCCI combustion. When approaching LTC combustion, the engine operation is done in the narrow corridors within several isolated islands of the air fuel ratio, EGR level, boost pressure, and injection parameters [26]. The employment of biofuels makes the pathway narrower and sometimes even the existence of this pathway needs to be confirmed by empirical work. As mentioned in the previous sub-sections, there are many differences between diesel and alcohol fuels in the fuel properties (both physical and chemical). This increases the complexity and uncertainty of conducting the biofuel application and optimization.

The objectives of this thesis are outlined as follows:

1) To prepare an engine platform with all the typical modern control and measurement devices for LTC study.

2) To implement the necessary modifications for biofuel applications on the diesel engine.

3) To document the entire engine platform preparation process for future references.

4) To perform preliminary engine experiments of verifying the performance of the engine platform and exploring the effect of the use of biofuels on engine emissions and efficiency.

1.6 Thesis Outline

The thesis outline is schematically presented in Figure 1-4. The preparation work is presented in Chapter Ⅰ and Chapter Ⅱ. A brief introduction to the diesel engine working principles, the LTC in diesel engines, alternative fuels, the beneficial effects and challenges of using biofuels are discussed in Chapter Ⅰ. The major equipment and

control systems used in this implementation are illustrated in Chapter Ⅱ. The technical data and a brief introduction of system setup are also presented in that chapter.

There are two main parts in the engine platform implementation: engine platform implementation and PFI system adaption. The engine platform implementation which is presented in Chapter Ⅲ includes the detailed process of dynamometer cell preparation, dynamometer and engine positioning, air management system setup, fuel delivery system and fuel pressure control system preparation.

The PFI implementation process is described in details in Chapter Ⅳ. In that chapter, the introduction to a PFI system, the whole system preparation, the safety consideration and an injector calibration are presented. The portable PFI injection bench is the first PFI application in the CDEL, thus a detailed documentation is necessary for future reference.

Chapter Ⅴ presents all the results and discussions, including the platform verifications, diesel baseline tests and PFI tests with ethanol and diesel. The encoder alignment, injection control of both diesel and PFI ethanol and the emission measurement were verified in the platform verification. Diesel low load SOI (start of injection) sweep, EGR sweep and medium load EGR sweeps were performed and the processed data were analyzed as the baseline for PFI experimental analysis.

Several preliminary tests with PFI ethanol ignited by DI diesel were performed and the results were analyzed. It was observed that the smoke emissions remained low over the entire ethanol PFI test and NOx production was under the control of EGR. The start of combustion could be controlled by the diesel injection timing. A second hump of heat release was noticed, which might be the indication of ethanol auto-ignition when more ethanol was injected into the intake manifold. Comparing with diesel combustion, more THC was emitted in the exhaust, which penalized the in-cylinder combustion efficiency. Ethanol accumulation in the intake manifold was also noticed via the ethanol switching-off test.

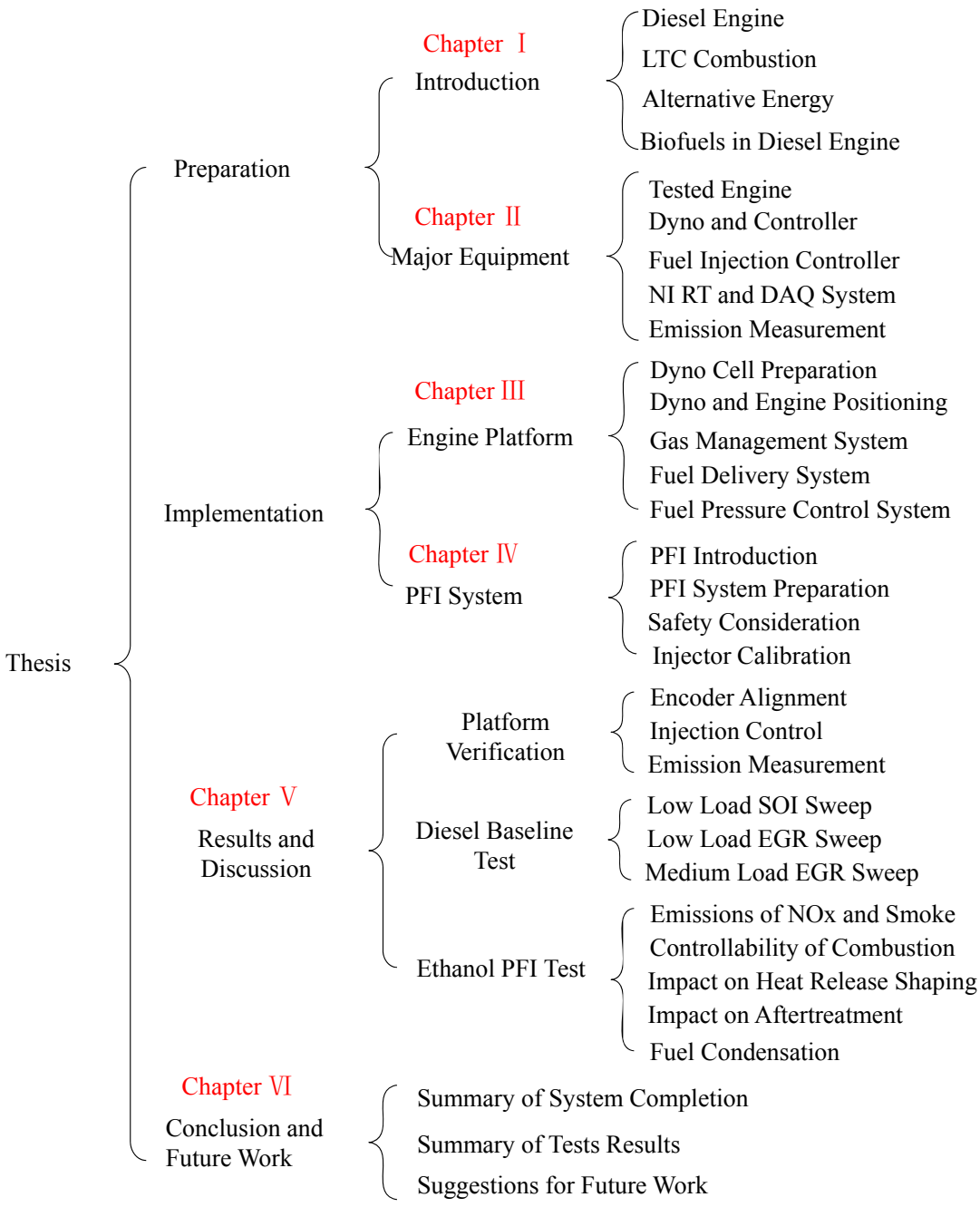

Figure 1-4 Thesis Outline

In Chapter Ⅵ of this thesis, the system completion and all the experiment results are summarized, and some suggestions for future work are proposed. The selected useful information and recordings are illustrated in the appendixes for references.

CHAPTER II

MAJOR EQUIPMENT AND DEVICES

2.1 Tested Engine

The tested engine in this platform setup is a Ford production diesel engine (Specifications in Table 2-1). It is a four-cylinder, four-stroke engine with a displacement of 2 liters. The compression ratio is 18.2:1. It is equipped with an advanced common rail diesel direct injection system and the peak fuel injection pressure can be up to 1600 bar. There are four solenoid diesel injectors utilized in the engine and up to six injections can be achieved by each injector.

Table 2-1 Specification of Tested Engine in the Platform

Engine Type	4-Cylinder, 4-Stroke Ford DuraTorq "Puma"
Displacement	1998 cm^3
Bore	86 mm
Stroke	86 mm
Connecting Rod	160 mm
Compression Ratio	18.2:1
Combustion System	DELPHI Common Rail Direct Injection System P_{rail} up to 1600 bar
Injection System	Independent Injection Control up to 6 Injections per Cycle

The engine was tested in the CDEL previously from 2006 to 2008 [14, 26]. Due to the new research planning, the engine was relocated to the newly constructed dynamometer cell. This engine was modified by a prior researcher in CDEL to the structure of three motoring cylinders (to stabilize the engine) and one research cylinder in which all the control strategies and measurements were performed. The engine control unit (ECU) from original equipment manufacturer (OEM) was removed from the engine. In this way, the engine control parameters were not constrained by ECU, thus their effects on engine performance could be explored independently through the control of each parameter. However, an additional control system to replace the ECU was necessary to operate the

engine safely and effectively. Moreover, a setup consisted of air management, fuel delivery and engine cooling systems was implemented in the platform preparation. Modifications were not made to the engine oil system except implementing the pressure and temperature monitoring.

An AVL GU13P piezoelectric transducer was installed in the engine to measure the pressure in the research cylinder (Cylinder #1). It was mounted through the glow plug hole with an adapter. The charge amplifier used is Kistler 5010B charge amplifier, from which the output is ± 10 Volts. The cylinder pressure measurement is an indirect observation of the combustion happening inside the combustion chamber and is the most commonly used method for the modern engine researches.

A Gurley rotary optical incremental encoder 9125S was installed at one side of the crankshaft. The outputs of this encoder are one index/revolution and one tick/0.1 CA, which provides an external timing of engine crankshaft rotation. Associated with the Hall effect CAM sensor signal, the TDC in the compression stroke can be identified from that of the exhaust stroke.

2.2 The Dynamometer and Controller

The dynamometer utilized in this platform setup is a Schenck WS230 eddy current high speed dynamometer. A dynamometer is a device to measure the torque and rotation speed of an engine. If controlled in the rpm mode, the dynamometer can maintain the engine rotating speed at the set value while the engine load levels varying. The highest rating power and torque for the dynamometer used in this platform are 230 kW and 750Nm respectively [27]. Figure 2-1 demonstrates the power curves for W-series eddy current dynamometers made by Schenck. The engine operating range is around 1000~3000 rpm at 10~30 kW power. Therefore, this dynamometer can meet the torque and power requirement of the current setup.

The excessive engine energy is absorbed by the dynamometer and converted to heat by the eddy current developed from the field iron [28]. Thus sufficient cooling water is required to maintain the operating temperature of the dynamometer. The cooling water used in this setup is supplied from the city water. A minimum upstream pressure of five

psi at the dynamometer water inlet port is recommended to maintain a sufficient cooling water flow for a medium to high load engine experiment. As another additional safety measure, a flow switch is also installed at the water inlet port to assure the required flow rate. The exhaust water from the dynamometer is directly connected to the water drain.

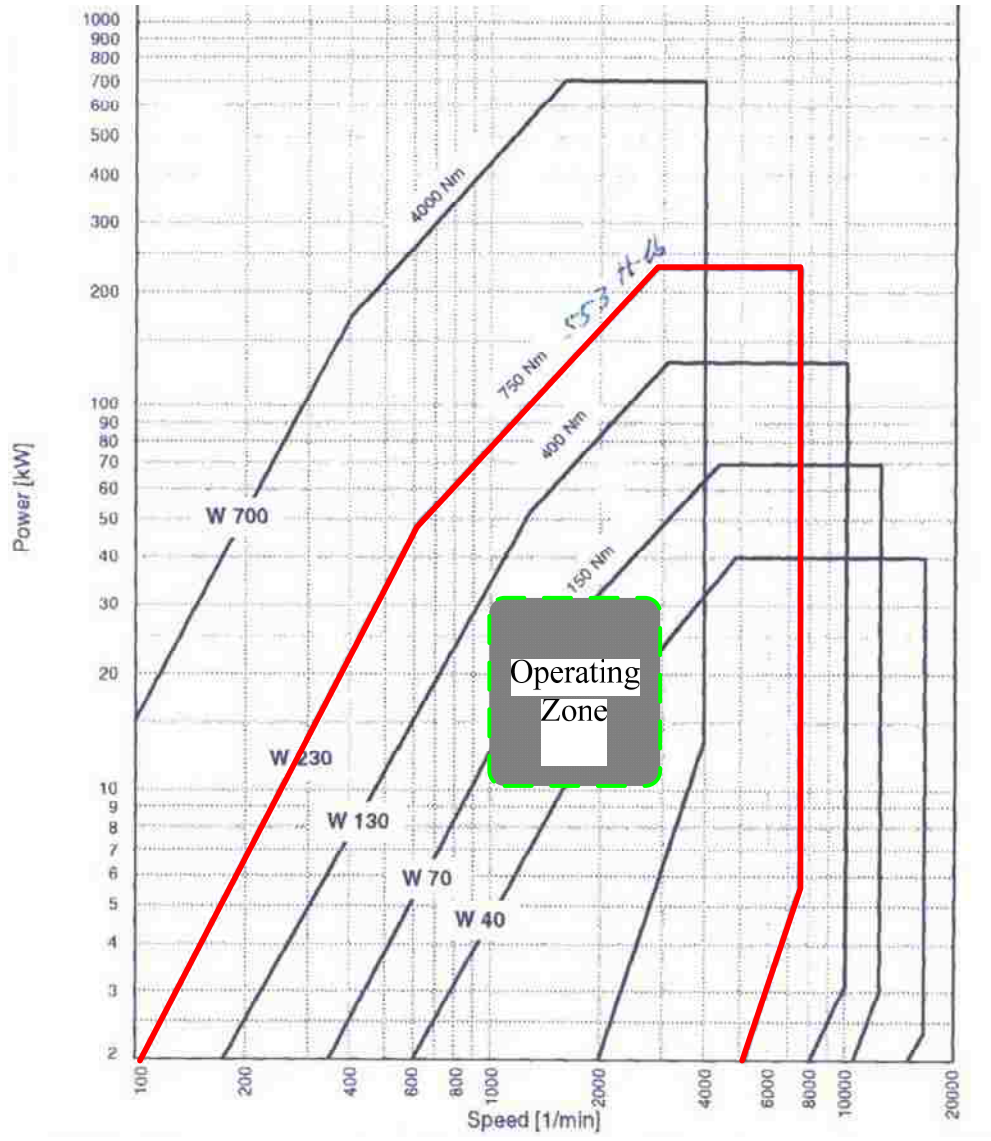

Figure 2-1 Power Curves for Selected Eddy Current Dynamometers [27]

There are two sensors equipped on the dynamometer, a speed sensor and a load cell. The connectors for those two sensors are seven pins and six pins MS connectors respectively. The speed sensor is a Magnetic Pickup. It picks the voltage developed by the rotating of a 60-tooth gear and the translation of the voltage frequency can provide an accurate speed

measurement. The recommended clearance between the Magnetic Pickup and the gear is 0.3mm [28]. The load cell is used to measure the tension or compression force on the strain gauges by measuring the voltage change. With the pre-defined arm-length from the center of the dynamometer to the load cell, the positive and negative torques corresponding to the engine clockwise and anticlockwise rotations can be calculated.

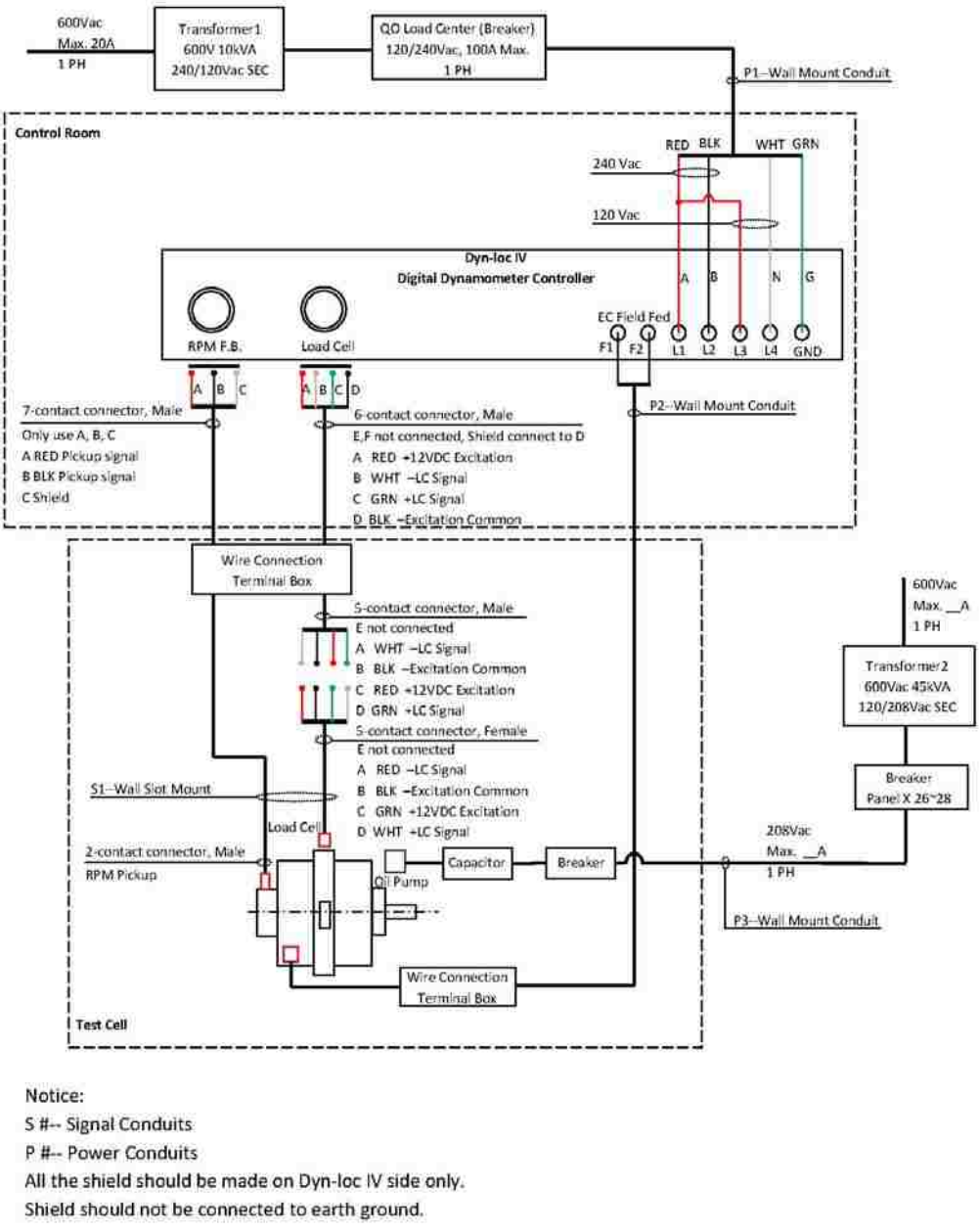

Notice:
S #-- Signal Conduits
P #-- Power Conduits
All the shield should be made on Dyn-loc IV side only.
Shield should not be connected to earth ground.

Figure 2-2 Wiring Diagram for WS230 Dynamometer Used in the Platform [29]

Figure 2-2 demonstrates the detailed wiring connections from the dynamometer to the power supply and the dynamometer controller. The power supply to the dynamometer is a high voltage power and the connections were conducted by some professional electricians. The dynamometer in this setup is controlled by a Dyn-Loc IV digital dynamometer controller (as shown in Figure 2-3). The filtered and smoothed rpm and torque feedback are displayed on the front panel of the dynamometer controller. The power is calculated based on Equation (2-1).

$$P = \frac{2\pi nT}{60} \tag{2-1}$$

Where: n : *Speed* [rev/min]

T : *Torque* [Nm]

P : *Power* [W]

Figure 2-3 Front Panel of the Dynamometer Controller

The control of the dynamometer could be switched between torque mode and rpm mode. The rpm control mode was used in CDEL for the Ford diesel engine controlling. There were two analogue outputs through BNC (Bayonet Neill–Concelman) connectors from the controller for both rpm and torque, which could be input into the data acquisition card for remote monitoring and recording. In the current setup, those two signals were connected to a National Instruments (NI) temperature module and the readings were recorded in a computer. The conversions from voltages to rpm and torque are according to Equation (2-2) and (2-3).

$$rpm = 1000 \times V_{rpm} \tag{2-2}$$

$$Torque = 100 \times V_{T} \tag{2-3}$$

The default display units for the power, speed and torque on the dynamometer controller are horsepower, rpm and pound-feet standard. But the standard displays in CDEL are kW, rpm and Nm. Therefore, it is necessary to set the controller to metric units. The unit selection switches are behind the torque bezel at the front panel. The bezel can be removed with fingernails. When Switch Six is on and Switch Seven is off, the display units are Nm for torque and kW for power [30].

The decimal position of the display can also be set in the controller. For the rpm display, it was set to be no decimals by default, and it is the desired display in the current setup in CDEL, otherwise the controller needs to be opened to change the setting on the mother board. One decimal for the torque display is required. The way to change it is to open the torque bezel and set Switch Four on, Switch Five off [30]. The decimal position of the power display matches the setting of the torque display.

2.3 Diesel Injector Driver

EFS 8232 programmable electro-valve power drivers are employed to control the solenoid injectors for the prepared setup (Figure 2-4). There are four sets of drivers to control the four solenoid injectors independently. One module can control one injector with a speed up to 400 drives per second [31], which is equivalent to 20 injections per cycle at 2400 rpm engine rotation speed, in case the injector can response fast enough.

Due to the physical limitation of the injectors (Injector opening delay and closing delay) in the Ford Puma engine, up to six injections can be realized with the prepared setup. Therefore, the controllability of this injection driver is sufficient for in-depth exploring the capability of the solenoid injector.

The power to drive the injector is supplied from an auto battery (12~15V). The injection and injection select command signals are TTL (Transistor-transistor Logic) type signals generated from an NI real-time controller via Labview programs developed in CDEL. The injection command is amplified by an EFS driver according to the TTL command and sent to the driven injector. There are four checking LEDs on the front panel of the EFS injector driver, which indicate the general operating status of the injector driver. There is also one 25-pin sub-D monitoring connector which can be used to check several parameters in the driver: such as EV current, selection signals, effective injection monitoring and others.

Figure 2-4 EFS IPOD Inputs and Outputs [31]

All the user parameters for those four IPOD drivers could be set via one computer by a program WinIPOD (Interface as shown in Figure 2-5) through RS232 communications. The version of the software used in this platform setup in CDEL was 2.3.6. The communications between each driver were through daisy chain as demonstrated in Figure 2-6. When starting the program all the powered IPODs were detected and the setting for both local at computer and remote at IPOD were displayed. The battery voltage and the engine speed could also be monitored in the program.

The overall injection system is illustrated in Figure 2-7. A TTL type injection select command was generated from a realtime controller and sent to all four IPODs via the physically connected cables. The injection command was sent to each IPOD independently. Various injection control strategies could be applied to each injector simultaneously. However, fixed injection timing and duration were used for the injectors in the other three cylinders and varied injection timings and durations were applied in the research cylinder.

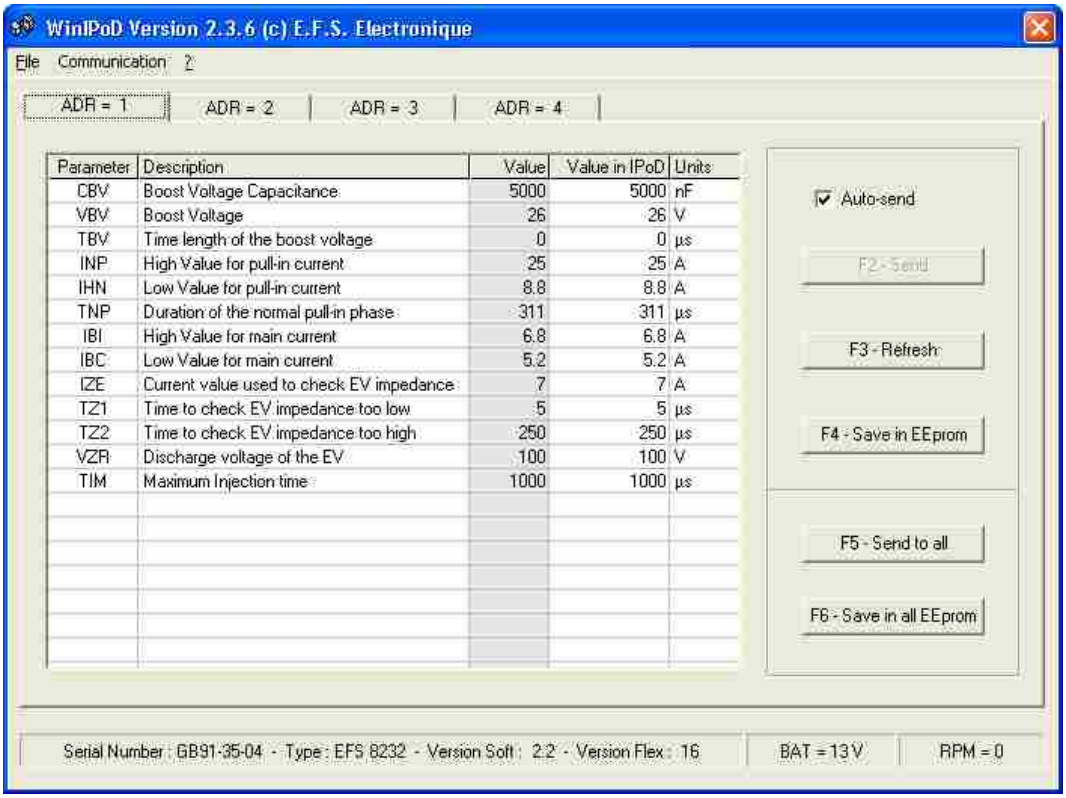

Figure 2-5 Control Parameters Setting Software Interface of WinIPOD

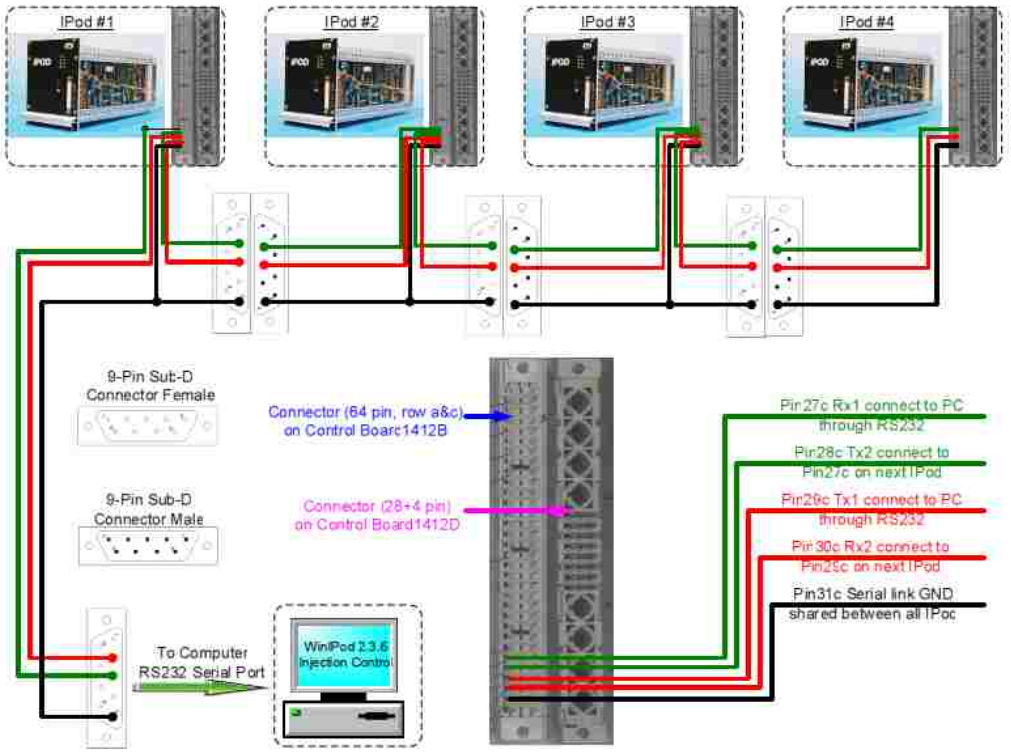

Figure 2-6 Daisy Chain Connections between Four Controllers

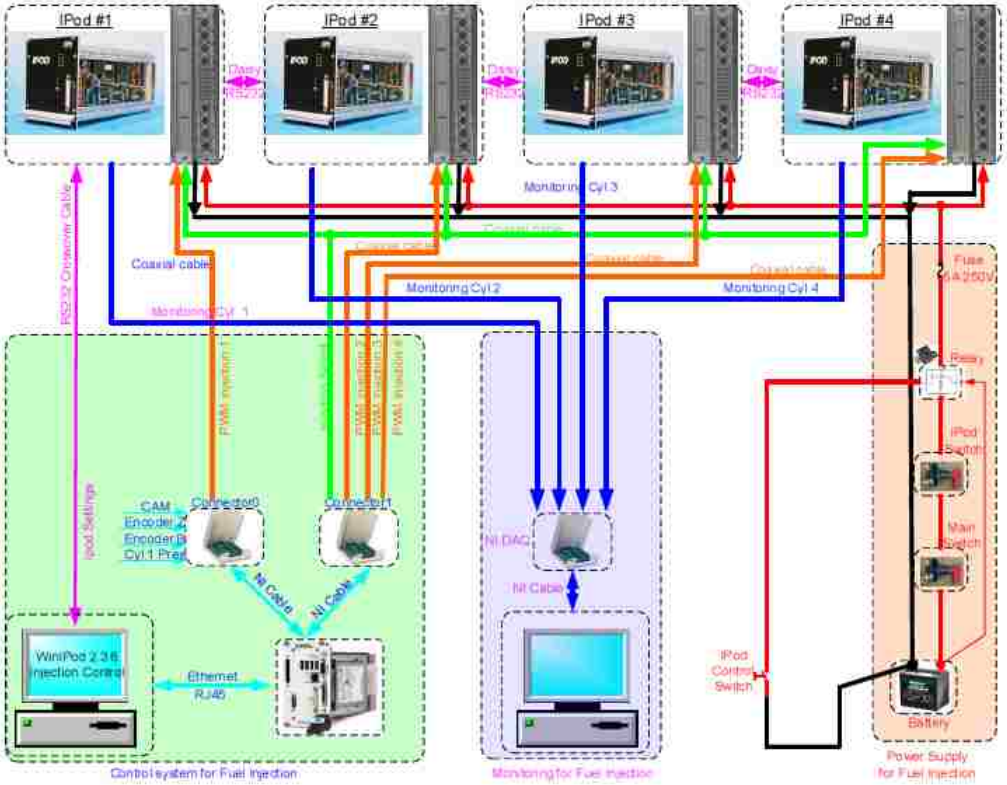

Figure 2-7 Schematic for Overall Fuel Injection Control System

2.4 NI Control and Data Acquisition (DAQ) System

The NI control and data acquisition system includes the hardware purchased from National Instruments. They support the input and output from the Labview programs which were widely used in CDEL for the engine control and monitoring. In this section, a brief introduction to the real time controller with the embedded field programmable gate array (FPGA), the temperature module, and various DAQ cards are described.

2.4.1. Real Time Controller

In this platform setup, two NI real time controllers (NI PXI-8110) were employed to control the common rail fuel pressure and fuel injections (both diesel and ethanol). These Real time controllors (RT) were installed on a nineteen-inch rack, as shown in Figure 2-8. Both RTs were with the same configuration. The chassis type is NI PXI-1031, which have four available slots, one for the controller and three for the embedded user configurable FPGAs (two FPGAs were installed in the current configuration). The types of these FPGAs are PXI-7813R with 160 bidirectional digital inputs/outputs (DIO) and PXI-7853R with 8 independent analogue inputs (AI), 8 independent analogue outputs (AO), and 96 DIOs [33]. Due to the requirement of analogue input from the injection programs, only FPGA PXI-7853R was utilized in this project.

The maximum DIO clock rate for FPGA PXI-7853R was 40 MHz, which was more than the requirement of the injection control. This fast speed provided more flexibility for the applications of various control strategies, such as combustion adaptive control. A host computer was employed to provide the user friendly interface. The control command from the host computer was sent to RT via RJ45 standard Ethernet cable. Both the host computer and RT were connected to a switch box under the same IP (internet protocol) group. The core injection control program was running on the FPGA. All the DIOs (Encoder index and ticks, CAM, injection select and command) and AI (the cylinder pressure) were connected to the FPGA through an NI terminal box. To assure the reliability of the injection control, the signals from the engine and the command to the

engine were directly connected without any signal duplication or filtering (the cylinder pressure signal was directly picked up from the output of the charge amplifier).

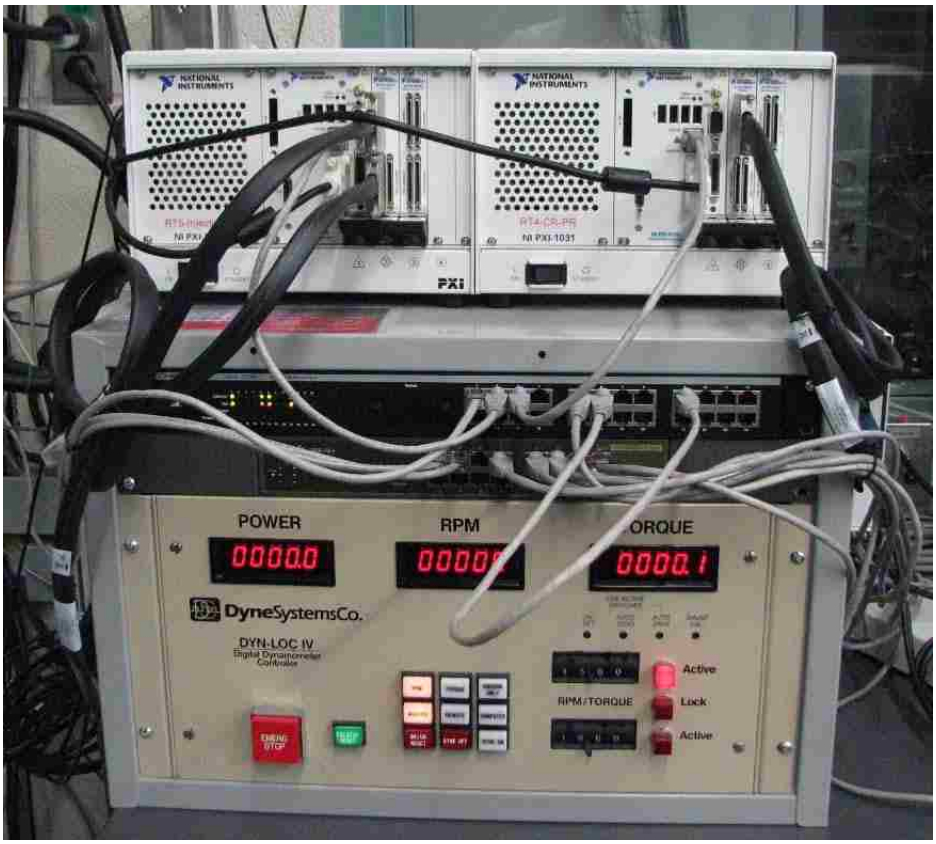

Figure 2-8 Installation of Two Real Time Controllers

2.4.2. Temperature Module

The temperature module consists of three NI SCXI-1303 temperature modules and one NI SCXI-1302 terminal block. The NI SCXI-1303 temperature module is specially designed for the high-accuracy thermocouple measurements. For each module there are 32 input channels in total for both T-type and K-type thermocouples. The NI SCXI-1302 terminal block with 16 AIs was mainly used as the measurement of analogue inputs of various sources from the engine and from the associated devices, such as pressure sensor readings, fuel flow readings, rpm and torque readings.

The whole engine temperature measurement system was primarily prepared by the author and shared use with the related group members in CDEL. As a summary, there are fifteen T-type and seven K-type thermocouples, and six analogue inputs from various sources connected to the temperature module. A new Labview program was also developed by the author to monitor and record the measurements.

2.4.3. DAQ System Summary

As shown in Figure 2-9, eight computers were employed to control and monitor the whole Ford engine test system. Among all the computers, two were connected to the real time controllers to command the primary and secondary fuel injections. Additional DAQ cards were installed to five computers. These cards were PCI-6122 Simultaneous Sampling Multifunction DAQ, PCI-6229 M series card, and three PCI-6220 M series cards, one card on each computer. Because of the availability of DAQ cards, different cards were utilized. The low cost PCI-6220 M series card had 16 analogue inputs and 24 digital inputs and outputs and two counters. It was sufficient for most of the data acquisition requirement of the prepared Ford engine experimental platform, except the control of intake and EGR which required two analogue outputs to drive the SMC pneumatic regulators.

For each DAQ card and FPGA, one or more terminal boxes were necessary for signal inputs and command outputs. In this engine platform preparation, all the terminal boxes used were the same type SCB-68. However, the pinouts for each type of cards were different, thus it was necessary to refer to the pinout diagram in the manual for that specific card when any of the physical connections were made. A detailed table of physical channel connections of all the DAQ cards and temperature modules for the prepared engine platform were illustrated in the appendix.

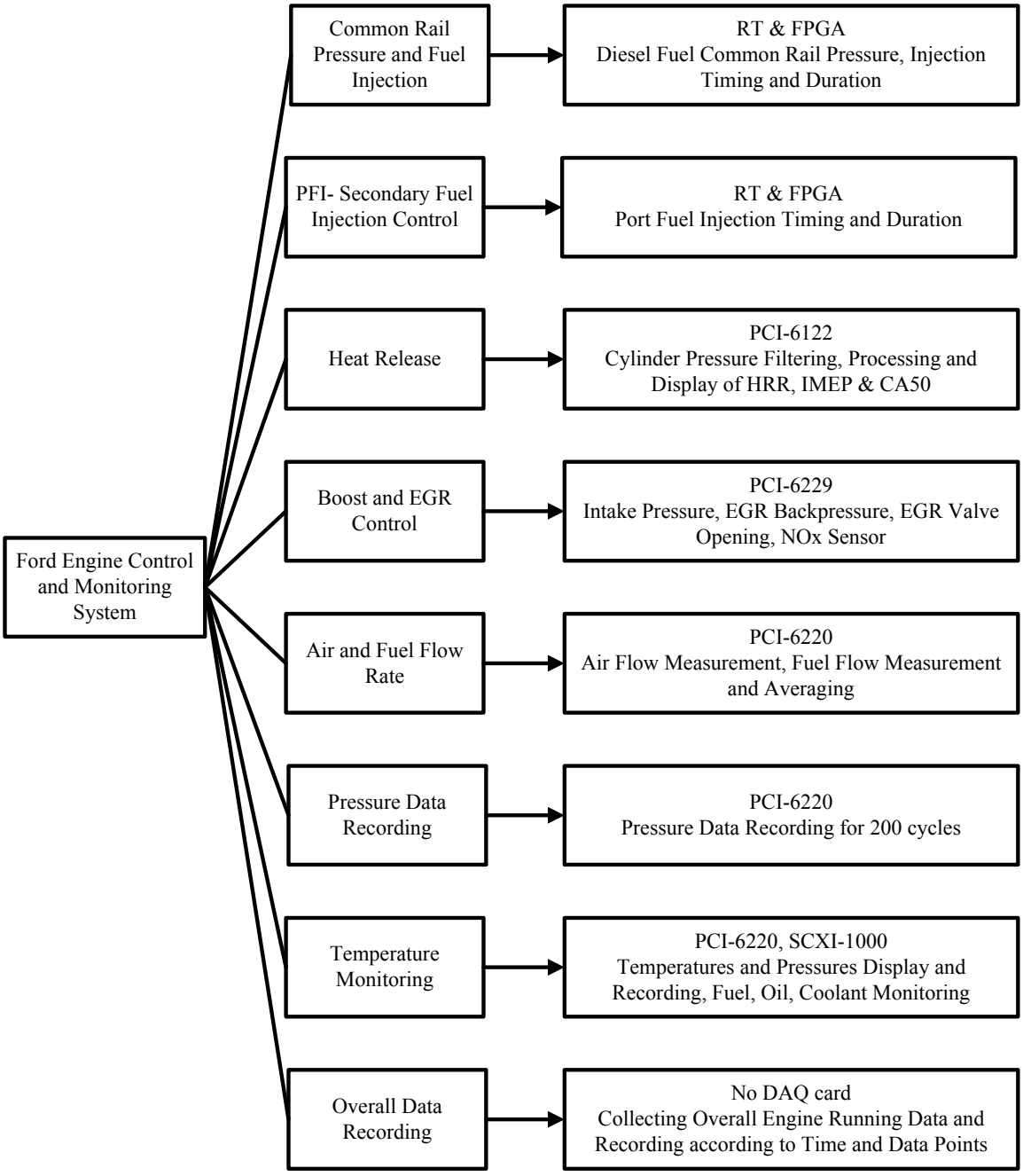

Figure 2-9 System Diagram for Ford Engine Control

2.5 Emission Measurement System

The intake and exhaust gas concentrations of the Ford engine were measured by a dual-bank CAI analyzer system and an AVL smoke meter, as demonstrated in Figure 2-10. The gas analyzers, smoke meter, and the conditioning unit were shared with the other

engine test platform. The gas samples from the engine intake and the exhaust were routed to the conditioning unit for water and soot removal. The gas was pumped to the CAI analyzers for measurement after the removal. The smoke sampling is through a separate sampling line from the engine to AVL 415S smoke meter "Sample 2". CO_2 and oxygen (O_2) concentrations in the engine intake were monitored by the intake CAI analyzer bank while the emissions of NO_x, CO, CO_2, O_2, THC and smoke in the engine exhaust were quantified via CAI analyzer exhaust bank and AVL smoke meter. The simplified diagram in Figure 2-10 illustrated the names, working principles and operating ranges of the CAI analyzers and the smoke meter.

The intake gas was sampled after EGR mixing with fresh air. The measurement could be considered as the in-cylinder mixture concentration. The exhaust sampling port was on the exhaust pipe before the DOC. The exhaust samples contained the raw exhaust emissions from the engine with all unconverted species. However, the exhaust sampled gas passed through a long cold sampling line and a chiller in the conditioning unit, thus the heavy hydrocarbon emissions were mostly condensed in the line and the chiller instead of going into the analyzer. Due to the low backpressure requirement of the smoke sampling, the smoke probe was installed after the DOC and the exhaust backpressure valve. The smoke produced by the engine might be burnt partially by the DOC when the exhaust gas passing through the DOC.

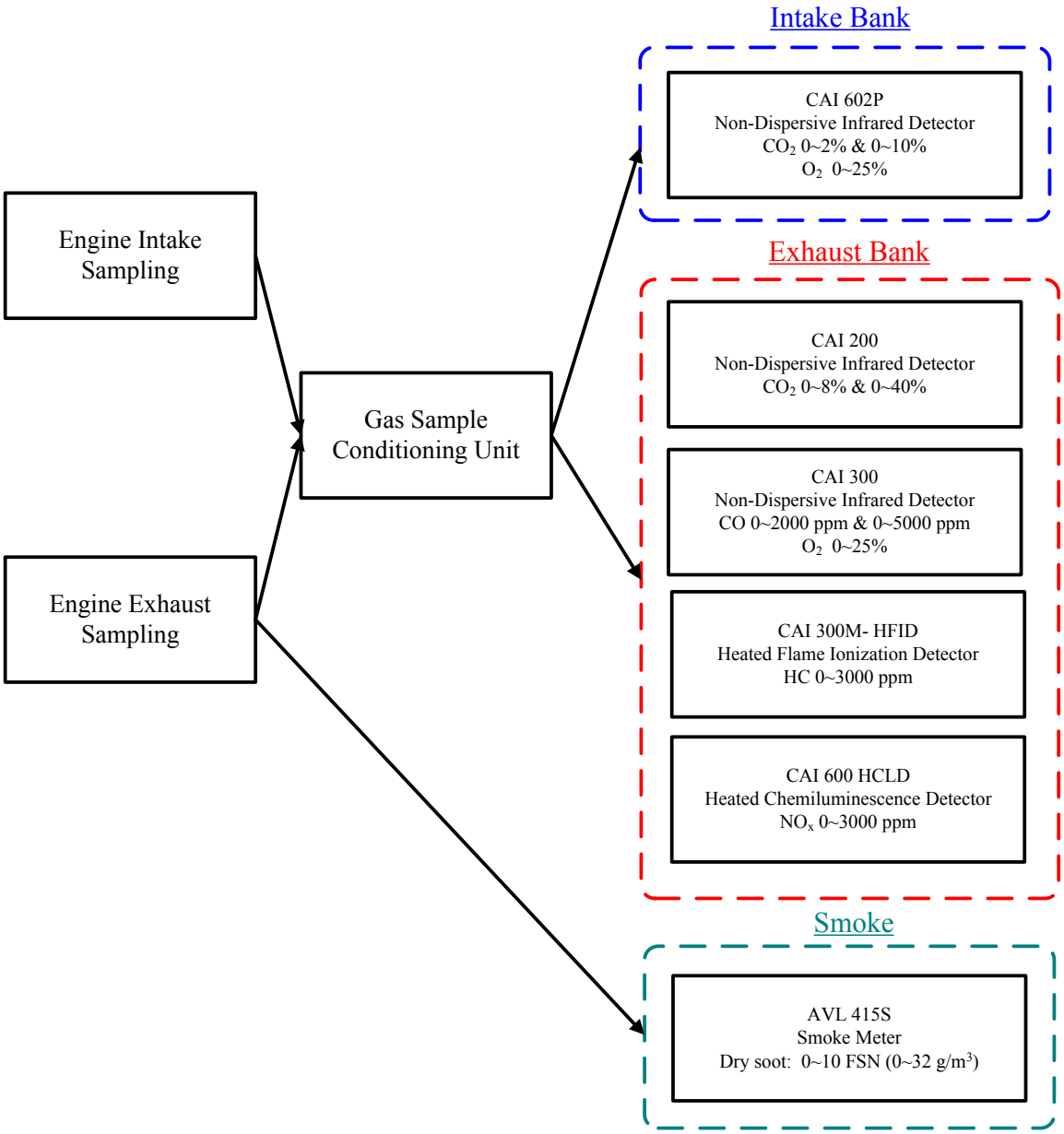

Figure 2-10 Emissions Measurement System for Ford Engine Setup

CHAPTER III

PLATFORM PREPARATION AND IMPLEMENTATION

3.1 Dynamometer Cell Preparation

The research engine in this thesis was relocated to a newly constructed dynamometer cell. A brief introduction to the dynamometer cell preparation will be given in this section. The main process of the dynamometer bed preparation is demonstrated in Figure 3-1. There are mainly two types of dynamometer beds used in the engine dynamometer experiment research: rigid bed and spring anti-vibration bed. Both types have advantages and disadvantages. The dynamometer bed used in CDEL is the rigid base with a 5-foot thick concrete pad, which provides the stability during the engine running. On top of the concrete are two pieces of steel base plates with slots, on which the dynamometer, the engine and all kinds of instruments can be attached. In between of the steel base and the concrete, grouts of M-bed Standard were filled to improve the contacting between the plate and concrete.

Figure 3-1 Dynamometer Test Bed Preparation

Besides the dynamometer test bed, the electricity supply of different voltages (110V, 208V, 220V, 480V and others), clean compressed air supply, enhanced air ventilation, water supply and coolant supply for the engine platform were also prepared. More than

one electricity transformer was installed during the dynamometer cell preparation, which satisfied all the power supply demands from various instruments. The shop compressed air was routed into the dynamometer cell. The original ventilation system was enhanced and additional equipment was used to fulfill the air recirculation requirement of the engine tests. A ditch around the dynamometer test bed was prepared for pipes of water and coolant, air supply to the engine, and engine exhaust. Aluminum cable holders were mounted on the wall for routing the cables of engine monitoring and control.

3.2 Dynamometer and Engine Positioning

A practice of aligning the dynamometer with the engine is shown in Figure 3-2. The dynamometer was placed at a side of the engine bed and aligned with one slot on the bed using the side frame of the dynamometer as a reference. In this way, the dynamometer shaft was roughly parallel to the slot. The projection of the dynamometer shaft was found with a laser pointer and marked on the engine bed. The centerline projection of the engine crankshaft was found by using a plumb-bob from both the flywheel side and the encoder side. After overlapping those projection lines, the engine crankshaft height was adjusted to be slightly lower than that of the dynamometer shaft. This was consistent with the practices in other engine to dynamometer connections in CDEL. In this setup, the heights of the crankshaft and dynamometer shaft were 697mm and 657mm. A commercial heavy duty drive shaft was used between the dynamometer and the engine.

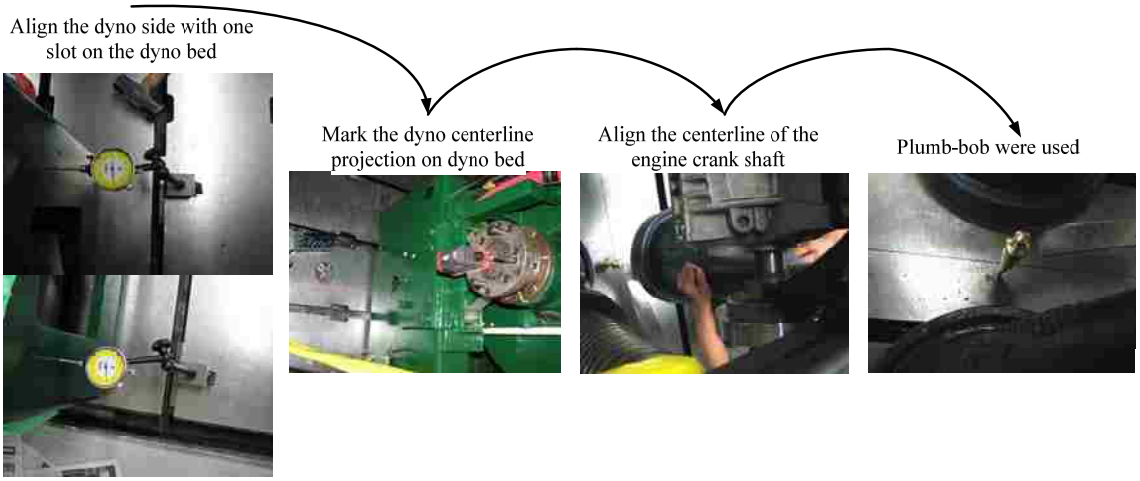

Figure 3-2 Steps of Aligning Dynamometer with Engine

The engine was mounted with two flexible mounting devices with rubber vibration absorbers. The engine can swing in a small angle during experiments. Each of the devices was supported by two heavy duty screw jacks. Two more screw jacks were used as the engine mounting safety backups. One more rubber absorber was installed to further reduce the engine operating vibration.

3.3 Gas Management System Preparation

Figure 3-3 demonstrates the overall layout for the whole engine gas management system, which consisted of the boosted intake system, the engine exhaust system and a EGR loop. The engine boost system was simulated with the compressed air. The engine exhaust was recirculated to the air intake, controlled by an exhaust backpressure valve and an EGR valve.

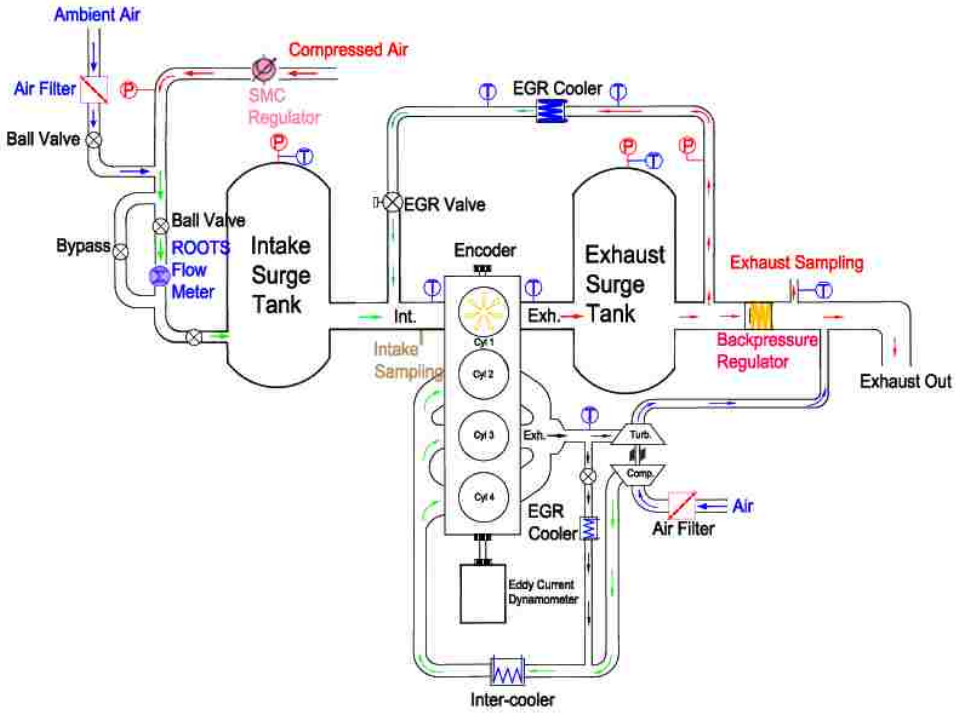

Figure 3-3 Overall Schematic of Gas Management in Ford Engine Test Platform

The engine intake can be switched between naturally aspirated and compressed air simulated boost by turning on/off the specific valves. When boosted intake was utilized, a clean and oil free air source was required and the air pressure was to be regulated. In this setup, two filters in series were employed for a better filtration of the shop compressed air

supply and a SMC electro-pneumatic regulator series ITV-3000 was used to accurately regulate the intake pressure.

3.3.1 Air Flow Measurement

The engine intake air flow is necessary for the calculation of air fuel ratio, mass EGR fractions, and the emissions conversions from ppm level to power based emission values [34]. Three potential air flow meters from Roots Meters & Instruments Dresser Inc. are compared in Table 3-1. The normal engine test speed range was from 1000 rpm to 3000 rpm. The type 2M175 was chosen in this engine platform preparation, which was sufficient to measure the intake flow rate across the tested speed range. A Roots ICEX counter with an electronic transmitter was purchased together, which could provide a non-compensated and high frequency pulse output [35]. The two-wire output from the ICEX was connected to an NI terminal box and the pulses were counted by an in-house developed Labview program.

Table 3-1 Specification Comparison of Potential Flow Meters

Technical Data	Units	2M175	3M175	5M175
Flow Rate	ACFH	2000	3000	5000
Base Rating(Q max)	m^3/h	56.6	85	141.5
Max. Operating Pressure	bar	12	12	12
Rangeability +/- 1%	ratio	68:1	76:1	120:1
Start Rate	m^3/h	0.0538	0.0595	0.034
Stop Rate	m^3/h	0.0311	0.051	0.0227
Avg. Differential, 100% Flow	mbar	0.7	1.1	1.1
Nominal Pipe Size	mm	50	50	80
Flange-to-Flange	mm	172	172	172
Flange Connection	ANSI	150#FF	150#FF	150#FF
Net Weight-CTR Version	kg	11.8	13.2	15.9
Engine Displacement/cyl	L	0.5		
Max. rpm		3774	5666	9434

3.3.2 Intake and Exhaust Surge Tanks

The engine intake and exhaust flow fluctuated severely due to the intake and exhaust valves opening and closing [28], which lowered the accuracy of the intake air measurement and the exhaust EGR control. An effective way to reduce this fluctuation in CDEL was by using large surge tanks in the gas loop for both engine intake and exhaust.

The specifications of the intake and exhaust surge tanks used in this prepared engine platform are shown in Table 3-2. The volumes for both tanks were more than 100 times of the research cylinder displacement (0.5 L), which was sufficient to damp the gas pressure fluctuations in the stream [34].

Table 3-2 Specifications of Intake and Exhaust Surge Tanks

	Intake	Exhaust
Height (Inches)	33	23.6
Diameter (Inches)	14	12.7
Volume (Liter)	>80	>60
Rating Temperature (ºF)	650	1000
Rating Pressure (psi)	200	300
Manufacture	Ontario Compressor	Prentex

High boost pressure was required to maintain the oxygen level in the intake when heavy EGR was applied to the cylinder. The intake pressure of one to five bar absolute was the typical operating range. The intake surge tank rating pressure was 200 psig at 650 °F, of which the safety factor was more than 3. The safety factor for the exhaust surge tank was even more than that of the intake surge tank. Therefore the selection of these two tanks was adequate.

3.3.3 Pressure and Temperature Monitoring

The gas pressures inside the intake surge tank and the exhaust surge tank were monitored by the Bosch differential pressure sensors (0261230093). The measurement output from this type of sensors was the gauge pressure because the reference pressure port on the sensor was open to the ambient. The measuring range was 0~ 500 kPa and the operating temperature ranges were from −40°C to 125°C [36]. The temperature range was too low for the direct exhaust gas pressure measurement. A long cold Teflon tube was used to route the exhaust gas to the pressure sensor. In this way, the measurement of the exhaust pressure may not be exactly accurate but could be taken as a reference.

An external wastegate (PBO085-1000) was installed in one of the ports of the exhaust surge tank as a safety measure of releasing the excessive pressure inside. The wastegate was made by Precision Turbo & Engine. Three sets of springs were used in the wastegate,

and they could provide 1.7 bar (25.5 psi) pressure on the diaphragm. Another two-bar compressed air was connected to the external boost port of the wastegate to increase the opening pressure to 3.7 bar gauge in total.

The temperatures of the system were measured from several locations via K-type and T-type thermocouples. A thermocouple was a temperature sensor with two kinds of dissimilar metals joined at the tip of the probe. A voltage was generated according to the change of the surrounding temperature. The voltage change was captured by the NI temperature module and converted to temperature. T-type thermocouples were used to measure temperatures of the intake tank and the intake port, while K-type thermocouples were utilized at the exhaust manifold, in the exhaust surge tank and across the EGR cooler. If the maximum measured temperature was lower than 200°C, the T-type thermocouple was recommended, otherwise K-type was recommended to be used.

3.4 Diesel Fuel Delivery System

A diesel fuel delivery system was assembled by the author to supply the diesel fuel to the high pressure common rail pump equipped on the Ford Puma engine. As shown in Figure 3-4, a daily ten-liter fuel tank was used to store the diesel fuel. A full tank of fuel was enough for one experiment of about two hours. Every time before the engine experiment, this tank was to be checked and refilled with diesel if necessary. The fuel flow from the tank was measured by a fuel flow detector (FP-2140H) and a meter (FP-210A), manufactured by Ono Sokki. Due to the resistance of the fuel supply line, a Delphi fuel pump was utilized to guarantee that a sufficient fuel flow was supplied to the engine. The fuel returning from the engine was directed to the downstream of the flow meter, passing through a heat exchanger. In this way, the measurement of the flow meter was the absolute engine fuel consumption. Two fuel filters were used to remove the particles in the fuel and also acted as the fuel reservoirs to damp out the fuel pressure waves generated by the pumping action. An ON/OFF valve was installed before the pump while a needle valve was installed bypass the pump. The fuel supply pressure could be regulated by adjusting the needle valve. The fuel temperatures across the engine were measured and monitored by a Labview program. If any of the temperatures were over the limit, an alarm was triggered.

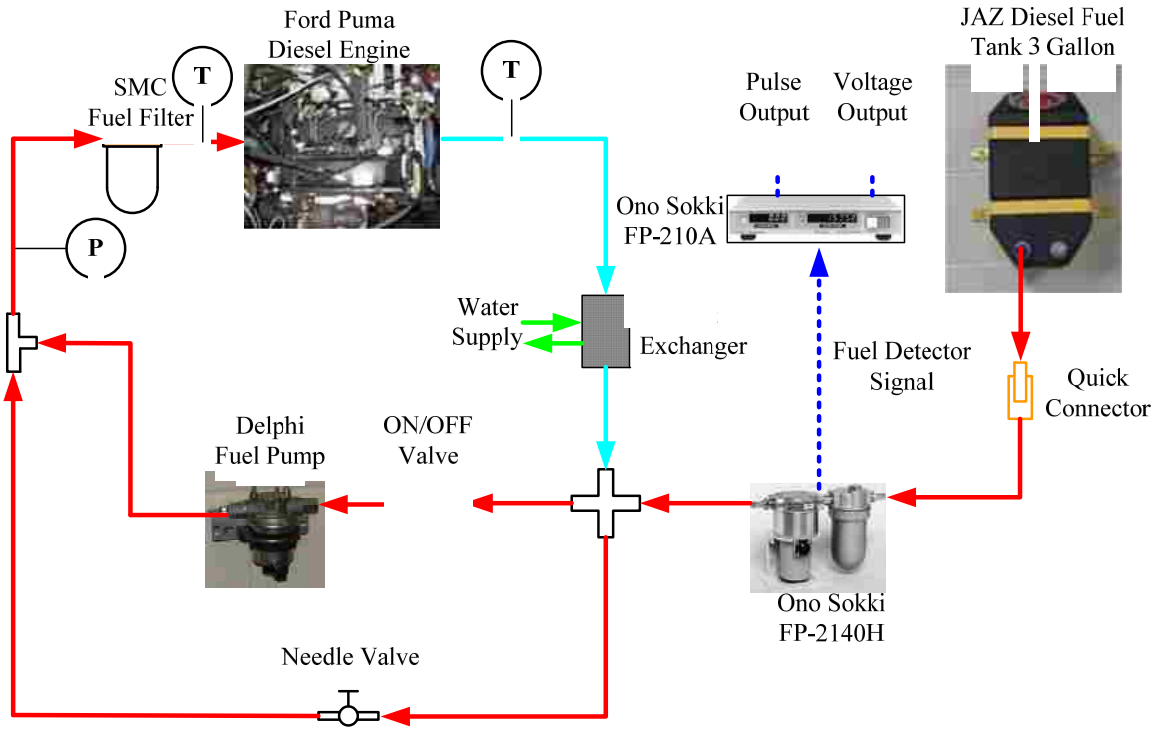

Figure 3-4 Diesel Fuel Supply System of Ford Puma Engine

The specifications of the fuel flow measurement system are demonstrated in Table 3-3. The FP-2140H fuel flow detector could detect the fuel flow in the range from 0.3 L/h to 120 L/h, which was relatively too high to detect the low load fuel consumptions in the single cylinder platform. However, in this prepared platform, the diesel fuel was supplied to all four cylinders and the detector was good enough to measure the fuel flow. The fuel returning from the engine could be hotter than 65°C when the engine was running at high loads. Therefore, a heat exchanger with a sufficient water flow was utilized to cool the fuel. The fuel flow meter FP- 210A was shared with the other engine test platform. The sensor selection and factor were to be changed during the change-over. Sensor "7" and factor "8982" were set to the fuel flow meter when the meter was connected to the FP-2140H fuel detector. The pulse output from the meter was connected to an NI DAQ card and the number of pulses was counted via a Labview program. The voltage output was connected to the NI temperature module and the total fuel flow was also monitored.

Table 3-3 Specifications of Fuel Flow Detector and Flow Meter [37]

FP-2140H	
Function	Flow Detector
Measurement Parameter	Flow Rate
Applicable Fluids	Gasoline/Light Oil/Petroleum Oils
Measurement Range	0.3-120.0 liter/hour
Accuracy	< ± 0.2% of the reading
Min. Resolution	0.1 ml
Max. Pressure	980 kPa
Temperature	0-65 °C
FP-210A	
Function	On-board Flow Meter
Measurement Parameter	Instantaneous Flow Rate
	Cumulative Flow Rate
Voltage Output	0-10V to 0-100 liter/hour
Pulse Output	0.1 ml/pulse
Power Requirement	11-15V DC @ 4VA
Temperature	0-50 °C

3.5 Diesel Fuel Pressure Control

The diesel fuel injection system on the prepared engine platform was a common rail injection system. The peak injection pressure of that system could be 1600 bar. The system consisted of a high pressure diesel pump, a fuel rail and four solenoid diesel injectors. The high pressure fuel was generated by the high pressure fuel pump, stored in the fuel rail, and injected into the cylinder when the injector was opened by the opening current supplied to the solenoid valve.

The fuel pressure was typically controlled via a PCV (Pressure-control Valve) and/or a VCV (Volume-control Valve) on the high pressure fuel pump by regulating the high pressure fuel amount leaking to low pressure fuel storage. In the prepared platform, there was only one PCV equipped on the fuel pump. A motor driver VNH2SP30 was used to drive the PCV. The schematic of the driving circuit is demonstrated in Figure 3-5. Basically the driver worked as a current amplifier which amplified the commanded PWM (Pulse Width Modulation) signal to drive the PCV. The PWM was generated from an NI

real time controller under the control of an in-house developed Labview program. The control channels of IN_A, EN_A, and EN_B were set to logic true by connecting them to +5 VDC while IN_B was set to logic false by connecting it to ground (GND). This configuration enabled the clockwise operation mode on the PCV [38].

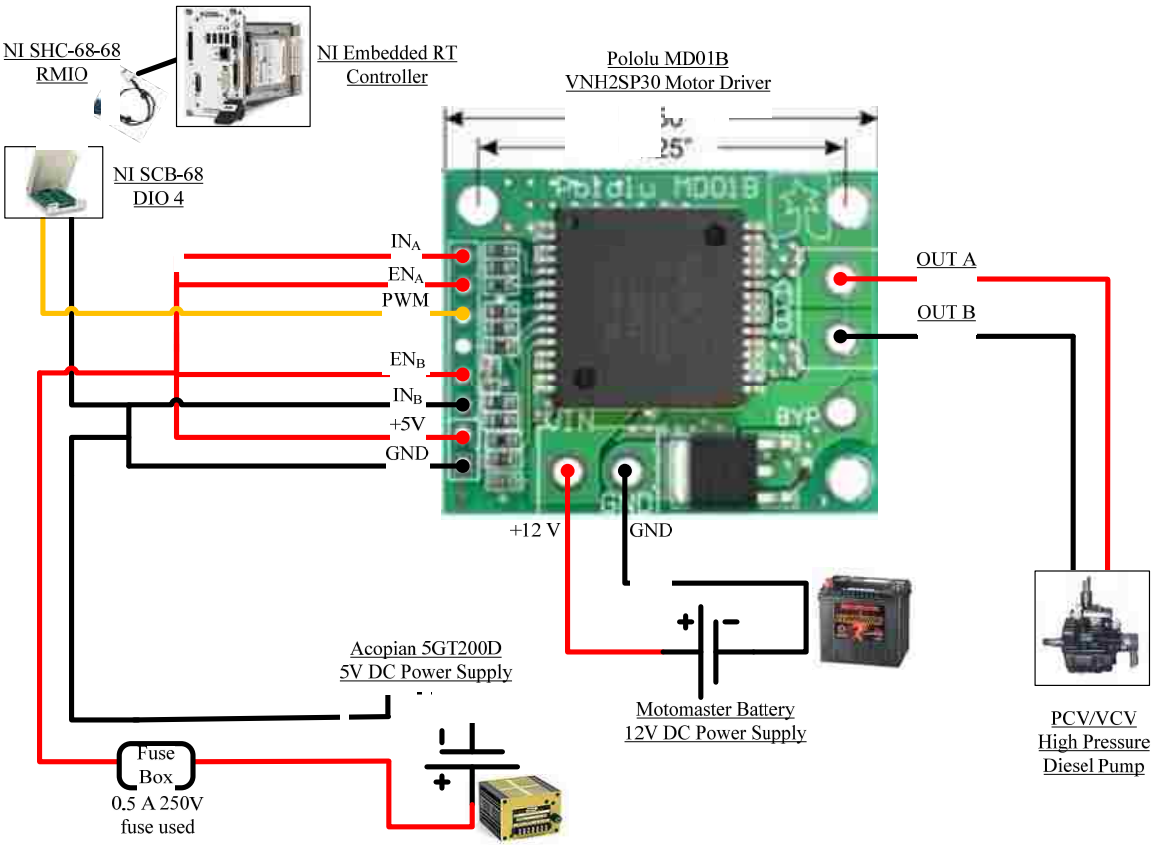

Figure 3-5 Diagram of PCV Control System

The specification of the driver VNH2SP30 was illustrated in Table 3-4. One of the most important parameters was the maximum PWM frequency, which differentiate this driver from the low-cost driver version VNH3SP30 with 10 kHz frequency. A low cost driver was also tested by the author in CDEL and the results indicated it could not respond as fast as the fuel pressure control required. Therefore, the VNH2SP30 was finally employed in this application. All the main components of the entire fuel pressure control system are illustrated in Table 3-5. All the parts were possible to be changed and the parts listed were tested to be working successfully.

Table 3-4 Specification of Driver VNH2SP30 [38]

Motor driver:	VNH2SP30
Motor channels:	1
Minimum operating voltage:	5.5 V
Maximum operating voltage:	16 V
Continuous output current per channel:	14 A
Peak output current per channel:	30 A
Maximum PWM frequency:	20 kHz
Reverse voltage protection?	Yes
Logic level compatible inputs:	5 V
Undervoltage or overvoltage shutdown?	Yes

Table 3-5 Parts List of Entire Fuel Pressure Control System

	Component	Part Number	Description and Function
H-bridge	Motor Driver	VNH2SP30	H-bridge main circuit
	Breadboard	922306-ND	The board supporting the system
	Encloser	377-1541-ND	The container for the breadboard and circuit
Control system	Computer	N/A	The host for the pressure control command
	Realtime controllor	NI PXI-8110	The FPGA modual for TTL generation
	Terminal box	NI SCB-68	Signal input and command output terminals
	Communication cable	NI SHC-68-68 RMIO	Communication between terminal box and FPGA
Power supply	5V power supply	5GT-200D	Power supply to the motor driver
	12V battery	10-3501-6	Power supply to the PCV

CHAPTER IV

IMPLEMENTATION OF PORT FUEL INJECTION

4.1 Port Fuel Injection Introduction

The technique of port fuel injection (PFI) is applied to deliver a fuel into the intake manifold near the intake port. A minimum of one injector is installed on the manifold. The fuel can be injected at any time from the start of the intake stroke, which provides abundant time for air and fuel mixing. The homogeneity of the air fuel mixture is improved by the extended mixing time. The premixed homogeneous mixture was desirable for the lean combustion strategies which can simultaneously suppress the production of NOx and smoke.

Compared to direct injection (DI), PFI requires lower fuel injection pressure thus no high pressure pumps are necessary, which simplifies the whole fuel delivery system. The fuel is injected into the manifold instead of the cylinder, which reduces the difficulty and complexity of the engine modification. In the PFI system, the fuel preparation process starts inside the intake manifold. This provides sufficient time to fully homogenize the air fuel mixture. However, because the fuel of a PFI system is injected outside the cylinder, it is difficult to determine the in-cylinder fuel amount for each cycle and it can lead to false calculation of the in-cylinder air fuel ratio. Meanwhile, due to more cold surfaces of the intake manifold, intake valve bodies and cylinder wall, the fuel impingement is more severe for the PFI system, thus the emissions of THC and CO can be dramatically increased and the efficiency might be penalized.

The introduction of another kind of fuel into the cylinder can be an effective breakthrough for both emission control and engine efficiency improvement. The desired fuel properties can be achieved by the combination of different fuels. The PFI system in this thesis was prepared for the application of a secondary higher volatile alcohol fuel, such as ethanol and butanol (the primary fuel was diesel ignited by compression ignition). The main purpose was to study the engine emissions and performance of using alcohol

fuel(s) ignited by diesel pilot injection and to explore the benefits and limitations of such applications.

4.2 PFI System

The PFI system was prepared by the author in CDEL. The entire system could be divided into three parts: fuel storage and supply, power supply and safety, and injection adaptation and control. Figure 4-1 demonstrates the schematic diagram of the whole PFI system. This was a completely independent and portable fuel delivery and injection system. Fuel was pressurized by an inline fuel pump, regulated by a mechanical fuel regulator and injected into the engine intake manifold through a Ford injector driven by an LM1949 injector driver. The fuel pressure relief and remote power cut-off for the fuel pump and injection were also integrated in the system.

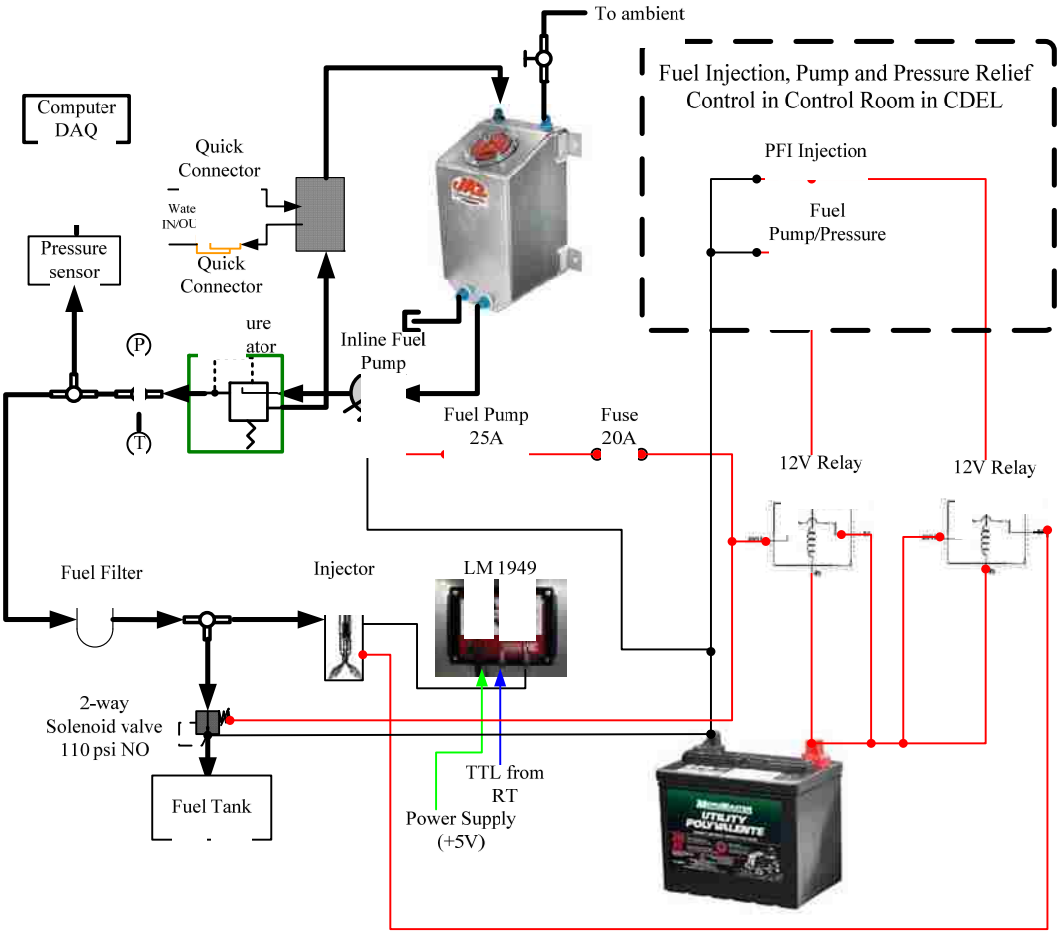

Figure 4-1 Schematic of Entire PFI System

4.2.1 Fuel Storage and Supply

The fuel storage and supply system were built on a portable stand with wheels, as shown in Figure 4-2. It was possible to move the whole PFI system to other engine platforms or test facilities to run a secondary fuel injection. It included a ten-liter fuel tank, a fuel pump, a regulator, a filter, a pressure sensor, a pressure gauge, a thermocouple, a solenoid valve and two quick connections to the injection adapter.

Figure 4-2 PFI Fuel Supply System on Portable Stand

The fuel pump used in this setup was a Walbro GSL392 inline external fuel pump. The flow rates of the fuel pump at different pressures are graphed in Figure 4-3. As highlighted, the typical operating pressure was set at 60 psi, of which the maximum flow rate was around 3.2 L/min at 12 VDC power supply. This flow rate was more than twenty times of the fuel injection to the research cylinder. Therefore, sufficient fuel flow can be supplied by the pump at a stable fuel pressure. The excess fuel flow was bypassed via a

regulator back to the fuel tank. The continuous fuel flow protected the pump from overheating. Both the inlet and outlet of the pump were M10mm x 1.0 female threads. In this setup, these threads were adapted to 1/8 NPT (national pipe thread) threads.

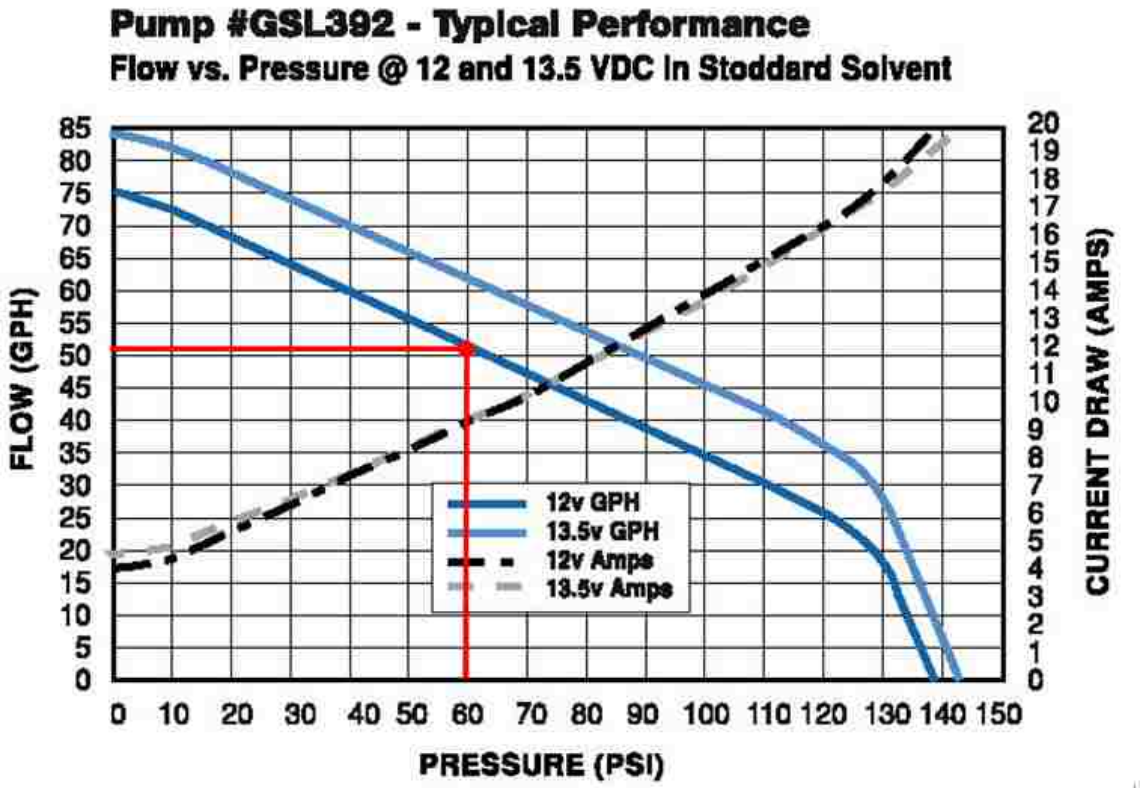

Figure 4-3 Inline Fuel Pump Flow Rate VS Pressure Curve [39]

The fuel in the PFI system was regulated by a mechanical fuel regulator Mallory 4305M installed at the downstream of the fuel pump. This regulator was a return type regulator with an adjustable pressure range from 207 kPa to 690 kPa. The fuel pressure could be adjusted by turning the setting screw on top of the regulator. The fuel pressure was completely controlled by the regulator, and the pressure fluctuations in the fuel line were partially compensated by the spring inside the regulator. The fuel pressures were stable at both ends of the pump. The fuel flow through the pump was also guaranteed, which could extend the life of the pump [40].

4.2.2 Power Supply and Safety

The fuel pump required a twelve VDC power supply with a current up to twenty Ampere. The power was supplied from an automotive battery. A 20A fuse and a 25A ON/OFF automotive switch were connected in the loop of the power supply to the fuel pump. A 12VDC relay was employed to remotely start the fuel pump inside the control room. The power to the fuel pump was also connected to a two-way fuel pressure relief solenoid valve. The valve was a normal-open (NO) valve, which became closed when it was energized. In this system, the valve became closed when the pump was on and opened when the pump was off to release the residual pressure. The injector power was also from the same battery and powered independently through another relay and a switch inside the control room.

4.2.3 Injection Adaptation and Control

A fuel injector was installed on the intake manifold with an adapter designed and fabricated by the author, as shown in Figure 4-4. Two quick connectors were utilized, one (blue) for the fuel supply and another (red) for the pressure relief. Based on the prepared installation, the fuel spray was perpendicular to the air flow into the engine.

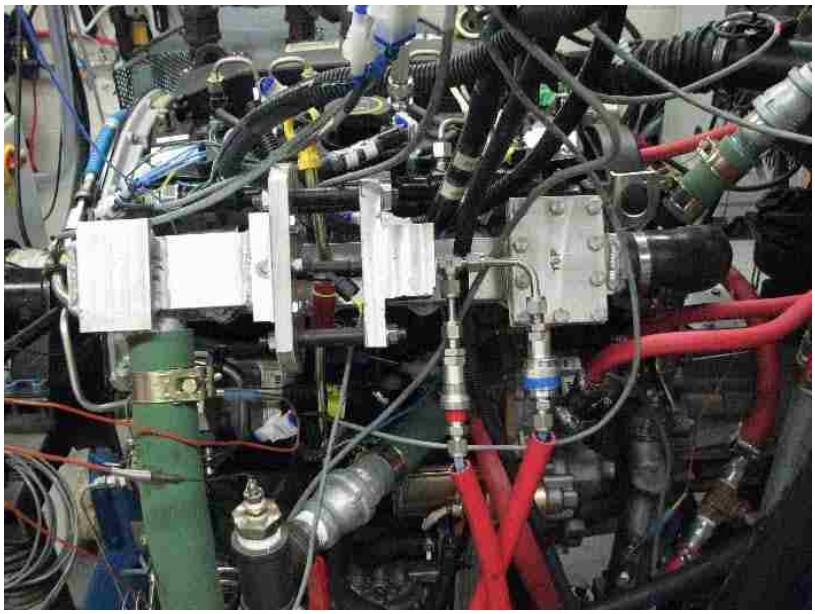

Figure 4-4 PFI Injection Installation on Ford Engine

The injector adapter consisted of a bottom plate, a top block and four spacers made from steel tubes. Ten bolt holes were drilled according to the original dimensions on the manifold as shown in Figure 4-5. The adapter was installed to the manifold without modifying the manifold.

As shown in Figure 4-6, there was a volume chamber inside the top block before the injector. The volume of the chamber was about 0.03 liters and it was in the range of 500~1000 times of the fuel injections each cycle. That volume was sufficient to be a reservoir to damp out the pressure waves caused by the fuel injections.

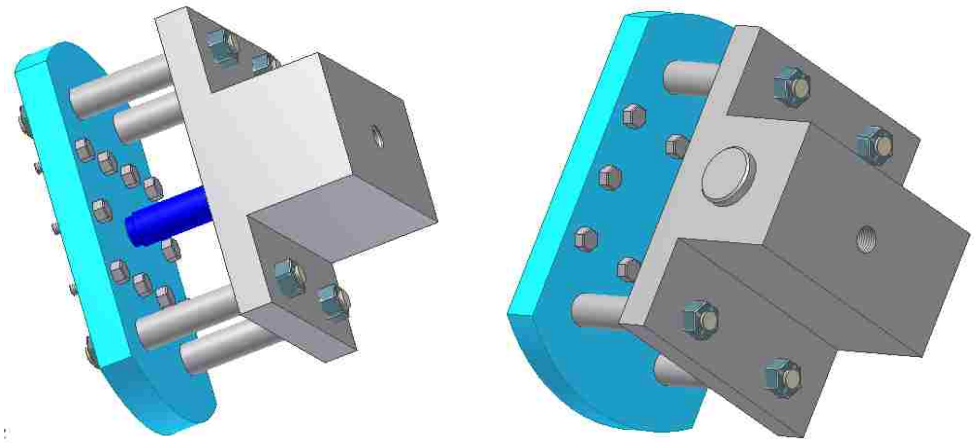

Figure 4-5 Three-Dimensional Assembly of PFI Injection Adapter

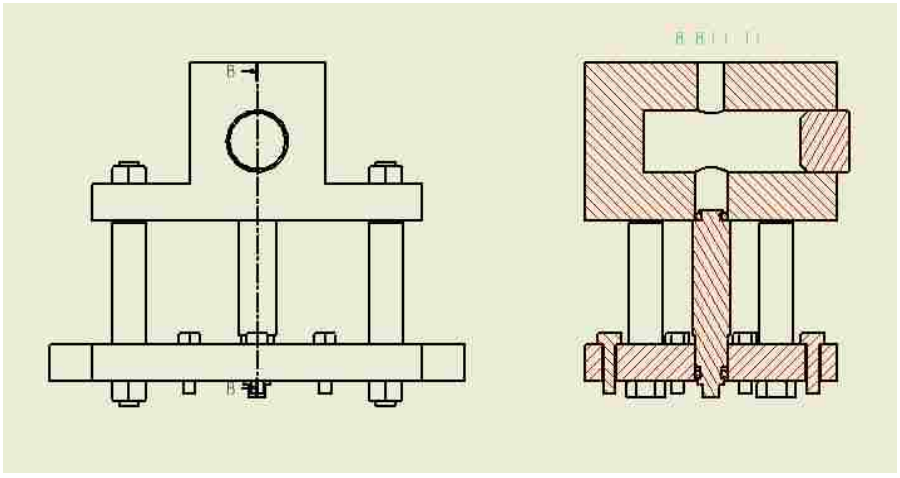

Figure 4-6 Section View of PFI Injection Adapter

The injector used in this setup was a Ford gasoline injector. The driver used was a LM1949 injector controller. As shown in Figure 4-7, a circuit based on the [41] was prepared. The driver worked as a high current switch connecting to the GND according to the injection command. When the other end of the injector was connected to GND, the injection current passed through the solenoid inside the injector and generated the force to lift the injector needle. Then the fuel came out of the injector. When the current was cut off, the spring inside the injector pushed the needle to close the injector.

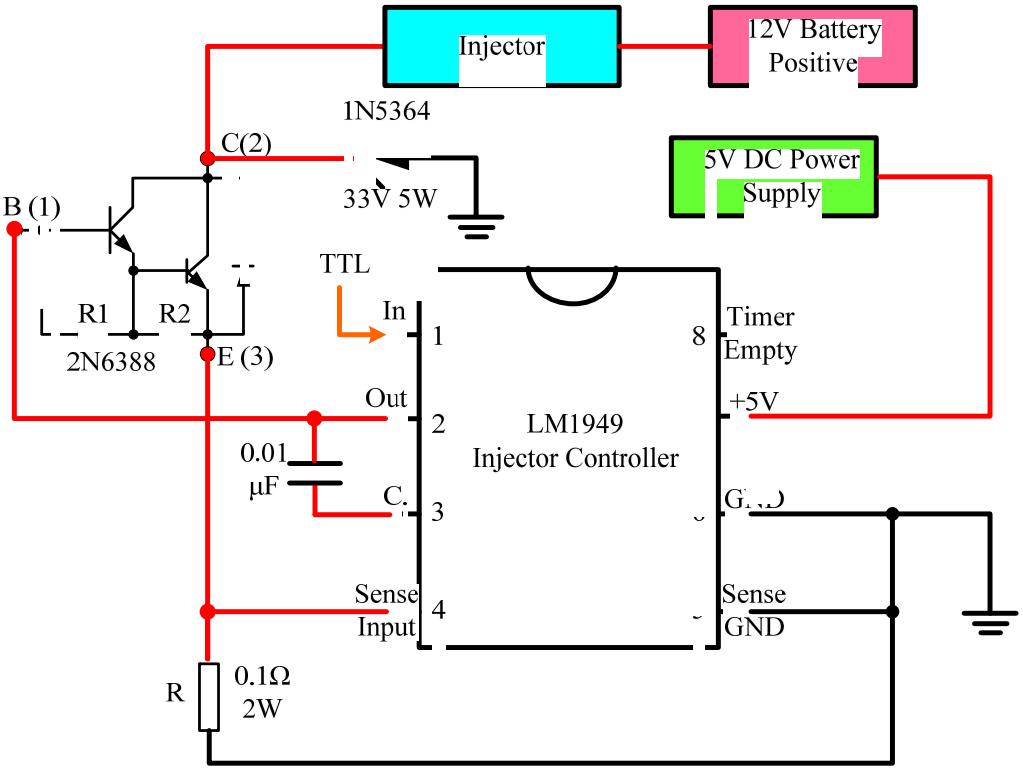

Figure 4-7 Injector Control Circuit Diagram [41]

Table 4-1 summarizes the major components of the injection control system. The photo of the physical box was shown in Figure 4-8. The injector driver required a five VDC power supply. A BNC connector was connected to the solenoid injector and another BNC connector was connected to the TTL signal output from a real time controller dedicated for the PFI fuel injection control.

Table 4-1 Components Summary of Injection Control System

	Component	Part Number	Description and Function
Injector driver	Injector Driver	LM1949N	Main controller
	Breadboard	922306-ND	The board supporting the system
	Capacitor	0.01 μF	Connect Pin2 and Pin3
	Transistor	2N6388	High current control
	Resistor	0.1Ω, 2W	
	Zener diode	1N5364-33V, 5W	Voltage safety
	Encloser	377-1541-ND	The container for the breadboard and circuit

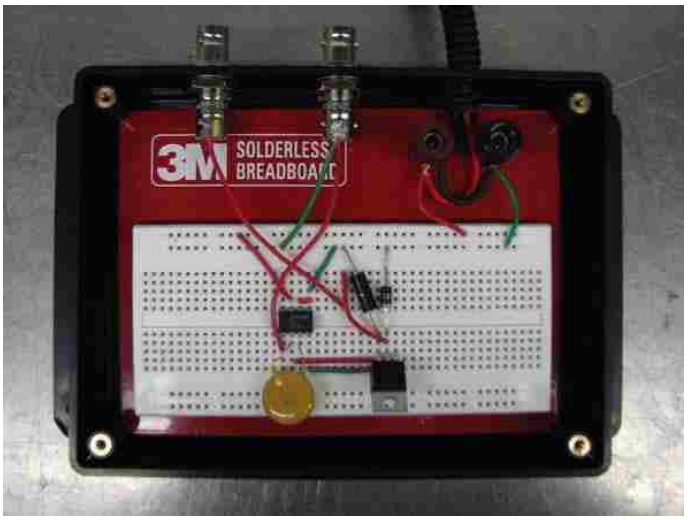

Figure 4-8 Photo of Injection Control Box

4.3 Safety Consideration

4.3.1 Corrosion

All the common biofuels, due to the nature of fuel properties and the production process, have corrosion issues, especially the targeted fuel of this thesis: ethanol. The concern of corrosion by a fuel grade ethanol has been raised by many researchers, vehicle manufacturers and biofuel producers [42~45]. The cause of corrosion could be water content or chloride ions or the solubility of ethanol itself. Ethanol is corrosive to

aluminum, copper and rubber at certain conditions. Therefore, the material selection of the ethanol fuel delivery system has been researched carefully.

In the PFI system made by the author, the fuel delivery tubes were made from either stainless steel or Teflon, which were commonly believed to be highly resistant to ethanol corrosion [46]. The o-rings on the injector, the diaphragm inside the fuel pump and the seals inside the solenoid valve were made from Nitrile [47], which also had excellent corrosion resistance to ethanol [46]. A new Teflon gasket was made for the intake manifold on the Ford Engine. Another new Teflon gasket was made for the injection adapter.

The fuel tank was made from aluminum. Some of the fitting used in this PFI system were made from copper. The water content inside ethanol might oxidize aluminum and copper. However, the thin layer of oxide outside aluminum and copper provided the improved resistance to ethanol for short time storage. Thus, the tank and these fittings can be used for the prepared application but addition attentions needed to be paid to check the system status regularly.

4.3.2 Flammability

The alcohol fuels, especially ethanol, have a higher volatility. The exhaust emissions from the engines burning alcohol fuels normally contain high level of THC. The unburnt THC could go either into the exhaust surge tank, or back into the intake with EGR. The mixture of THC and the fresh air could possibly reach the flame limit of ethanol. As shown in Table 4-2, ethanol and butanol have wider range of flame limit than diesel fuel and the flash points are under room temperature, which increased the risk of explosion.

Table 4-2 Flammability Comparison of Alcohol Fuels and Diesel and Gasoline [48]

Substance	Lower Flame Limit %(Volume)	Higher Flame Limit %(Volume)	Flash Point
Diesel Fuel	0.6	7.5	> 62ºC
Gasoline (100 Octane)	1.4	7.6	< -40ºC
Ethanol	3-3.3	19	12.8ºC
Butanol	1	11	29ºC

In order to avoid the high concentration of THC in the exhaust surge tank and EGR, a diesel oxidation catalyst (DOC) was installed in the exhaust loop to burn the THC and catch the flame in the engine exhaust. A commercial DOC was cut into a diameter of 54mm cylindrical shape and pressed into a stainless steel pipe, as demonstrated in Figure 4-9. The length of the DOC was 154mm and the tube length was 170mm. The volume of the DOC was around 0.35 L. A DOC with the same volume was tested to be effective to remove diesel at one g/s flow rate based on the experiments done in CDEL by another researcher. It was also sufficient for the application of ethanol PFI experiments.

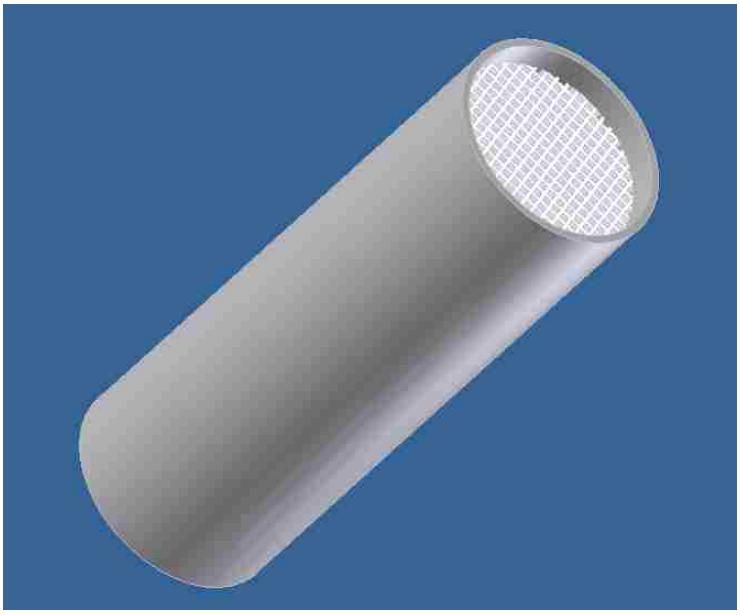

Figure 4-9 CAD Demonstration of DOC Installation

As demonstrated in Figure 4-10, two pipe unions were welded at both ends of the DOC to provide the flexibility for changing or repairing (no need to rework on the whole piece of exhaust pipe). A thermocouple was installed to the center of the DOC to measure the inside temperature. Typically if the temperature was higher than 200°C, the DOC was considered to be activated and it could effectively remove hydrocarbons. The original exhaust pipe and the current exhaust pipe with a DOC are compared in Figure 4-11. They were exactly the same shape with a section of flexible pipe on each. Both of them provided a connection for hot EGR by bypassing the exhaust surge tank. The exhaust emission sampling port for the new exhaust pipe was before the DOC. The measurement of THC was the raw emissions before conversion.

Figure 4-10 Photo of DOC Made by Author

Figure 4-11 Current and Original Exhaust Pipes

4.4 Injector Calibration

The fuel injection utilized in this PFI system was a Ford commercial gasoline injector. All the parameters and calibration curves of that injector were based on gasoline. On the other hand, the in-house developed injection program required the relationship between fuel mass and injection timing. Therefore, an injector calibration was performed with the same fuel delivery system and injector as used for the engine tests. The fuel pressure was

set at 60 psi and the injection frequency was 12.5 Hz to simulate 1500 rpm engine speed. The result is demonstrated in Figure 4-12. A thousand fuel injections at each injection duration from 3.5 ms to 9 ms were conducted. The total fuel was collected in a bottle and weighed on an electronic scale. Each measurement was repeated for three times and the average value was used for calculation and plotting in Figure 4-12. The injected fuel mass followed the injection duration linearly. An assumption of indicated mean effective pressure (IMEP) based on a 40% burning efficiency was calculated for each calibrated fuel point and plotted in the figure too. The IMEP of three bar could be generated from 3.5 ms injection duration, while nine bar IMEP could be produced from injection duration of 9 ms.

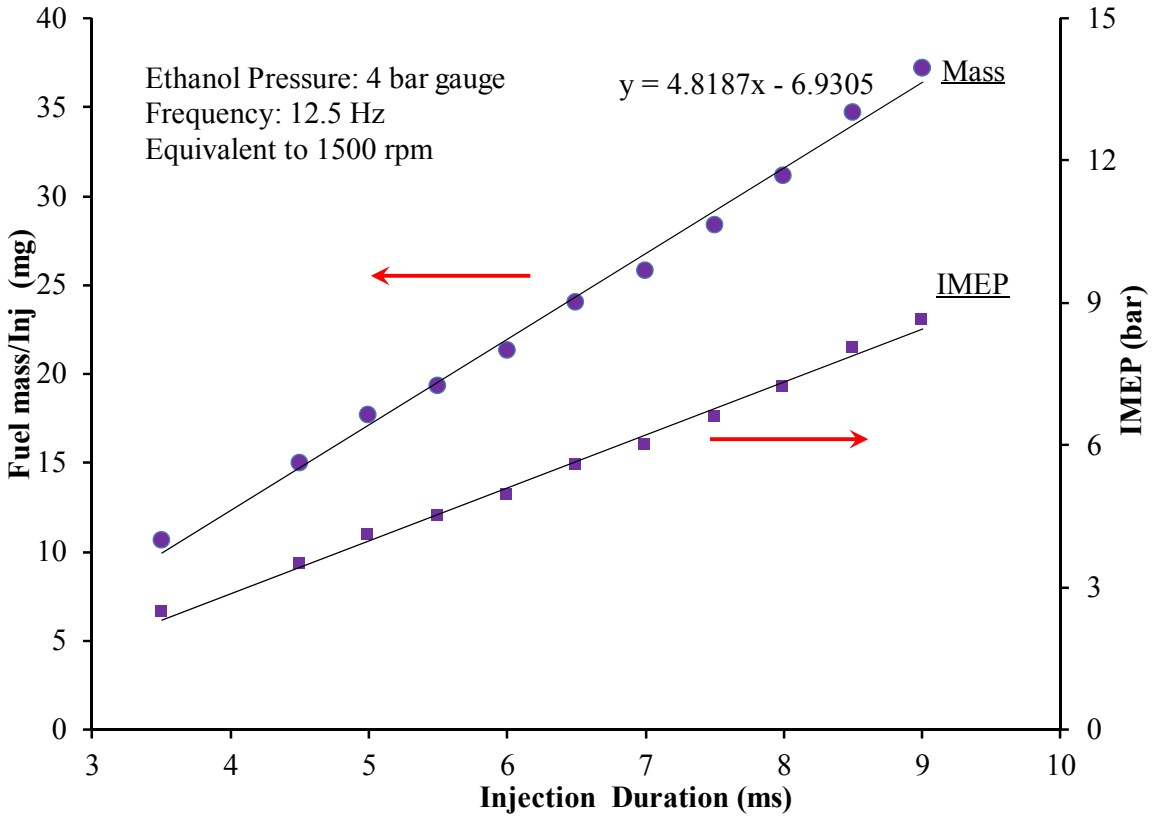

Figure 4-12 Calibration Curve of Ethanol Injection

A high speed camera and an oscilloscope were used to study the injector spray characteristics and opening and closing delays. Figure 4-13 illustrates the plot of injection command, camera trigger and the injection current. Both the injection command and camera trigger signals were generated from an NI FPGA. The square wave of injection

command was sent to the injection driver LM1949 to drive the injector. The camera was triggered by the rising edge of the camera trigger signal and started recording at the same time. The current passing through the injector was also monitored by a current probe and plotted in the figure.

The video frame at the camera trigger can be considered as the injection command starting (50 ns deviation @ 20000 fps). By counting the quantity of frames, the real injection opening and closing were decided and converted back to time. Several videos were taken for injection commanded durations increased from 3 ms to 9 ms. The result of 4 ms injection command is demonstrated in Figure 4-14. From the video, there was around 1.8 ms injection opening delay and 1 ms closing delay for all the tested injection durations. Therefore, the real opening duration was 0.8 ms less than the commanded for all the measured injection durations.

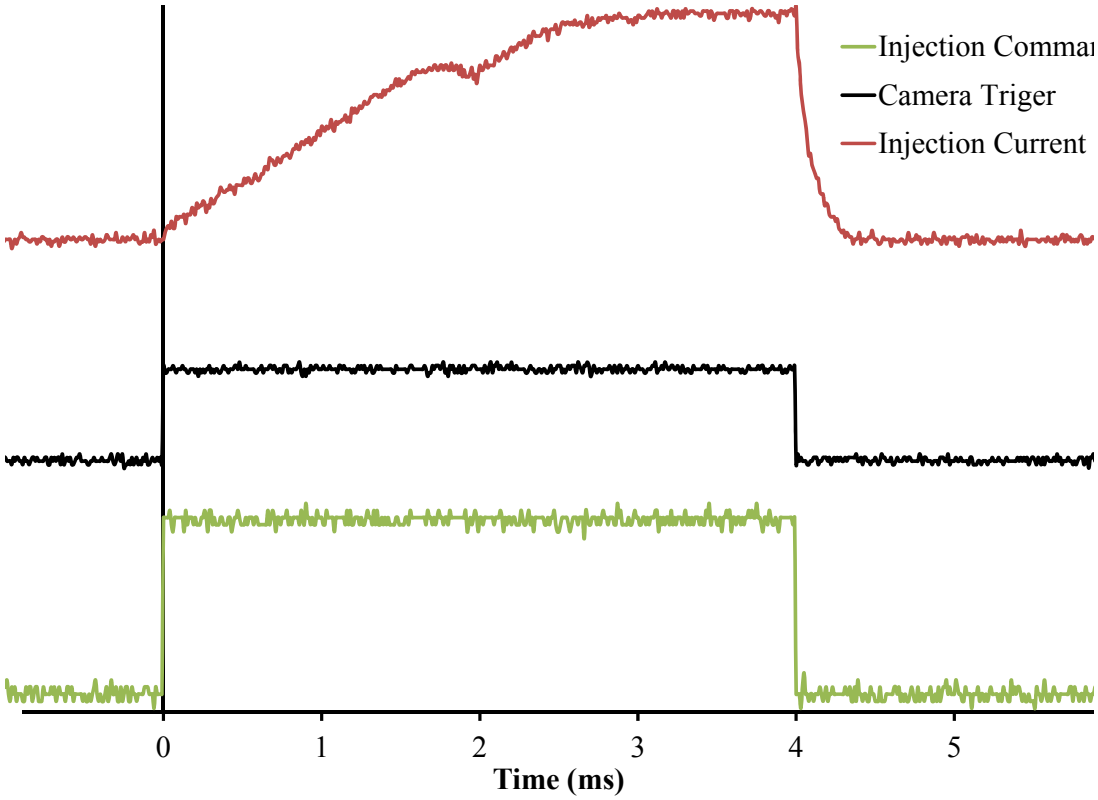

Figure 4-13 Recording of Camera Trigger, Injection Command and Current

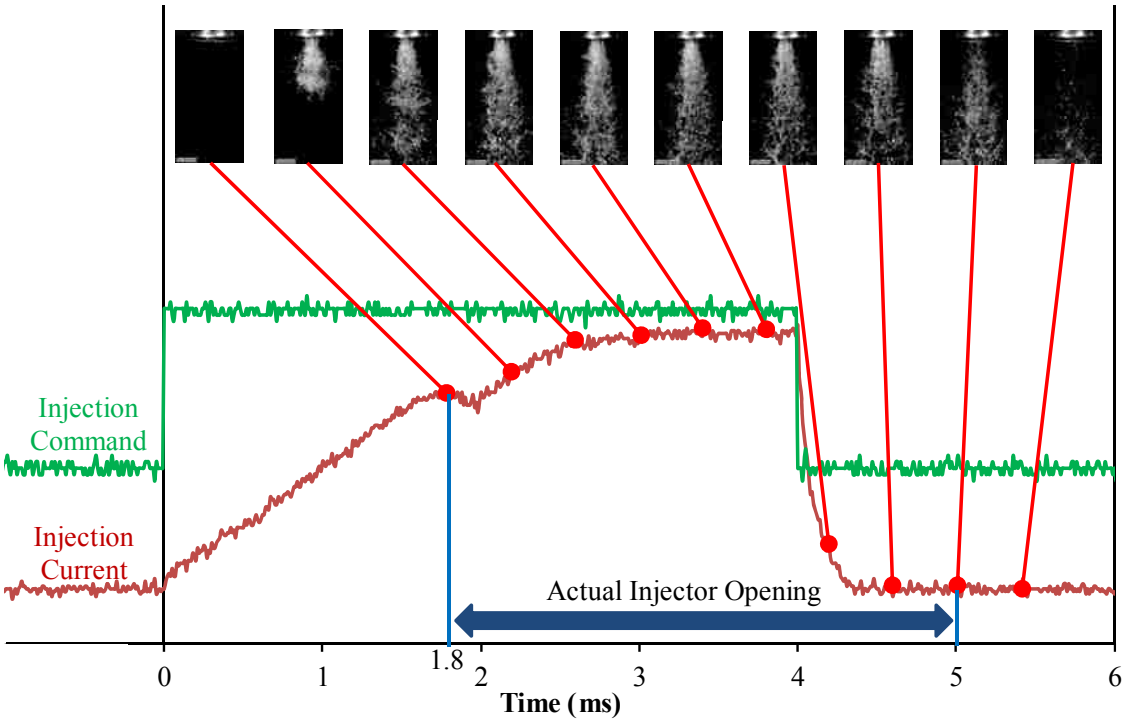

Figure 4-14 Fuel Spray with Injection Current and Command

CHAPTER V

RESULTS AND DISCUSSION

Empirical investigations were performed with both diesel and ethanol in part to verify the newly prepared engine platform, which included exploring the LTC with ethanol PFI. The test matrix is shown in Table 5-1. The test results are analyzed and discussed in this chapter.

Table 5-1 Summary of the Test Matrix

Series	Purpose	rpm	Boost (kPa)	P_{inj} (DI, bar)	IMEP (bar)	Test Content
1	System Verification	1500	50	N/A	N/A	Motoring for Encoder Alignment
2		1500	50	900	6	Diesel Multi-Injection
3		1500	50	900	8	PFI Injection Check
4		1500	50	900	4	Whole Engine Platform Verification
5	Diesel Baseline	1500	50	900	3	SOI Sweep Diesel Low Load Baseline
6		1500	50	900	4	EGR Sweep Diesel Low Load Baseline
7		2400	50	900	4	EGR Sweep Diesel Low Load Baseline
8		1500	75	1500	8	EGR Sweep Diesel Medium Load Baseline
9		1500	100	1500	8	EGR Sweep Diesel Medium Load Baseline
10	Preliminary Ethanol PFI	1500	100	1500	8	Ethanol PFI EGR Sweep D5E3
11		1500	100	1500	8	Ethanol PFI EGR Sweep D3E5
12		1500	100	1500	10	Ethanol PFI EGR Sweep D3E7
13		1500	100	1500	10	Ethanol PFI SOI Sweep D3E7
14		1500	75	900	8	Ethanol Switching-off D1E7

5.1 Platform Verification

Part of the objectives of this thesis was to prepare a whole engine test platform for both diesel and biofuels experiments. The physical setup process was finalized and described in the previous chapters. The conditions of the whole platform need to be verified by different tests. The major verifications and results are discussed in the following sections. The performance of the whole platform was evaluated and the limitations were addressed.

5.1.1 Encoder Alignment

An optical encoder was mounted to the crankshaft of the Ford engine, which produced one digital index and 3600 pulses per revolution. These encoder signals were used for the injection control and the cylinder pressure recording to determine the engine crankshaft rotation angle. Therefore, aligning the encoder index with the engine physical TDC is critical to have the correct engine control and data analysis.

The encoder was aligned to the compression stroke TDC of the first cylinder in the Ford Engine. The recorded motoring curve is demonstrated in Figure 5-1. The compression stroke TDC was well aligned with the encoder TDC (the encoder TDC was set to be 360°CA in the program). No miss-alignment could be observed from the curve. From the record pressure data, the peak cylinder pressure was at 359.7°CA, which was 0.3°CA off from the TDC. Based on the experience from CDEL, this was considered as encoder aligned, and the 0.3°CA off could be compensated by adjusting the program.

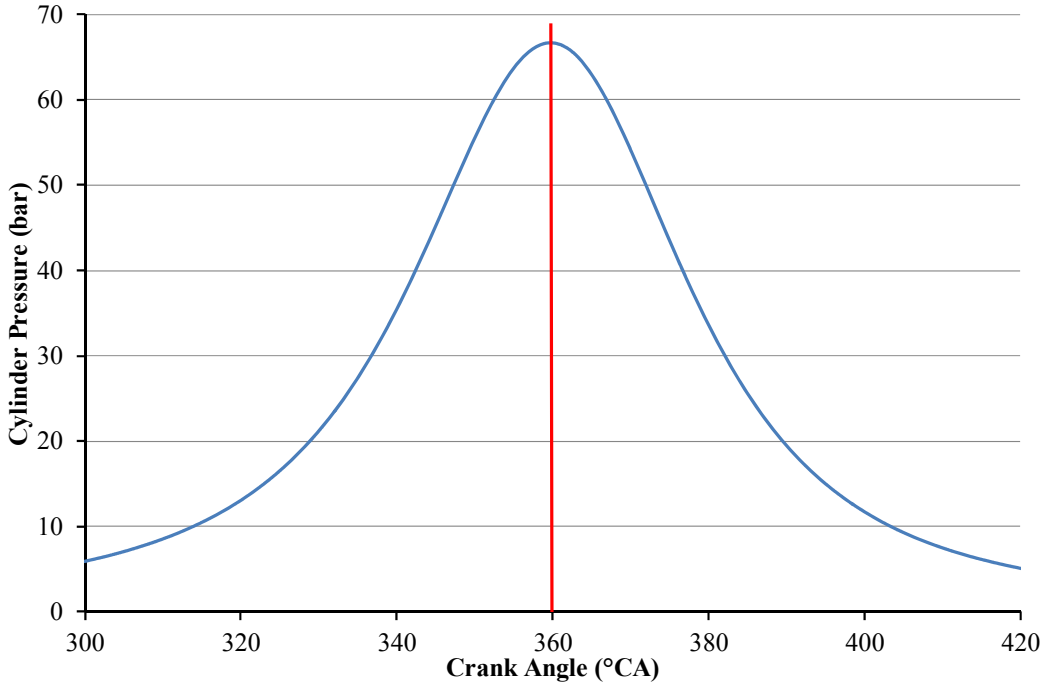

Figure 5-1 Research Cylinder Motoring Curve for Encoder Alignment

5.1.2 Fuel Injection Control

The diesel injection was controlled by a RT with an embedded FPGA. The control programs were developed in-house by CDEL and adapted for the Ford engine platform. As stated in the previous section, the engine compression stroke TDC was aligned with the encoder index. A low CAM signal was produced near the compression stroke TDC from a hall effect CAM sensor on the Ford engine. With these two signals, the compression stroke TDC could be differentiated from the exhaust stroke TDC. All the injection timing controls were based on the compression stroke TDC.

The waveforms of encoder index, CAM, cylinder pressure trace and injection command signal recorded by an oscilloscope is shown in Figure 5-2. It was confirmed that the low CAM signal was at the compression stroke TDC. The injection timings and durations were under the control of the Labview program. Multiple injections could be enabled and controlled. Maximum six injections can be realized with the solenoid injectors on the Ford engine. The response of the cylinder pressure to injection was quick. No time delay could be observed from the recording.

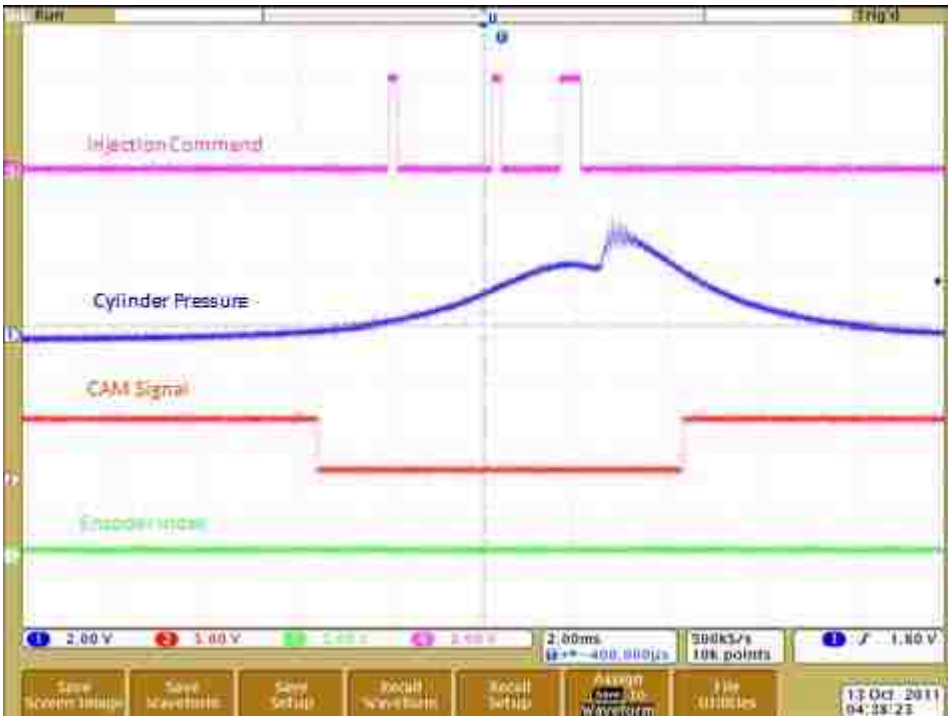

Figure 5-2 Oscilloscope Recording of Multiple Diesel Injections

The PFI injection was controlled independently via another injection control system. The fuel was injected at the start of the intake stroke. In Figure 5-3 the PFI injection timing was 350°CA before the compression stroke TDC. The injection current corresponded with the command. From the waveforms recorded, the control program, the injector driver, and the physical connections between the driver and the injector were verified to be working properly.

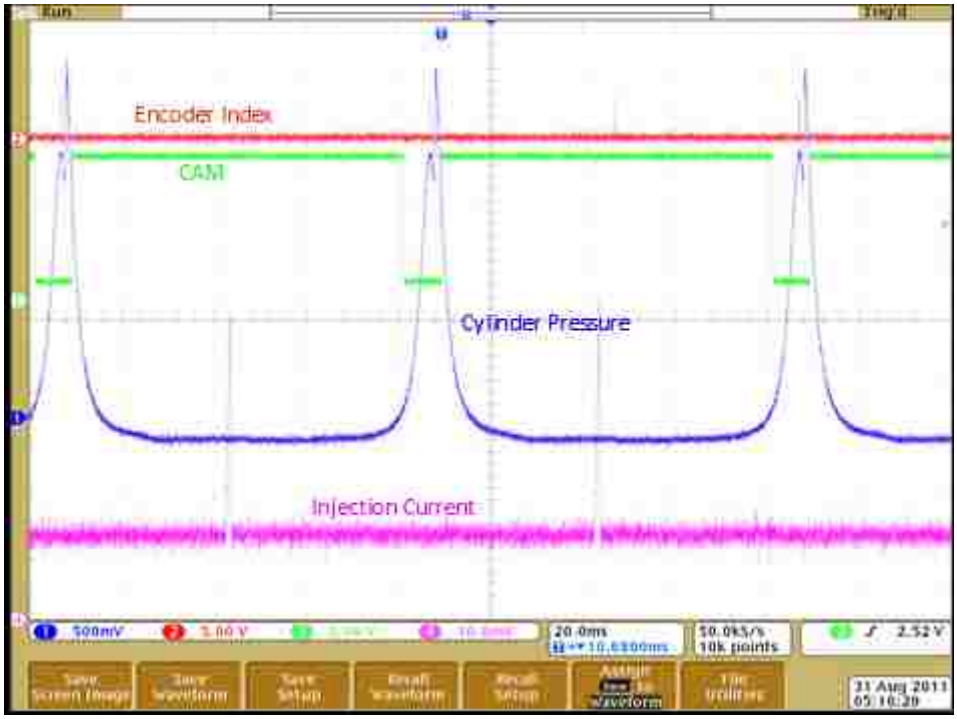

Figure 5-3 Oscilloscope Recording of PFI of Ethanol

5.1.3 Whole Platform Verification

A low load (3.5 bar IMEP) engine experiment with diesel was performed to verify the working conditions of the whole system, including the test of boost and EGR control, emission measurements, temperature measurements and data recording. During the whole test process, the boost was maintained at 1.5 bar (abs). The boost pressure was stable and the small oscillation was comparable with the other engine platform. The EGR was built up via an exhaust backpressure valve by partially blocking the exhaust flow. The EGR

was confirmed to be under the control and was capable to be applied up to 70%. The NOx and smoke measurements were similar to the previous data at a similar condition. The response time to changed conditions was fast. The emission comparisons of experiments conducted on 2011-06-02 and 2007-04-04 is plotted in Figure 5-4. If focused on the shaded area (NOx lower than 100 ppm and smoke lower than 0.5 FSN), both test results overlapped each other, which indicated that the emission measurement setup was at a similar level to the previous one. The temperatures of intake, exhaust, coolant, oil, fuel and others were monitored and recorded properly in the temperature computer. Both the cylinder pressure data and the emission data were correctly recorded.

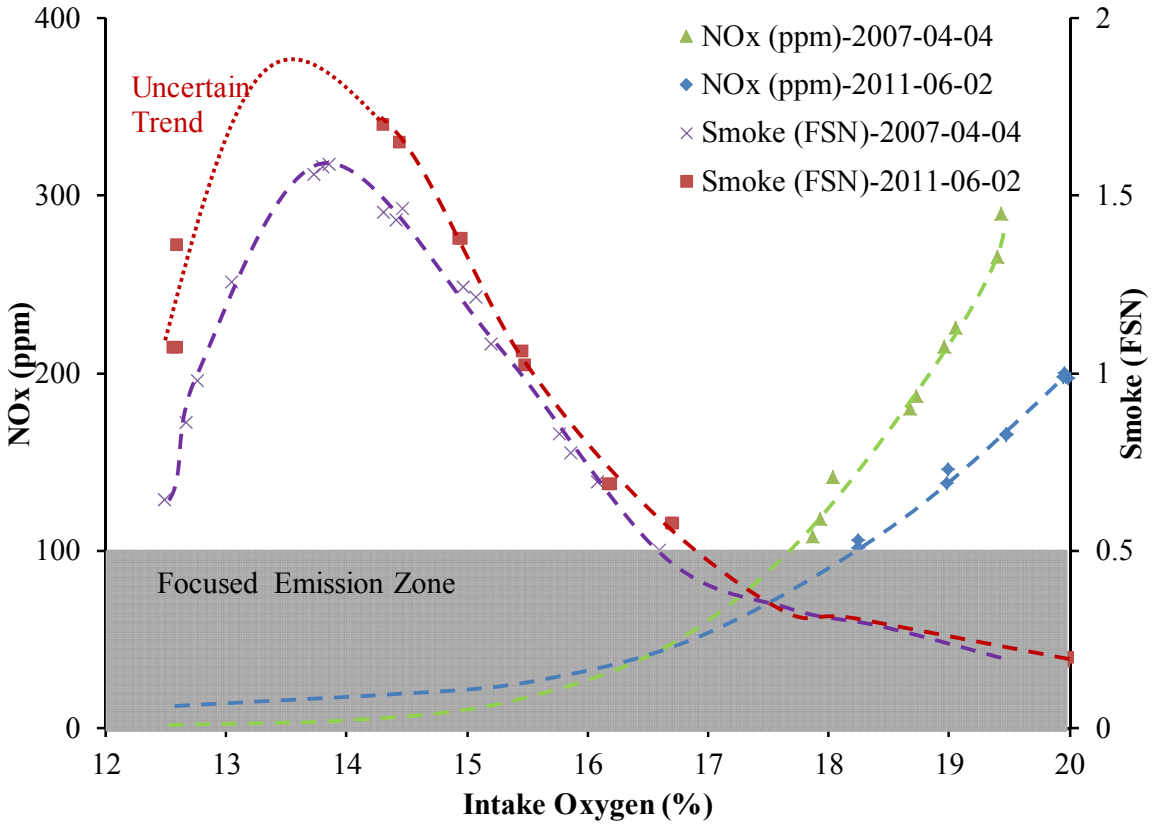

Figure 5-4 NOx and Smoke Emissions Compared with Previous Test

5.2 Diesel Baseline Experiments

A. SOI Sweep at Low Load

A low load engine experiment of SOI sweep was performed on the Ford engine test platform. The engine speed was fixed at 1500 rpm with an intake pressure of 50 kPa (gauge). The fuel injection pressure was set at 900 bar. The injection timing was advanced from 361°CA to 300°CA and retarded from 361°CA to 370°CA. The fuel injection duration was adjusted to produce three bar IMEP at 361°CA and kept constant during the entire SOI sweep. The 200-cycle averaged IMEP and the engine emissions of NOx, smoke, and THC were measured and plotted in Figure 5-5 and Figure 5-6.

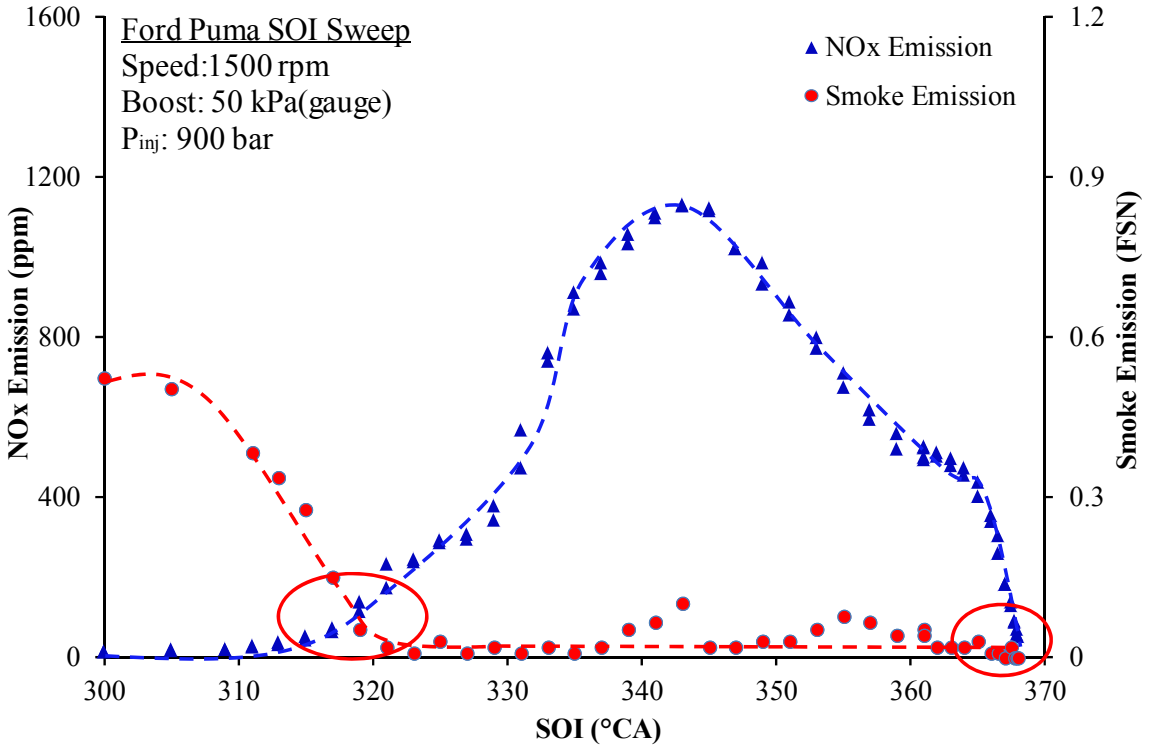

Figure 5-5 NOx and Smoke Emissions of SOI Sweep

The emissions of NOx and smoke are shown in Figure 5-5. The smoke emissions remained around 0.1 FSN until the SOI was advanced to 320°CA and further. This might be because the injection timing was too early. The fuel was sprayed onto the cylinder wall when the piston was near BDC. The smoke emissions might be generated near those regions. The NOx emissions peaked at around SOI 342°CA, which might indicate the

potential highest combustion temperature at that SOI. As circled in Figure 5-5, there were two SOIs with the simultaneously low emissions of NOx and smoke, at around 320°CA and 368 °CA. The indicated THC emissions and IMEP of the research cylinder were plotted in Figure 5-6. The indicated power-based THC emissions were converted from the measured volumetric exhaust THC emissions based on Equation (5-1).

$$e_{ind} = \frac{3600 \times e_{ppm} \times (MAF + m_f) \times M_{emission}}{0.5 \times 60 \times 0.01 \times n \times IMEP \times V_d \times M_{air}} \tag{5-1}$$

Where: e_{ind} : *Indicated emission* [g/kWhr]

e_{ppm} : *Raw emission* [ppm]

MAF : *Air flow* [g/s]

m_f: *Fuel flow* [g/s]

n : *Engine speed* [rev/min]

$IMEP$: [bar]

V_d : *Engine displacement* [m^3]

The IMEP was calculated from Equation (5-2) [34].

$$IMEP = \frac{\int P_{Avg} dV}{V_d} \tag{5-2}$$

The THC emissions were lower than 0.5 g/kWhr, except for the conditions with SOI earlier than 330°CA and later than 365°CA. The THC emissions from early SOIs were because of the incomplete combustion zones from the fuel impingement and the THC emissions from late SOIs were because of the insufficient time to complete the combustion and low in-cylinder temperature. The HCCI and LTC were enabled with a single injection at these SOIs. Therefore, the high THC emissions of HCCI and LTC thus resulting in fuel penalties were the common challenge, which could also be observed

from the IMEP curve in Figure 5-6. The highest IMEP was at the SOI near TDC, of which CA50 (crank angle of 50% heat release) was around 5°CA after top dead center (ATDC). From the study in [49], the efficiency of combustion with CA50 near 5°CA ATDC was higher. The IMEP dropping before TDC was due to the negative work done on the piston and the high THC emissions from unburnt fuel for the very early SOIs. The IMEP penalties for the SOIs after TDC were because of the off phasing and high emissions of THC and CO [50]. The exhaust temperatures of those late SOI points were higher. The energy remained in the exhaust stream reduced the engine efficiency but might benefit the exhaust after-treatment devices by activating the catalysts on them.

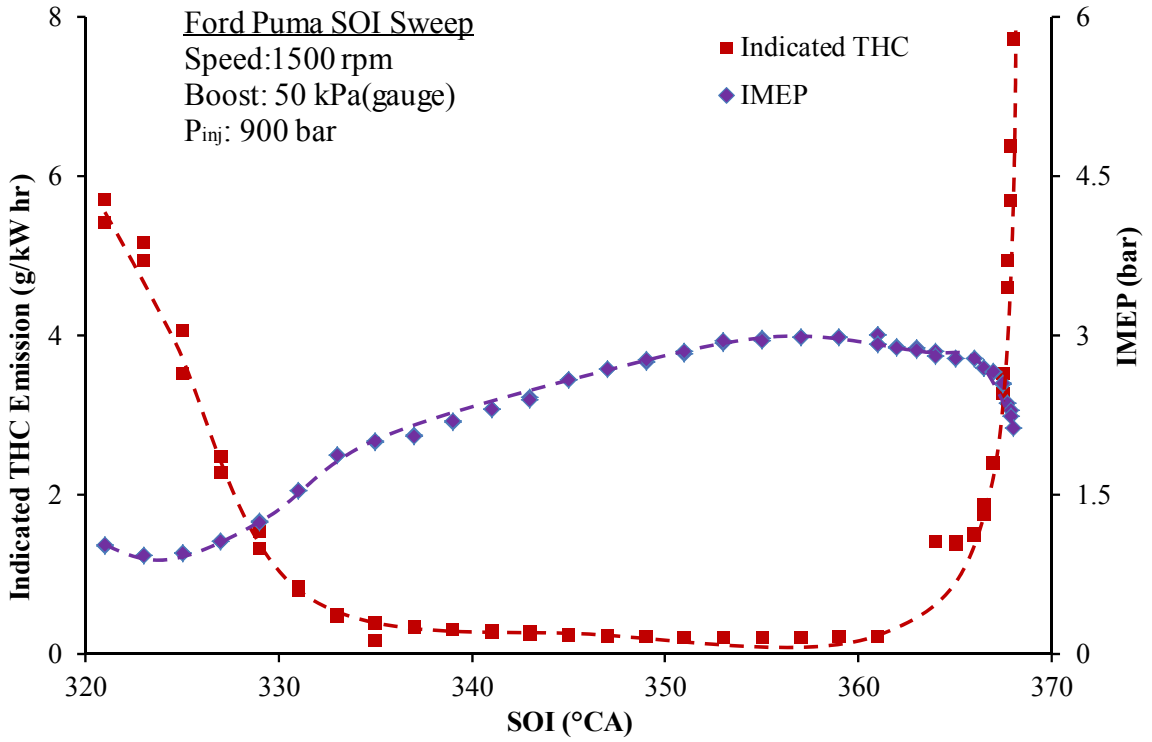

Figure 5-6 Indicated THC Emissions and IMEP of SOI Sweep

B. EGR Sweeps at Low Load

To explore the EGR effect on engine parameters, several low load engine experiments of EGR sweeps were performed on the Ford engine test platform. The engine experiment

plotted in Figure 5-7 was conducted at 1500 rpm with 900 bar single diesel fuel injection. The IMEP was fixed at around 3.5 bar by locking up the injection duration at 440 µs/cycle. The CA50 was maintained at about 367ºCA by adjusting the injection timing commands. The calculated CA50 and injection command timing are plotted in Figure 5-7 and the distance these two curves departing from each other could be an indication of the ignition delay. The high level of EGR increased the heat capacity and diluted the oxygen concentration of the cylinder charge. The auto-ignition of diesel fuel became more difficult and the combustion preparation time was prolonged. It was observed that the injection timing was advanced more the 5 ºCA to maintain a similar CA50 for the EGR over 70%. The longer ignition delay was desirable for diesel LTC. The homogeneity of the cylinder charge with a longer ignition delay was improved and the NOx and smoke emissions were lower compared to those from conventional diesel high temperature combustion.

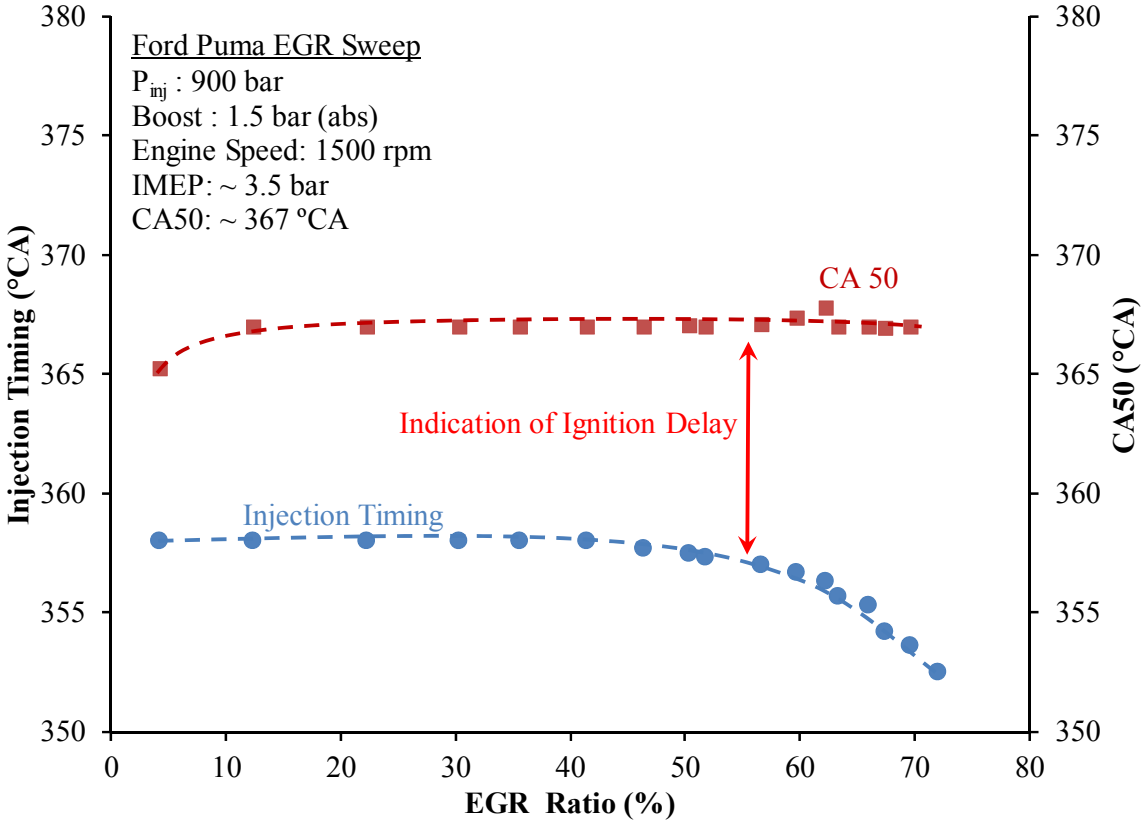

Figure 5-7 EGR Effect on Ignition Delay

Furthermore, two low-load (3.5 bar) EGR sweeps at different engine rotation speeds were done to explore the EGR impact on NOx and smoke emissions. The NOx emissions for both engine speeds followed the same trend, dropping with the increase of EGR and reaching ultra-low level with EGR over 60%. For the smoke emissions, curves for both engine speeds tend to increase with EGR to the peak smoke and falling rapidly to ultra-low level with further increased EGR. The first rising slope of the smoke curve was identified as the HTC slope and the dropping slope was defined as the LTC slope, also called "Slope 2" [51]. When Slope 2 was achieved, the combustion entered LTC. In Figure 5-8, both EGR sweeps reached LTC, because the low engine load required less oxygen and higher level EGR could be applied to push the combustion into LTC. Comparing these two engine speeds, the higher engine speed emitted more smoke at the same level of EGR. The reason might be the absolute time of air fuel mixture preparation was shorter for higher engine rotation speed thus the homogeneity was worse.

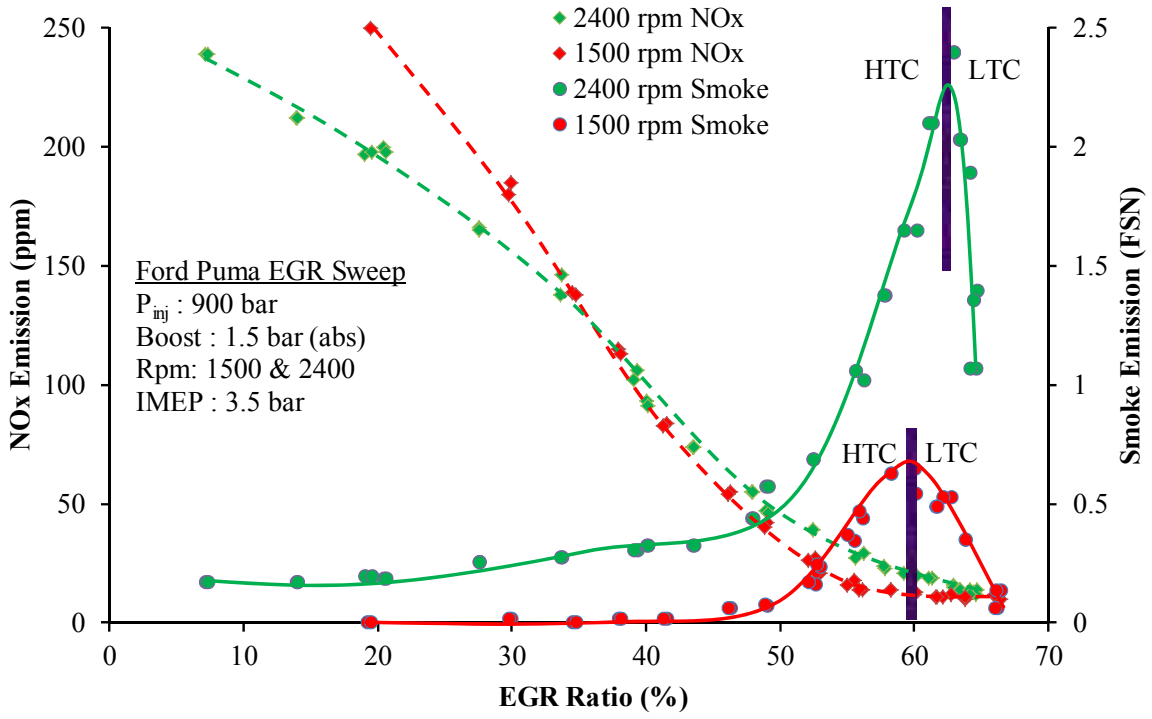

Figure 5-8 EGR Effect on NOx and Smoke Emissions

Two data points with the same injection timing and duration were chosen from the EGR sweeps in Figure 5-8. The cylinder pressure traces and calculated heat release rate (HRR)

are presented in Figure 5-9. The EGR applied at both data points were 20.6% and 54% respectively. Due to the different EGR, the intake oxygen concentration was diluted from 18.8% to 13.2%. The smoke emissions increased about 5 times to 2.6 FSN, while NOx emissions were grounded at 27 ppm. The pressure trace for higher EGR was lower than the other one and the combustion roughness was improved with a smoother pressure curve, thus combustion noise and dp/dθ was also improved. The start of combustion (SOC) was postponed by higher EGR, which can be observed from the HRR curves. The ignition delay with higher EGR was prolonged, thus the air fuel mixture preparation was improved. The overall combustion temperature with higher EGR could be lower, which helped to suppress the production of NOx. The better mixing improved the homogeneity of the cylinder charge and the detonation combustion was less. However, because of the lower oxygen concentration, incomplete combustion produced higher smoke, THC and CO emissions and penalized the fuel efficiency.

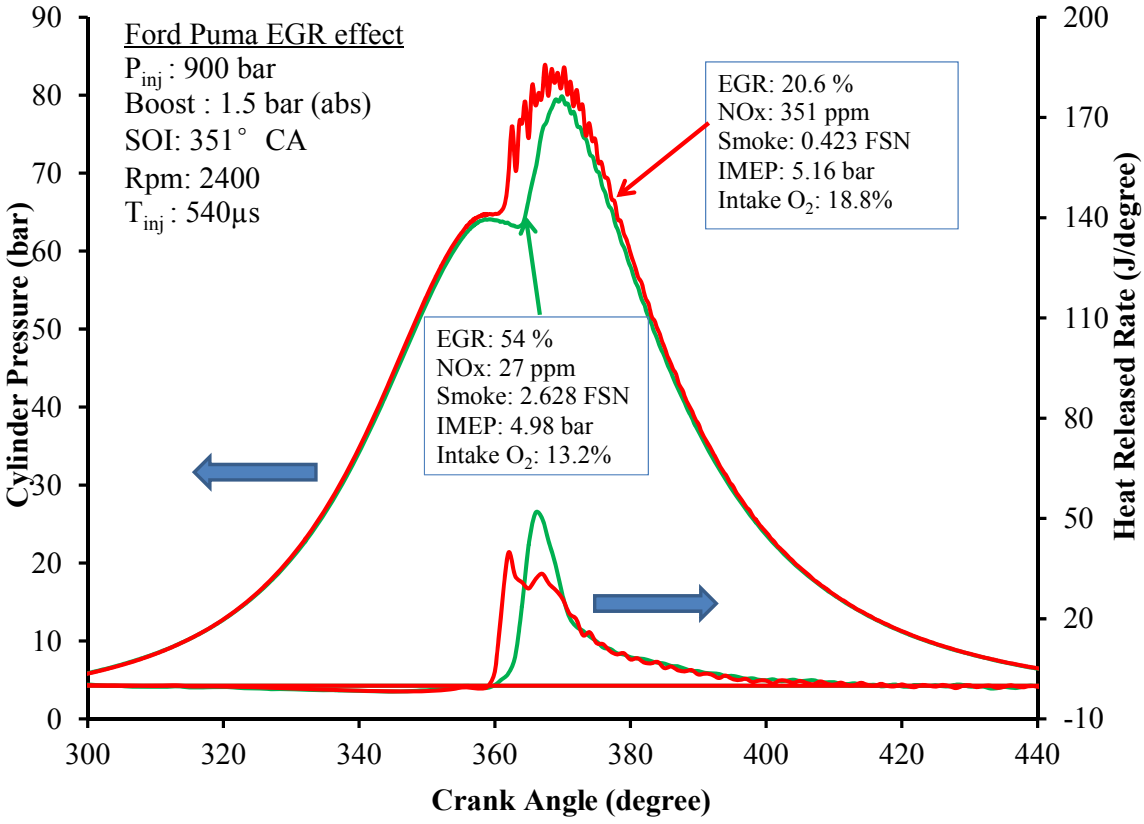

Figure 5-9 EGR Effect on Cylinder Pressure Traces and Heat Release Rate

C. EGR Sweeps at Medium Load

Two medium load data points and one low load data point were selected from the engine tests performed on the Ford engine platform. The EGR applied was similar for all three data points. The cylinder pressure traces and heat release rate curves are plotted in Figure 5-10.

Comparing the HRR curves for medium load and low load, the SOC was earlier for medium load conditions. The cylinder charge preparation time was less and the homogeneity was worse. Thus medium load might produce more NOx and smoke and higher level of EGR might be necessary to improve the homogeneity. On the other hand, high engine load required more oxygen in the intake cylinder charge. This was the trade-off between higher EGR and higher load. This scenario made the operating zone narrower and it was one of the challenges of applying the modern emission control strategies to higher engine loads.

In order to overcome the challenge, increasing the amount of intake oxygen by boosting the intake air was tested and the emission results are shown in Figure 5-10. When the engine load was increased from three bar to eight bar, smoke emissions jumped from 0.065 to 1.379 FSN. This was due to the shorter ignition delay as stated in the previous paragraph. Either higher EGR level to prolong the ignition delay or higher intake boost to make the air fuel ratio leaner was required to suppress the high smoke emissions. In the performed test, a higher boost level of 100 kPa (gauge) was applied and the smoke emissions were reduced by about 20%. However, the smoke emissions were still higher than the US heavy duty truck emission standard. Therefore, a combination of several emission control methods (EGR, fuel injection, and after-treatment technology) was often essential for high engine load conditions to control the emissions and meet the emission requirements. The NOx emissions remained at a similar level for all these three conditions, which might be because of the comparable oxygen concentrations of these conditions.

The energy to boost the intake air was also coming from burning of the fuel. Higher boost consumed more energy thus reducing the overall engine efficiency. High intake pressure also increased the peak cylinder pressure and temperature, which required better material to make the engine body. Those were the limitation from both the fuel cost and the engine production cost, which needed to be balanced with the emission control requirements.

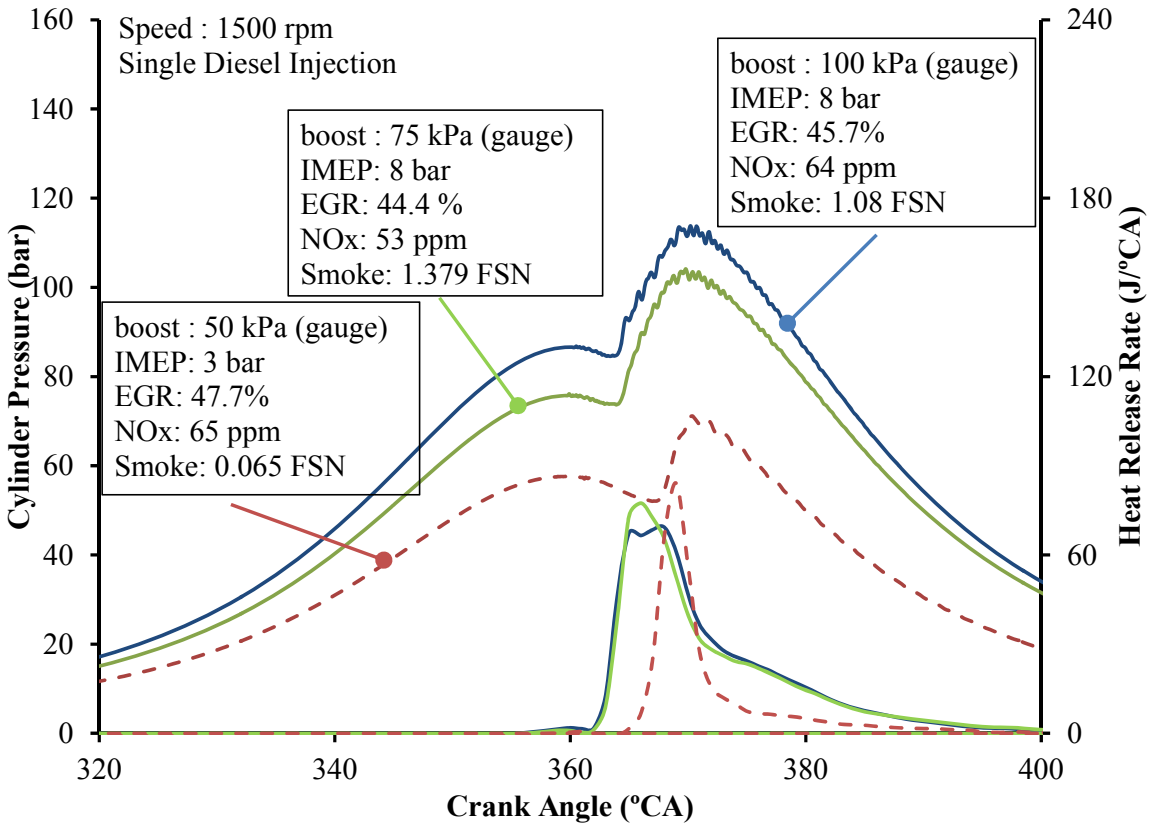

Figure 5-10 Selected Cylinder Pressure Traces and HRR Curves

The emission results of NOx and smoke from two EGR sweeps with different intake boost pressures are shown in Figure 5-11. The raw emissions were converted into the indicated emissions using Equation (5-1). The estimated emission standards for NOx and smoke were shaded in red in the figure. For the EGR sweep at 75 kPa boost pressure, the smoke emissions increased rapidly after intake oxygen concentration became lower than 15%. And it reached 4.75 FSN smoke at 11% intake oxygen and 3% exhaust oxygen. It was decided to stop further increasing the EGR because of the already low exhaust

oxygen. For the engine test at that load, boost and EGR, it could not reach smoke "Slope 2". However, another EGR sweep with increased boost pressure was conducted and the smoke emission reached the peak and then achieved "Slope 2", which was indicated approaching LTC. The smoke emission met the emission requirement together with NOx emission. Comparing the smoke emissions of both curves in Figure 5-11, it was observed that higher boost combustion produced less smoke at the same intake oxygen level. The NOx emissions for both boost levels overlapped each other, which indicated that intake boost pressure might not have direct impact on NOx production.

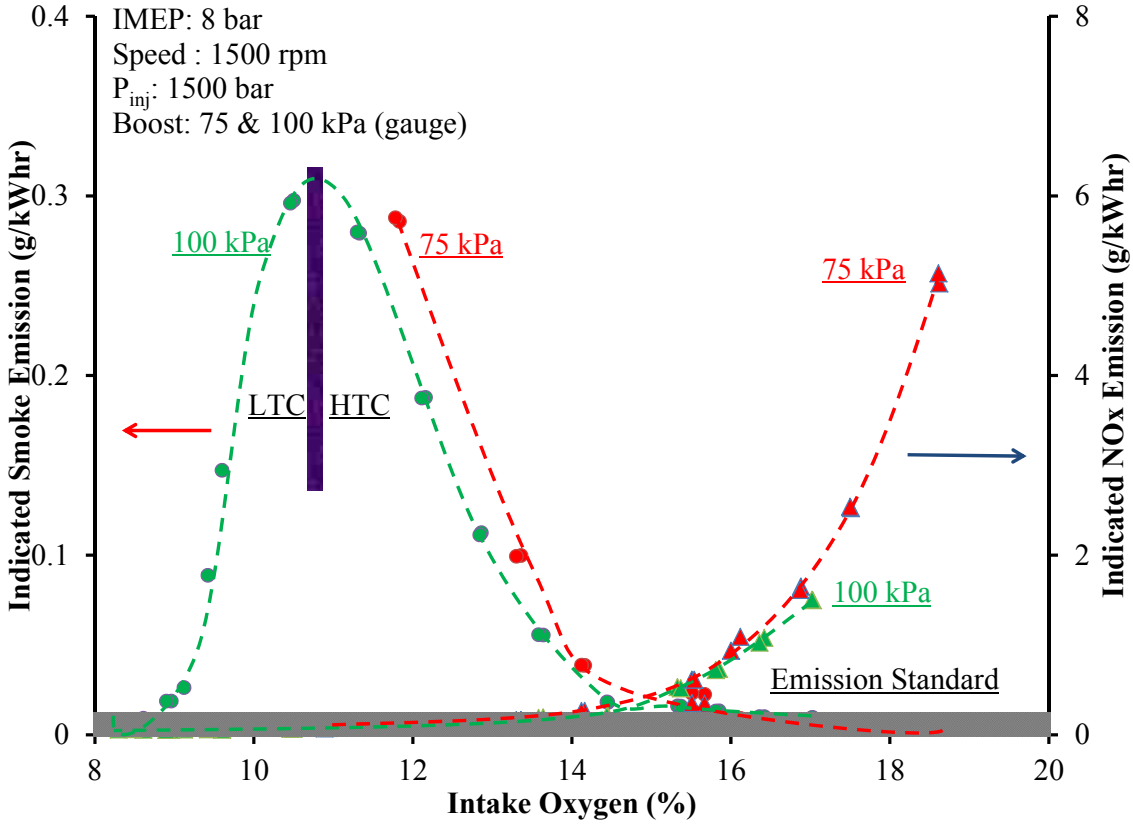

Figure 5-11 Boost and EGR Effect on NOx and Smoke Emissions

The cylinder pressure traces of three data points chosen from the 75 kPa EGR sweep in Figure 5-11 are plotted in Figure 5-12. From the enlarged cylinder pressure traces, it was shown that the peak compression pressure was lower for the higher EGR. The EGR brought high concentration of CO_2 from the exhaust, and increased the heat capacity of the cylinder charge. Thus the peak compression pressure with higher EGR was lower. The peak combustion pressure was also lower and the oscillations on the pressure curve

were less. The reason for that might be the combustion flame temperature in the high EGR case was lower and the combustion occurred slower. Thus the overall in-cylinder temperature was lower, which helped reduce the NOx production. THC could not be burned completely under the lower flame temperature. Therefore, more THC emissions and CO emissions were generated from high EGR combustion.

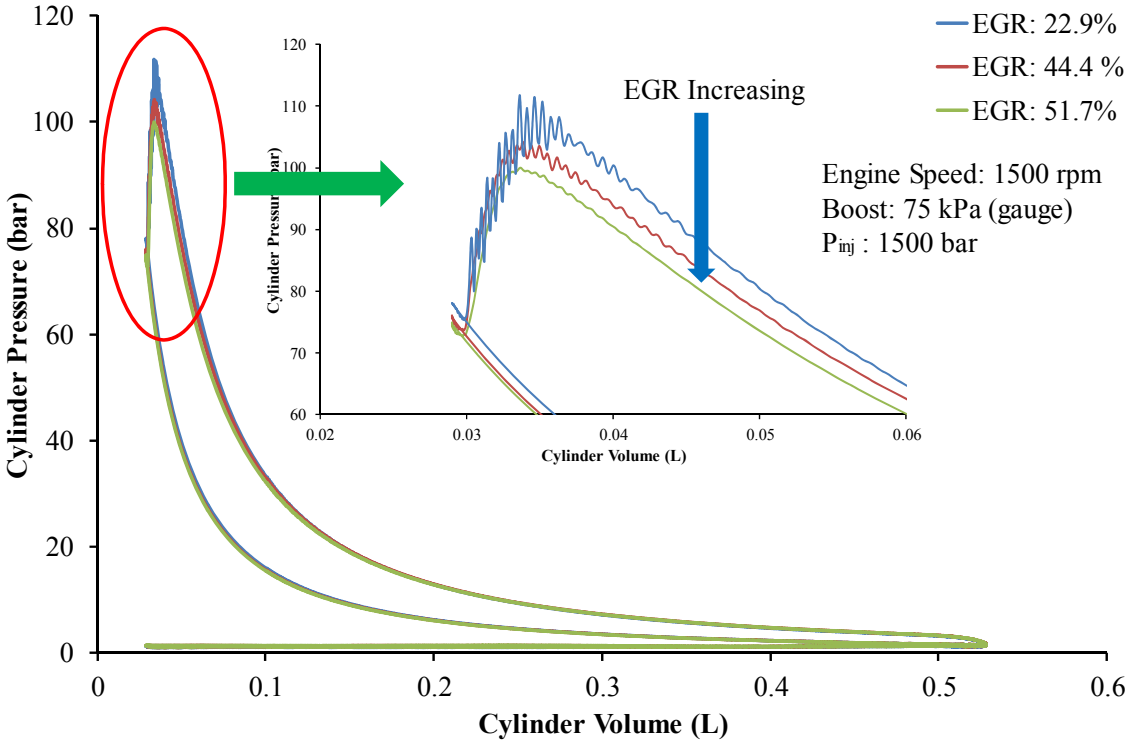

Figure 5-12 EGR Effect on Cylinder Pressure Curves

5.3 PFI Preliminary Tests

Several preliminary engine experiments were conducted on the Ford engine platform with diesel (DI) and ethanol (PFI). Diesel fuel was injected directly into the cylinder via a common rail high pressure injection system, while ethanol was injected into the intake manifold with a portable PFI system. The ethanol used in the experiments was the absolute anhydrous ethanol. The properties of the ethanol fuel are illustrated in Table 5-2.

Table 5-2 Properties of Anhydrous Ethanol in PFI Tests [52]

Name	Anhydrous Ethanol
Formula	CH_3-CH_2-OH
CAS Number	64-17-5
Flame Limit % V/V	3.3-19
Auto-Ignition point °C	422
Molecular Weight	46.07
Boiling Point, ºC @ 760mm Hg	78.3
Freezing Point, ºC	-114.1
Density, kg/L @ 20ºC	0.7883
Coefficient of Water/Oil Distribution	Separates from oil
Miscibility in Water	Complete
% Volatiles by Volume	100

The cylinder pressure of every engine cycle was measured by an in-cylinder piezoelectric pressure transducer and recorded in a computer. The exhaust emissions were measured by the dual bank CAI gas analyzers and an AVL smoke meter. The fuel injection parameters, intake boost and EGR were varied independently throughout the entire experiments to explore the impact on the performance with ethanol fuel. The selected experimental results and analysis were discussed in the following paragraphs.

An EGR sweep with diesel and another EGR sweep with diesel and ethanol were performed on the Ford engine platform. During the whole experiment, the intake boost was kept at one bar (gauge) and the diesel fuel injection pressure was maintained at 1500 bar. The combined IMEP remained at 8 bar. The indicated NOx and smoke emissions of both EGR sweeps are shown in Figure 5-13. The red line in the figure was the US heavy duty truck 2010 emission regulation for both NOx and smoke. For the diesel-only engine test, the NOx emissions dropped with the increased EGR. Smoke emissions reached Slope 2 when intake oxygen was lower than 11%, and met the emission standard at around 9% intake oxygen. For the ethanol PFI test, the smoke emissions remained ultra-low over the entire EGR sweep, under the emission standard. With the EGR increasing, the NOx emissions for ethanol PFI reached the emission standard with 15% intake oxygen. Therefore, the simultaneously ultra-low NOx and smoke emissions were achieved by the utilization of ethanol PFI rather than heavy EGR.

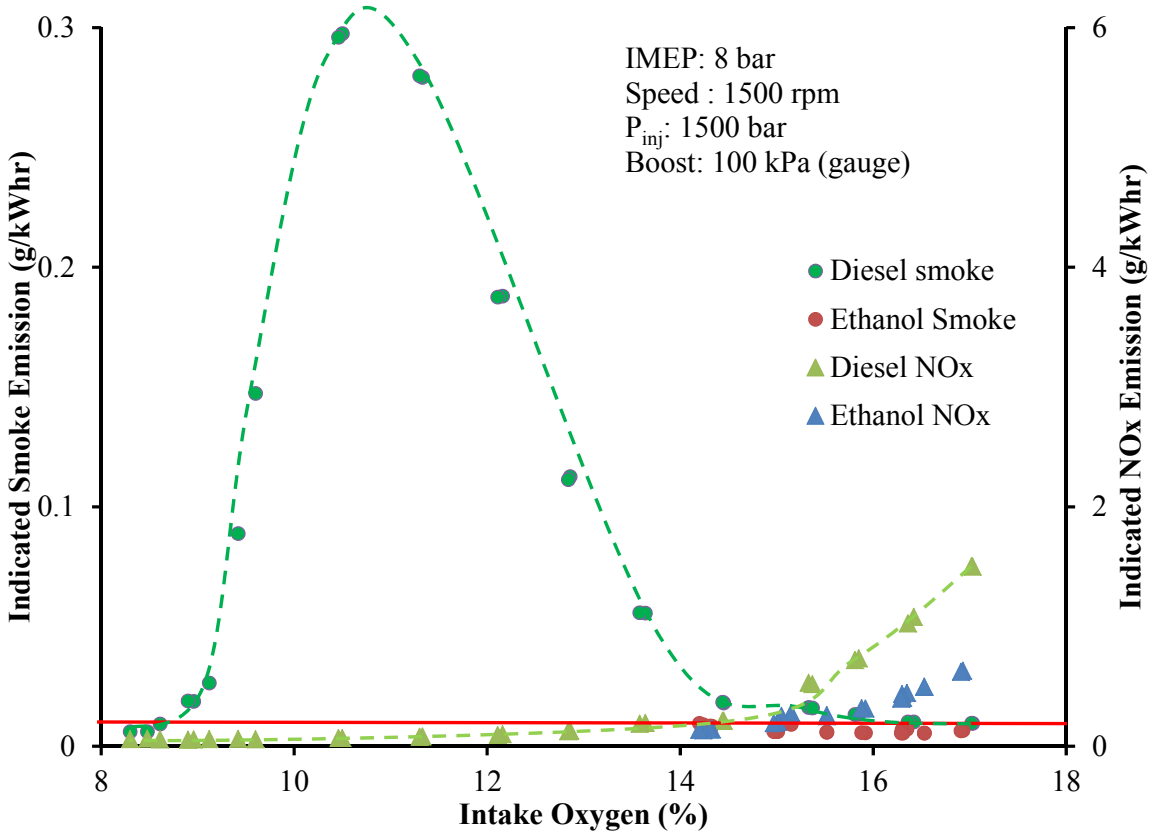

Figure 5-13 Ethanol Impact on NOx and Smoke Emissions

The engine experiments shown in Figure 5-13 indicated that the smoke emissions from combustion with ethanol could meet the emission standard across the tested EGR sweep. Therefore, the smoke emissions were not an issue for current load with ethanol PFI. The methodology of reducing NOx emission became critical. More tests were conducted to explore the effect of ethanol on NOx production, and the results are demonstrated in Figure 5-14 and Figure 5-15.

The indicated NOx emissions with different EGR levels are shown in Figure 5-14. In the legend of Figure 5-14 “100_D3E5” and “100_D3E7” stand for “three bar IMEP from diesel and five bar IMEP from ethanol at 100 kPa boost” and “three bar IMEP from diesel and seven bar IMEP from ethanol at 100 kPa boost”. In the experiment, the diesel injection remained constant and the injection timing was adjusted slightly to maintain the combustion phasing. The use of EGR was effective in suppressing NOx production for

both EGR sweeps. The NOx emissions dropped with the increased EGR. The ethanol injection amount was increased thus the IMEP contributed from ethanol was increased from five bar to seven bar and the combined IMEP was increased from 8 bar to 10 bar. Normally for the conventional diesel combustion, NOx emissions were increasing with load, because of the higher combustion temperature for higher loads. However, this barrier was overcome by the utilization of the secondary ethanol fuel. As shown in Figure 5-14, the NOx emissions (green curve) were lower for the increased IMEP. Thus the NOx emission standard was achieved easily (~40% EGR) for higher engine loads. Therefore the engine load could be extended to higher level without much penalty in NOx emissions with the use of ethanol.

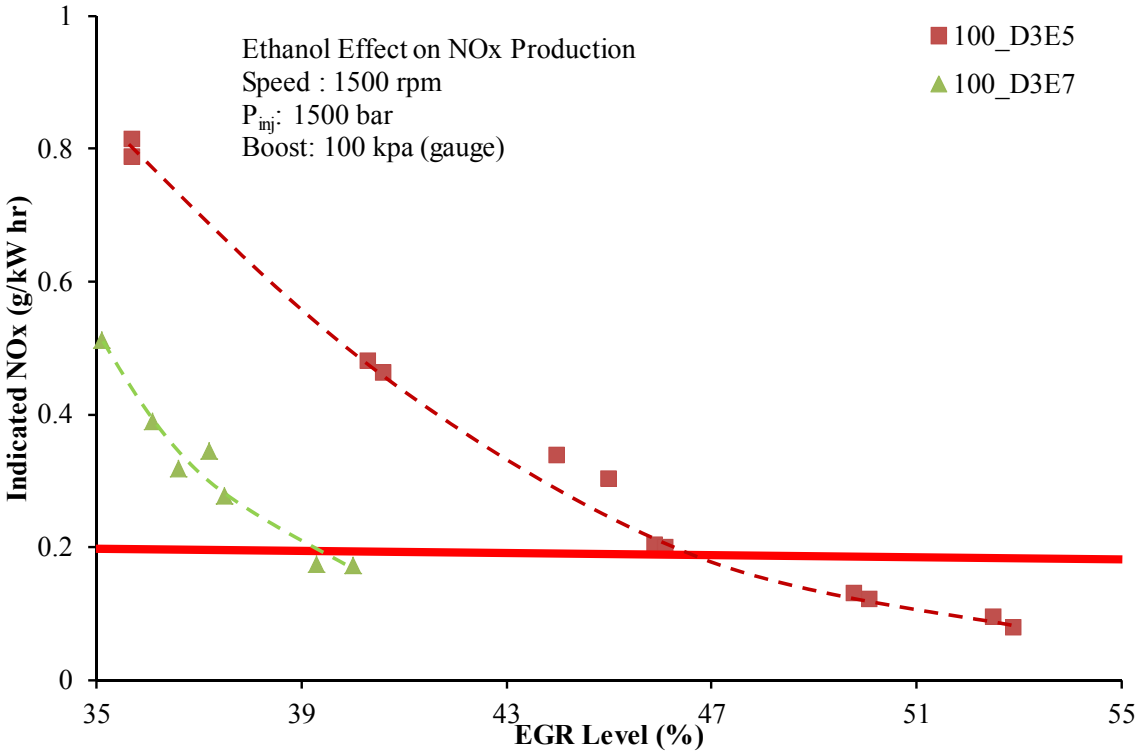

Figure 5-14 Ethanol Ratio Effect on NOx Production with Same Diesel Injection

Another test was performed with a combined eight bar IMEP. The NOx productions of two cases (D3E5 and D5E3) are plotted in Figure 5-15. D3E5 and D5E3 represented three bar IMEP from diesel plus five bar IMEP from ethanol and reversely. It was observed that the NOx production was suppressed by the higher ratio of ethanol. The reason might be the heat absorption of ethanol evaporation to lower down the overall

temperature and higher octane number of ethanol to restrict the fast burning. The benefits of ethanol could be extended by further reducing the ratio of diesel to improve the engine performance and emissions. The possibility of ethanol compression ignition could be evaluated from in future studies.

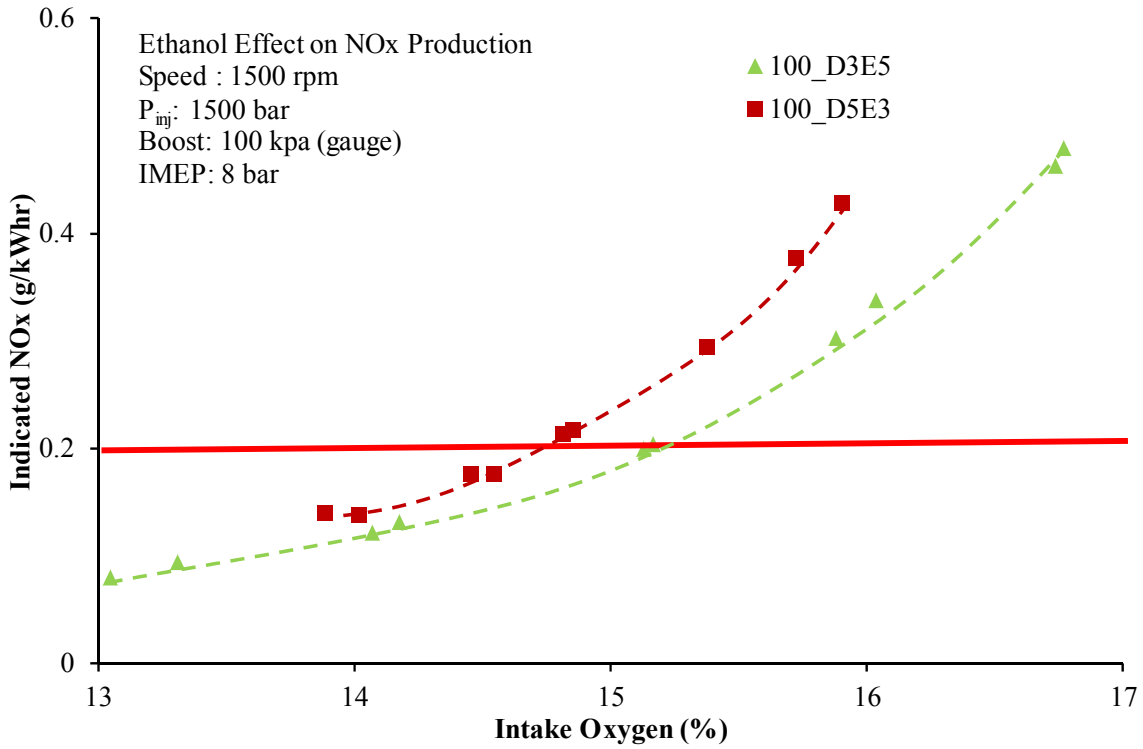

Figure 5-15 Ethanol Ratio Effect on NOx Production with Same IMEP

The cylinder pressure and heat release rates were analyzed to explore the ethanol effects on in-cylinder combustion. A data point with diesel injection and another one with diesel and ethanol were chosen and the pressure traces and HRR are plotted in Figure 5-16 and Figure 5-17. From the pressure traces in Figure 5-16, it was observed that the compression pressure was lower for the combustion with PFI ethanol. Ethanol was in a liquid phase when it was injected into the intake manifold. It evaporated inside the manifold and cylinder, absorbed the heat in the cylinder charge and lowered the overall intake temperature. This evaporation occurred early of the intake stroke and the in-cylinder temperature and pressure were lower for ethanol enabled intake, which could be noticed from Figure 5-17 that the green curve was lower than the red curve before compression stroke TDC.

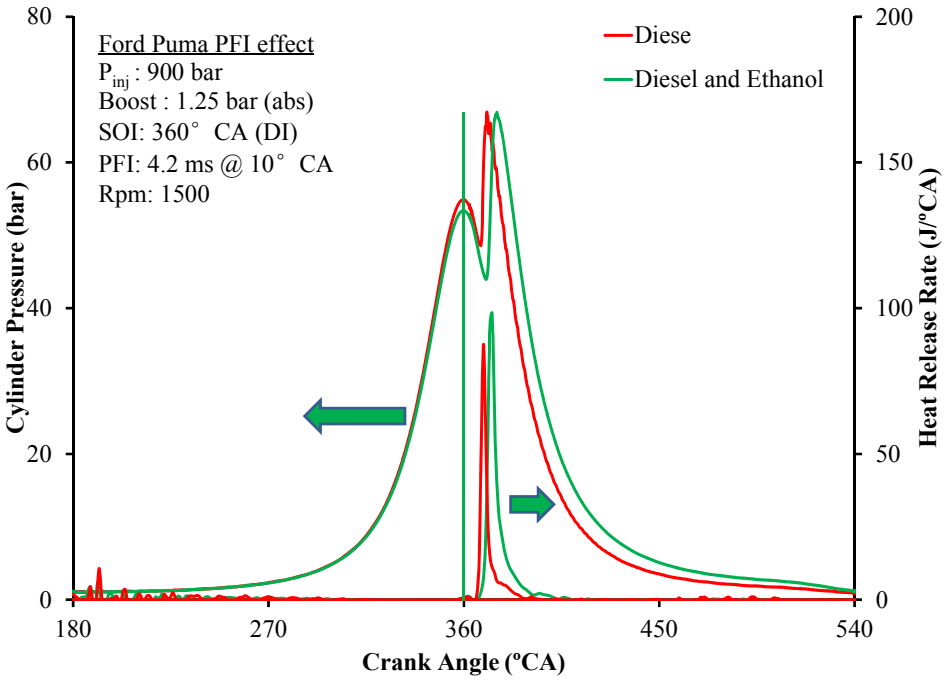

Figure 5-16 Comparison of Diesel and Diesel-Ethanol Combustions

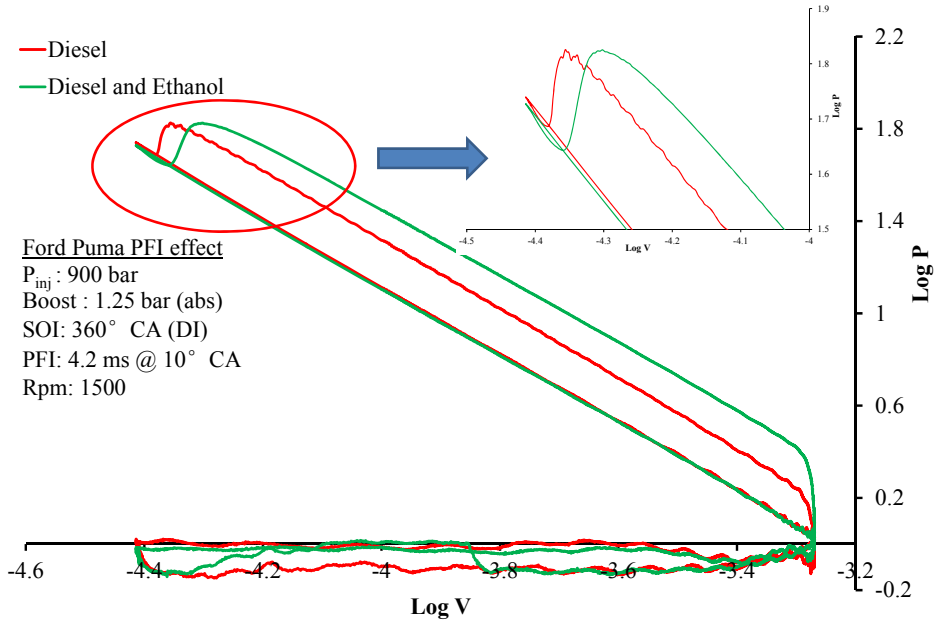

Figure 5-17 Logarithm Plot of Cylinder Pressure and Volume

From the heat release rate curves in Figure 5-16, the start of combustion and the CA50 were retarded by enabling ethanol. Combustion with a proper phasing produces better

emissions with emission control technologies applied [49]. In order to control the combustion phasing in the proper range, diesel fuel injection timing could be adjusted. The SOC and CA50 controllability was tested with a diesel injection timing sweep as shown in Figure 5-18. The engine test was performed at 10 bar IMEP, 3 bar from diesel and 7 bar from ethanol. With retarding the SOI, it was observed the whole heat release was postponed and the shape of each HRR was similar to each other. Therefore, the controllability of diesel-ethanol was good and the SOC and combustion phasing can be controlled by varying the diesel injection timing at 10 bar engine load. At the tested conditions, ethanol auto-ignition was not noticeable from the heat release shape. Thus the diesel fuel injection, acting as the ignition source of ethanol, was essential for diesel-ethanol combustion.

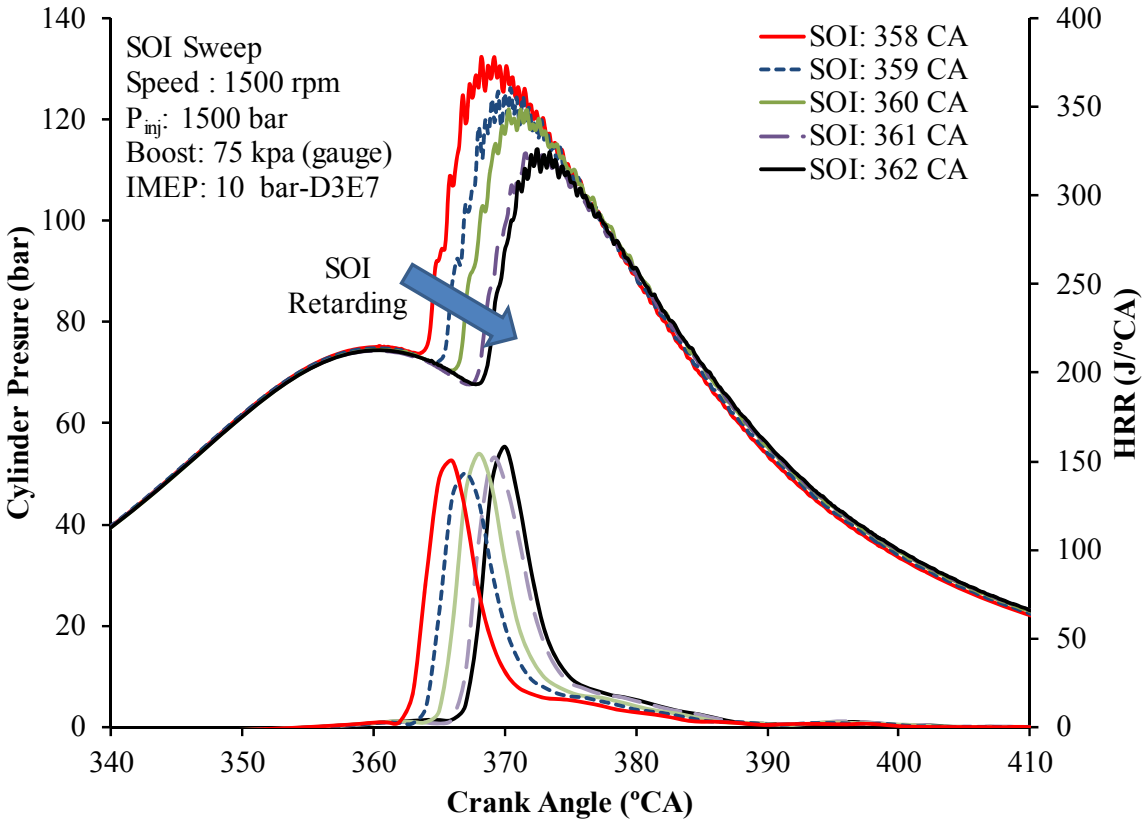

Figure 5-18 Combustion Phasing Controllability Test with Diesel SOI Sweep

From the practice in CDEL, NOx was produced mainly from diesel combustion. Thus a less percentage of diesel utilization was desirable to reduce NOx emissions. Engine experiments with different energy ratios of diesel and ethanol were conducted and three conditions were selected and plotted in Figure 5-19. These three conditions were performed at a similar EGR level (around 36%). The combined IMEPs were 8 bar and 10 bar. The combustion phasing was controlled at about 369°CA by adjusting the diesel injections. The start of combustion was at a similar crank angle. However, the heat release shapes were different from each other. With the ethanol ratio increasing, another heat release hump was observed. At the HRR of D5E3 (37% energy ratio), no second hump was visible, while a flat step was observed at HRR of D3E5 (63% energy ratio) and a clear second hump was noticed at HRR of D3E7 (70% energy ratio). The second hump heat release might be from the ethanol auto-ignition. The total ethanol was partially burnt by diesel, and partially was chemically activated to be auto-ignited when the cylinder pressure and temperature were high enough.

The second peak of HRR prolonged the combustion duration and the heat from diesel and ethanol was released gradually, thus the cylinder pressure rise rate and temperature were not too high. The combustion was more stable, thus the combustion noise was less. The NOx emissions were reduced by the lowered temperature. Part of the soot produced at the first peak could also be burnt by the combustion at the second hump, thus the soot emission was also reduced.

However, the THC and CO emissions were the common challenges for highly volatile fuels such as ethanol. The THC and CO emissions from diesel LTC and diesel-ethanol combustion are plotted in Figure 5-20. The combined IMEP was 8 bar with an intake boost pressure at 100 kPa (gauge) and the fuel injection pressure for diesel was kept constant at 1500 bar.

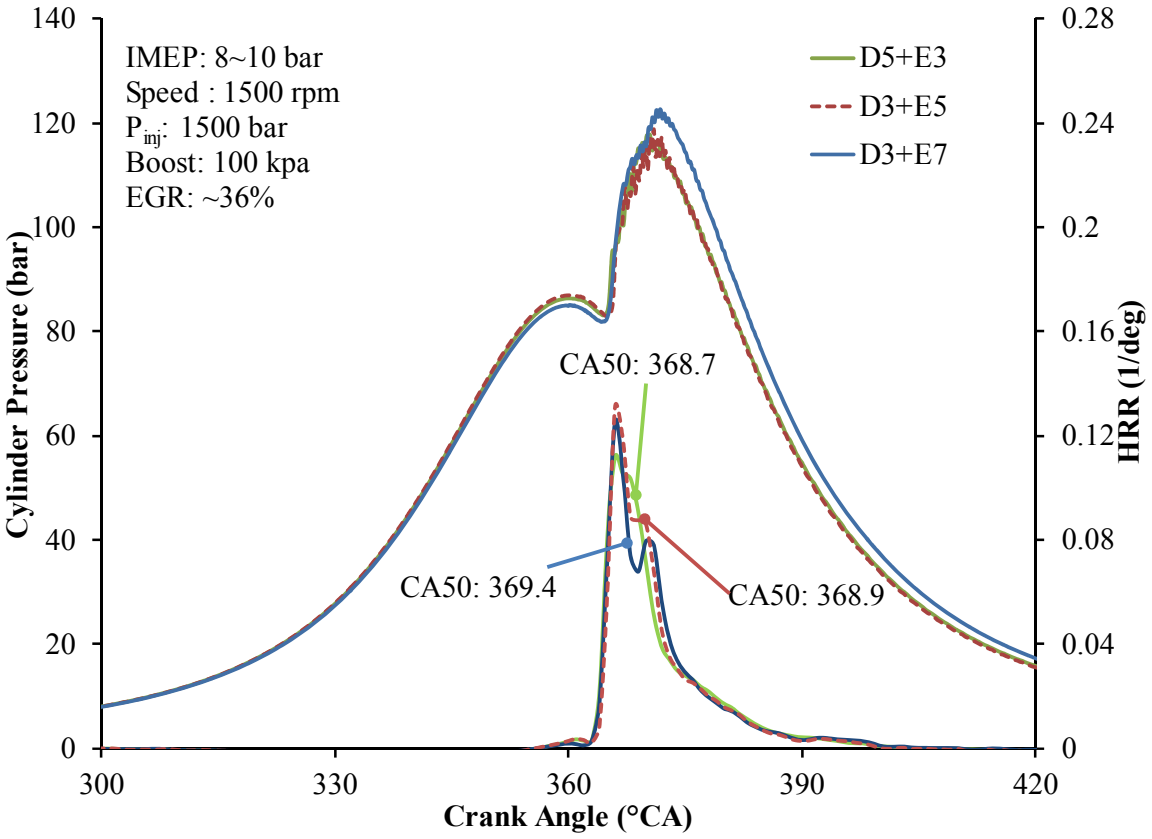

Figure 5-19 Diesel/Ethanol Ratio Effect on HRR Shaping

For the diesel combustion, THC and CO emissions remained low until heavy EGR was applied to further lower the intake oxygen. The THC and CO emissions increased dramatically when combustion entered LTC. The trends of diesel THC and CO emissions were similar, increasing with the reduced intake oxygen concentration. However, the emissions from diesel-ethanol combustion differed from the diesel LTC. The overall emissions of THC and CO were higher than diesel combustion at a similar oxygen level. The emissions of THC and CO remained flat for the whole EGR sweep until NOx and Smoke met the emission standard. If comparing the THC and CO emissions at the location where NOx and smoke emissions met the emission standard, the emissions from diesel-ethanol combustion were lower than those from diesel LTC.

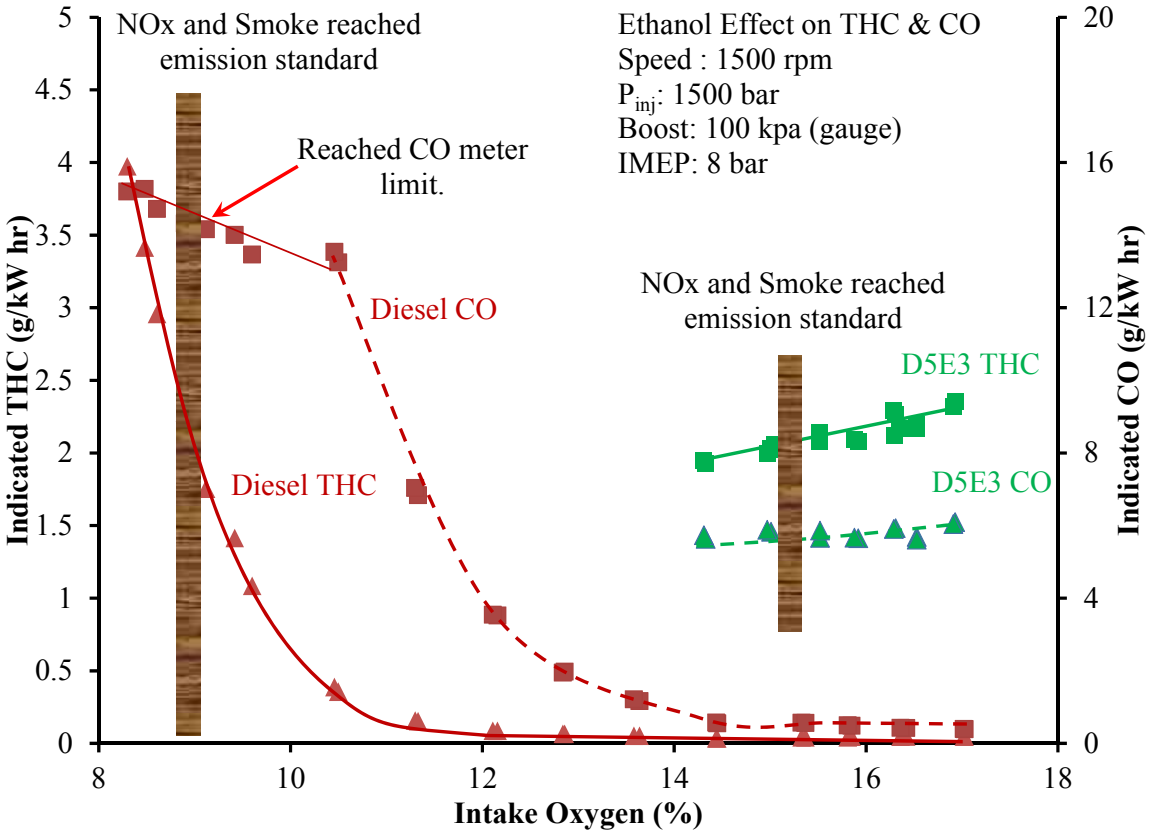

Figure 5-20 THC and CO Emissions from Diesel and Diesel-Ethanol Combustion

An ethanol injector was installed on the manifold. The distance between the injector and intake valves was about 300mm. The overall intake temperature was lower than the boiling temperature of ethanol, thus it was possible for ethanol to be condensed on the cold surface of the manifold and accumulate inside. To test the potential accumulation, an ethanol switching-off test was conducted. The combined IMEP from ethanol and diesel was eight bar IMEP and diesel contributed one bar IMEP. The 200-cycle cylinder pressure traces were recorded. The pressure traces of one out of every 40 cycles are plotted in Figure 5-21. It was noticed that it took about 160 cycles (4.8g of ethanol) to burn the accumulation in the entire switching-off process. This was because of the limitation of the prepared system. Fabricating a new intake manifold was planned to improve this condition and the detailed three-dimensional design has been proposed by the author.

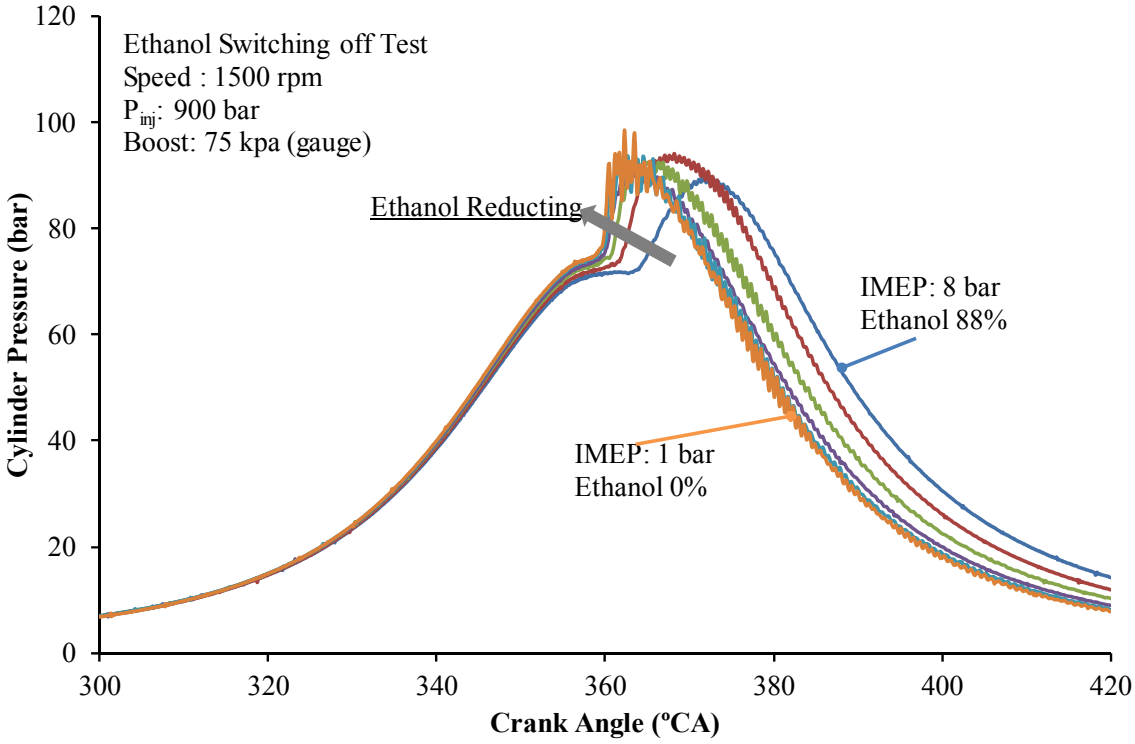

Figure 5-21 Cylinder Pressure Traces of Ethanol Switching-off Test

CHAPTER VI

SUMMARIES AND FUTURE WORK

6.1 Summary of System Completion

A diesel engine was relocated to a newly constructed dynamometer cell, with which a new engine test platform was built. The entire system of dynamometer and dynamometer controlling, air intake and measurement, implementation of EGR, fuel delivery and measurement, fuel pressure and fuel injection control, engine cooling, system monitoring, and emissions sampling and measurement was finalized and verified by specific tests. The results suggested that the condition of the new platform was qualified for performing diesel LTC experiments.

A new fuel delivery and control system for ethanol PFI was prepared and installed on the diesel engine test platform. The system enabled the platform to investigate biofuel effects on diesel LTC combustion. This system and controlling worked properly.

The documentation about the preparation of the diesel engine platform and PFI injection bench was stated in details in this thesis. The procedures, the precautions, and the system limitations were described. The selected important manuals, drawings, tables and photos were included either in the related chapters or appendixes.

6.2 Summary of Test Results

A series of system verification tests were performed on the new engine platform. The experiment results were comparable with the previous setup in the old dynamometer cell, which indicated the whole engine platform preparation work was properly conducted and finished. The findings were illustrated as follows:

- The encoder TDC was aligned with the combustion stroke TDC.
- Multi-injection of diesel and PFI could be realized and the injection timing and duration were under the control.

- Emission measurement results of NOx and smoke were comparable with the previous results produced in 2007.

Diesel baseline engine tests of SOI sweep and EGR sweeps at varied load conditions were conducted at the platform. The cylinder pressure, heat release, and engine emissions were analyzed. The effects of injection timing, EGR ratio, intake boost and rpm on engine emissions and efficiency were explored. The EGR was observed to be the most effective method among the tested parameters to push the combustion into LTC and further suppress NOx and smoke emissions. It was found that:

- NOx, smoke and THC emissions and IMEP were affected by diesel SOI.
- EGR prolonged the ignition delay and reduced flame temperature and combustion noise.
- Higher rpm tended to produce more smoke, but similar NOx emissions.
- The higher intake pressure provided the possibility of applying heavy EGR to suppress smoke to the second slope.

The preliminary engine experiments with ethanol PFI were also performed. The primary emissions of NOx, smoke, THC and CO were studied. The characteristics and controllability of diesel-ethanol combustion were explored. The ethanol effects on emission formations, cylinder pressure and heat release shaping were discussed. Following conclusions can be drawn from the PFI test:

- Ultra-low smoke emission was produced over the entire test matrix.
- NOx production was reduced by the increase of ethanol percentage.
- SOC was retarded by the ethanol PFI.
- Cylinder peak compression pressure was lowered by ethanol evaporation.
- SOC of diesel-ethanol combustion was closely controlled by diesel pilot injection.

- Higher percentage of ethanol tended to have a second stage heat release.
- Ethanol condensed in the intake manifold.

Overall, the results of diesel-ethanol are promoting and further in-depth experiments are essential to explore the beneficial effects of ethanol. The improvement of ethanol condensation was proposed, and will be implemented in the near future.

6.3 Suggestions for Future Work

Diesel baseline LTC experiments and preliminary diesel-ethanol combustion were investigated in the Ford engine test platform. More biofuel experiments were proposed. The following suggestions could provide the further insight of the biofuel research:

1) Fuel delivery improvement
    - New intake manifold with 2 injectors installed to extend the load range and improve the fuel condensation
    - Intake manifold heating
    - Fuel dosing directly into the intake port
    - Direct fuel injection system to provide higher injection pressure and precisely controlled injection timing
2) Fuel blend method
    - Try blending ethanol with other fuels (such as butanol), through PFI
    - Try blending ethanol with other fuels (such as diesel), through DI
3) More fuels

Biodiesel, butanol, gasoline, natural gas, and propane, and other fuels could be investigated with various fuel delivery methods and combustion technologies.

REFERENCES

1. J. B. Heywood (1988), "Internal Combustion Engine Fundamentals", McGraw-Hill Inc., ISBN-10: 007028637X.
2. DieselNet, "Emission Standard, Summary of Worldwide Diesel Emission Standards", http://www.dieselnet.com/standards/, Retrieved 2011-07-25.
3. R. Diwakar and S. Singh (2008), "NOx and Soot Reduction in Diesel Engine Premixed Charge Compression Ignition Combustion: a Computational Investigation", International Journal of Engine Research 2008 9: 195, DOI: 10.1243/14680874JER00308.
4. M. Potter and R. Durrett (2006), "High-Efficiency Clean Combustion Design for Compression Ignition Engines", 2006 Directions in Engine-Efficiency and Emissions Research Conference, Detroit, Michigan, August 20-24, 2006.
5. M. Zheng, G. T. Reader, R. Kumar and C. Mulenga et al (2006), "Adaptive Control to Improve Low Temperature Diesel Engine Combustion", 2006 Directions in Engine-Efficiency and Emissions Research Conference, Detroit, Michigan, August 20-24, 2006.
6. T. Fang, R. E. Coverdill, C. F. Lee and R. A. White (2006), "Combustion and Soot Visualization of Low Temperature Combustion within an HSDI Diesel Engine Using Multiple Injection Strategy", SAE Paper 2006-01-0078.
7. X. Han, T. Gao, M. Zheng and J. Tjong (2010), "Fuel Injection Strategies to Enable Low Temperature Combustion in a Light-Duty Diesel Engine", Global Powertrain Congress, Troy, Michigan, November 3-4, 2010.
8. Wikipedia, "Energy Density", http://en.wikipedia.org/wiki/Energy_density, Retrieved 2011-05-09.

9. A. Demirbas (2009), “Political, Economic and Environmental Iimpacts of Biofuels: A Review”, Applied Energy 86: S108–S117.
10. H. C. Greenwell, L. M. L. Laurens, R. J. Shields and R. W. Lovitt et al (2010), “Placing Microalgae on the Biofuels Priority List: a Review of the Technological Challenges”, J. R. Soc. Interface 6 May 2010 vol. 7 no. 46 703-726.
11. H. Eviana (2008), “A Promising Oil Alternative: Algae Energy”, The Washington Post, Retrieved 2008-06-10.
12. Department of Energy Aquatic Species Program (2006), “Biodiesel Production from Algae”, National Renewable Energy Laboratory, Retrieved 2008-08-29.
13. M. Zheng (2009), “Fundamentals of Clean Diesel Engine Technology”, Lecture Notes, University of Windsor.
14. M. Zheng, X. Han, Y. Tan and M. S. Kobler et al (2008), “Low Temperature Combustion of Neat Biodiesel Fuel on a Common-rail Diesel Engine”, SAE Paper 2008-01-1396.
15. P. Sementa, B. M. Vaglieco and F. Catapano (2011), “Influence of the Injection Pressure on the Combustion Performance and Emissions of Small GDI Engine Fuelled with Bio-Ethanol”, SAE Paper 2011-37-0007.
16. Alternative Fuels and Advanced Vehicles Data Center, “Properties of Fuels”, http://www.afdc.energy.gov/afdc/pdfs/fueltable.pdf, Retrieved 2011-06-09.
17. William De Ojeda, Tytus Bulicz, Xiaoye Han and Ming Zheng et al (2011), “Impact of Fuel Properties on Diesel Low Temperature Combustion”, SAE Paper 2011-01-0329.
18. S. Takahashi, K. Wakimoto, N. Iida and D. Nikolic (2001), “Effects of Aromatics Content and 90% Distillation Temperature of Diesel Fuels on Flame Temperature and Soot Formation”, SAE Paper 2001-01-1940.

19. R. T. Butts, D. Foster, R. Krieger and M. Andrie et al (2010), “Investigation of the Effects of Cetane Number, Volatility, and Total Aromatic Content on Highly-Dilute Low Temperature Diesel Combustion”, SAE Paper 2010-01-0337.
20. C. I. McCarthy, W. J. Slodowske, E. J. Sienicki and R. E. Jass (1992), “Diesel Fuel Property Effects on Exhaust Emissions from a Heavy Duty Diesel Engine that Meets 1994 Emissions Requirements”, SAE Paper 922267.
21. N. Ladommatos and J. Goacher (1995), “Equations for Predicting the Cetane Number of Diesel Fuels from Their Physical Properties”. Fuel Vol 74 No. 7, pp. 1083-1093, 1995.
22. T. Nakai and H. Ogishi (2010), “Verification of Influences of Biodiesel Fuel on Automotive Fuel-line Rubber and Plastic Materials”, SAE Paper 2010-01-0915.
23. ASTM D5186 (2009), “Standard Test Method for Determination of Aromatic Content and Polynuclear Aromatic Content of Diesel Fuels and Aviation Turbine Fuels by Supercritical Fluid Chromatography”, http://www.astm.org/Standards/D5186.htm, Retrieved 2011-07-15.
24. K. Saitoh and M. Hamasaki (2003), “Effects of Sulfur, Aromatics, T50, T90 and MTBE on Mass Exhaust Emissions from Vehicles with Advanced Technology-JCAP Gasoline WG STEP 2 Report”, SAE Paper 2003-01-1905.
25. S. pischinger, V. K. Rajamani and Y. Jeihouni (2011), “Impact of Fuel Properties on the Performance of a Direct Injection Diesel Engine under Part Homogeneous Operating Conditions”, SAE Paper 2011-01-1358.
26. M. Zheng, M. Wang, G. T. Reader and M. C. Mulenga et al (2008), “An Improvement on Low Temperature Combustion in Neat Biodiesel Engine Cycles”, SAE Paper 2008-01-1670.

27. Schenck (2001), “Technical Specification Eddy-Current Dynamometer W Series”, 2001-05-01.
28. Dyna Systems, “Water cooled Eddy Current dynamometer user manual”, Dyna systems, Inc.
29. S. Yu (2009), “Wire Connection Diagram for WS230 Eddy Current Dynamometer”, Internal diagrams.
30. Dyne Systems (2001), “Dyn-Loc IV Digital Dynamometer Controller Installation and User Manual”, Dyne Systems Co., LLC.
31. EFS Operating Manual (2003), “Electrovolve Control Module EFS 8232”, EFS, 2003-05-26.
32. EFS User Manual (2003), “WinIPoD Software V2.3.4 EFS 1543”, EFS, 2003-07-11.
33. NI R Series Multifunction RIO User Manual (2009), “for NI 781xR, NI 783xR, NI 784xR, and NI 785xR Devices”, National Instruments.
34. U. Asad, R. Kumar, X. Han and M. Zheng (2011), “Precise Instrumentation of a Diesel Single-Cylinder Research Engine”, Measurement 44 (2011) 1261-1278.
35. Dressor User Manual (2008), “Roots Meters and Instruments”, Dressor Inc..
36. Robert Bosch Datasheet, “Differential Pressure Sensor”, Robert Bosch GmbH Automotive Aftermarket.
37. Ono Sokki Catalog, “High-Precision Fuel Flow Meters FP/FX/FZ Series Detectors FM Series Display Units”, CAT. NO. 040907-01, Printed in Japan 053 (SK) 2K.
38. STMicroelectronics Datasheet (2005), “VNH2SP30 Automotive Fully Integrated H-bridge Motor Driver”, STMicroelectronics.

39. Auto Performance Engineering, “Walbro External Fuel Pumps GSL392 Flow Graph”, http://www.autoperformanceengineering.com/html/ext_pump.html, Retrieved 2011-10-13.
40. Century Performance Centre, “Fuel Pressure Regulators and the Benefits of Return Style Systems”, http://www.centuryperformance.com/mallory-fuel-pressure-regulators-selection-spg-81.html, Retrieved 2011-10-08.
41. National Semiconductor Datasheet (2008), “LM1949 Injector Drive Controller”, National Semiconductor, 2008-12-14.
42. A. C. Hansen, Q. Zhang and P.W.L. Lyneb (2005), “Ethanol-Diesel Fuel Blends—a Review”, Bioresource Technology 96 (2005) 277–285.
43. J. Galante-Fox, P. V. Bacho, C. Notaro and J. Zizelman (2007), “E-85 Fuel Corrosivity: Performance Effects on Port Fuel Injector Durability”, SAE Paper 2007-01-4072.
44. S. D. Clark and W. Studzinski (2010), “ Flex Fuel Vehicle Performance and Corrosion Study of E85 Fuel with Chloride Addition”, SAE Paper 2010-01-2088.
45. E. Torsner (2010), “Solving Corrosion Problems in Bbiofuels Industry”, Corrosion Engineering, Science and Technology, 2010, VOL 45, NO 1.
46. Chemical Resistance Chart, http://www.pumprite.com/chemre.pdf, Retrieved 2011-08-20.
47. ASCO Datasheet, “General Service Solenoid Valves”, ASCO.
48. Wikipedia, “Flammability Limit”, http://en.wikipedia.org/wiki/Flammability_limit, Retrieved 2011-08-10.
49. M. Zheng, Y. Tan, M. C. Mulenga and M. Wang (2007), “Thermal Efficiency Analyses of Diesel Low Temperature Combustion Cycles”, SAE Paper 2007-01-4019.

50. R. Kumar and M. Zheng (2008), “Fuel Efficiency Improvements of Low Temperature Combustion Diesel Engines”, SAE Paper 2008-01-0841.
51. M. Zheng, R. Kumar, Y. Tan and G. T. Reader (2008), “Heat Release Pattern Diagnostics to Improve Diesel Low Temperature Combustion”, SAE Paper 2008-01-1729.
52. Material Safety Data Sheet, “Ethyl Alcohol (anhydrous), NO. 1009”, Commercial Alcohols, Effective Date: February 1, 2008.
53. Product Drawings of 302404 from Supplier Ontario Compressor.
54. Product Drawings of PO-16696 from Prentex Alloy Fabricators, Inc.

APPENDIX A INFORMATION OF AIR MANAGEMENT SYSTEM

A.1 Intake Tank and Exhaust Tank

The drawings of the intake surge tank and the exhaust surge tank are shown in Figure A-1 and Figure A-2. The basic dimensions of the tanks and the available connecting ports are illustrated in the drawings. The intake surge tank is a vertical tank with self-stand. A simple support has been made to fix the tank to the slots on the engine bed. At the bottom of the intake surge tank, there is a 1/4 NPT port. A Swagelok fitting with a cap has been installed there, which can be used for the release of the accumulated water in the tank.

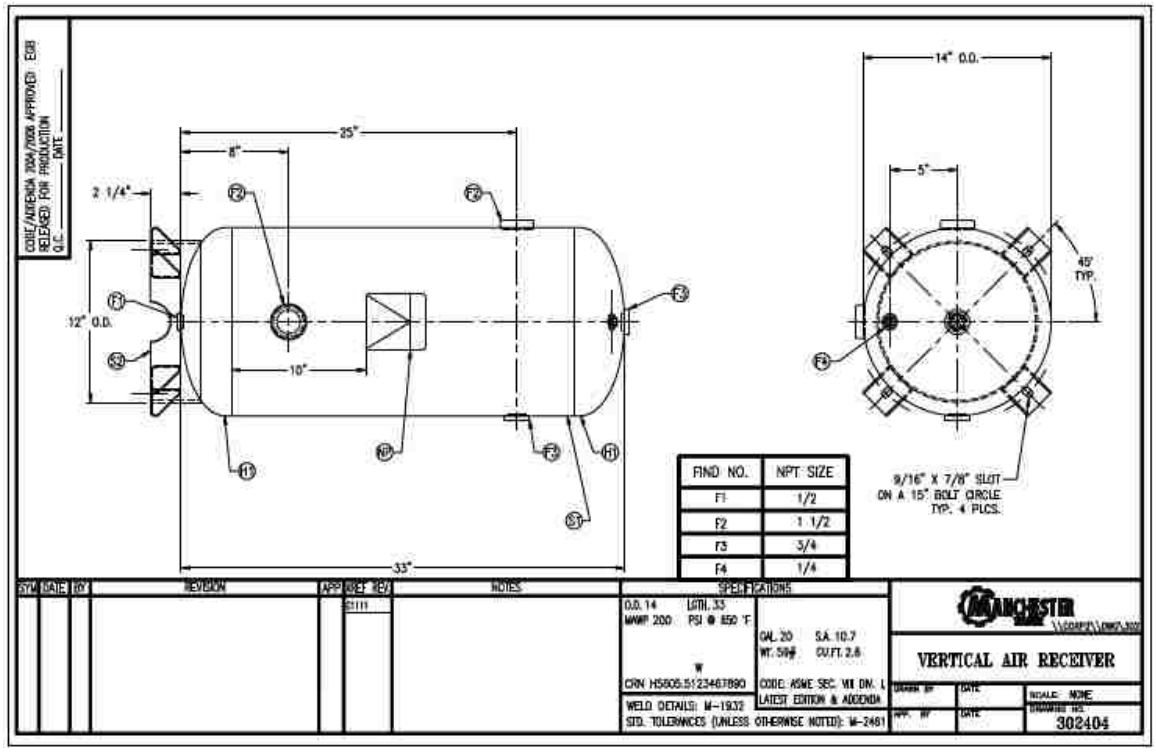

Figure A-1 Drawing of Intake Surge Tank [53]

The exhaust surge tank was without stand when purchased from the supplier. A new stand was made to hold the tank vertically, as shown in Figure A-3. Both ends of the exhaust tank were open and two new flanges were designed and made. The drawings of both flanges are demonstrated in Figure A-4 and Figure A-5. Those two flanges were made from stainless steel. Two stainless steel 54mm pipe fittings were welded on each of the flanges. Two copper gaskets were also made accordingly.

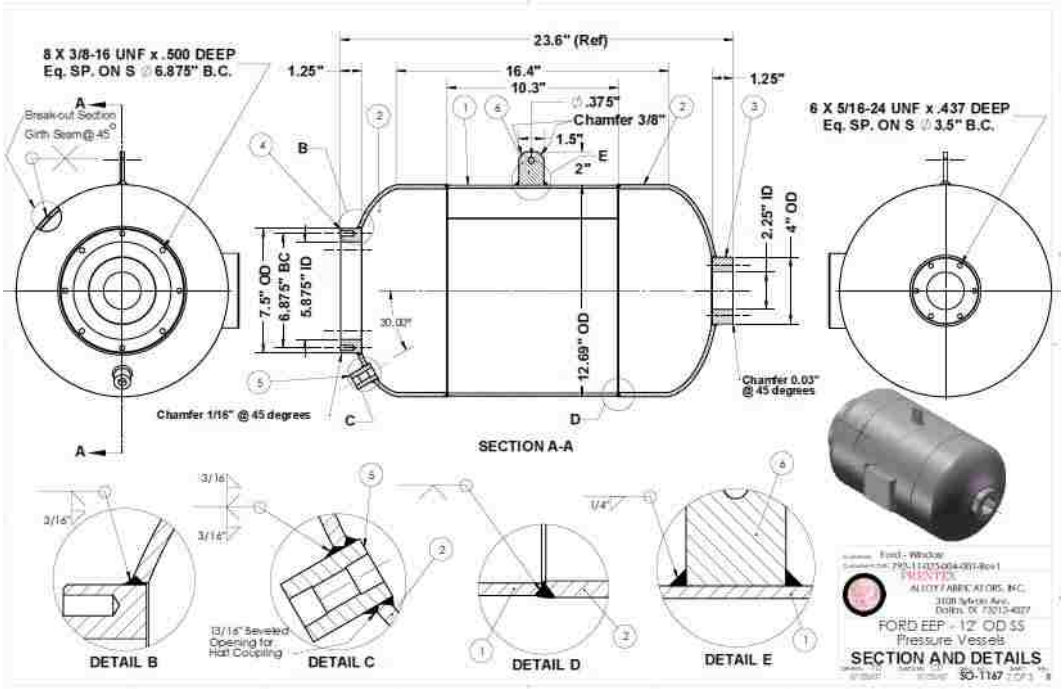

Figure A-2 Drawing of Exhaust Surge Tank [54]

Figure A-3 Stand of the Exhaust Surge Tank

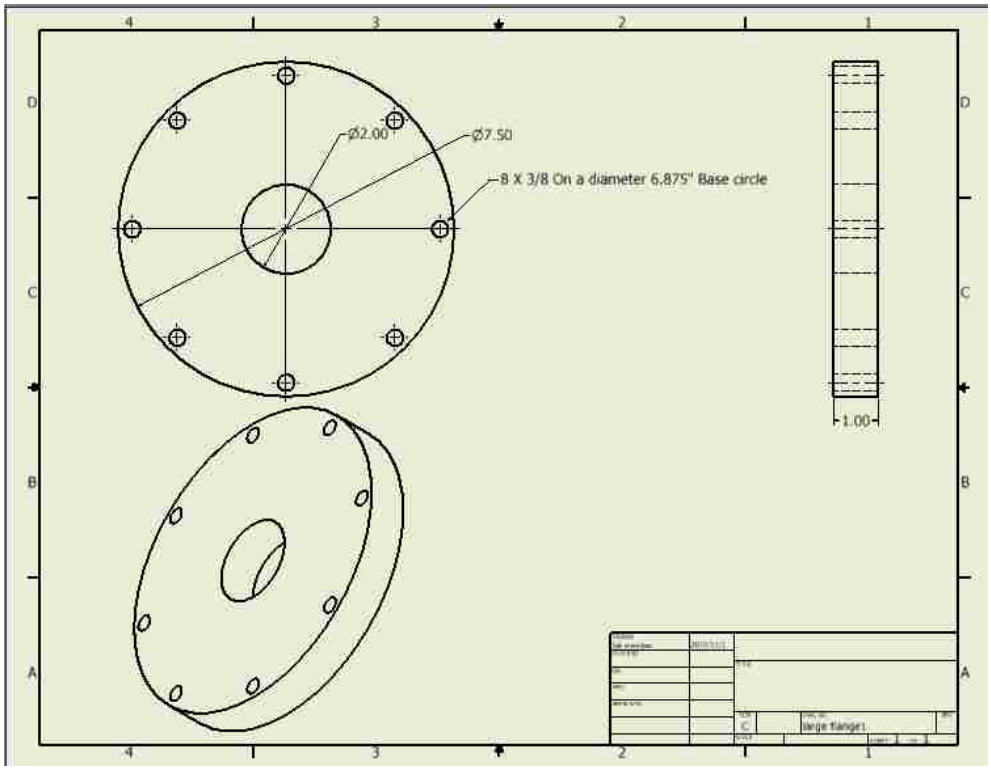

Figure A-4 Drawing of Big Flange on Exhaust Surge Tank

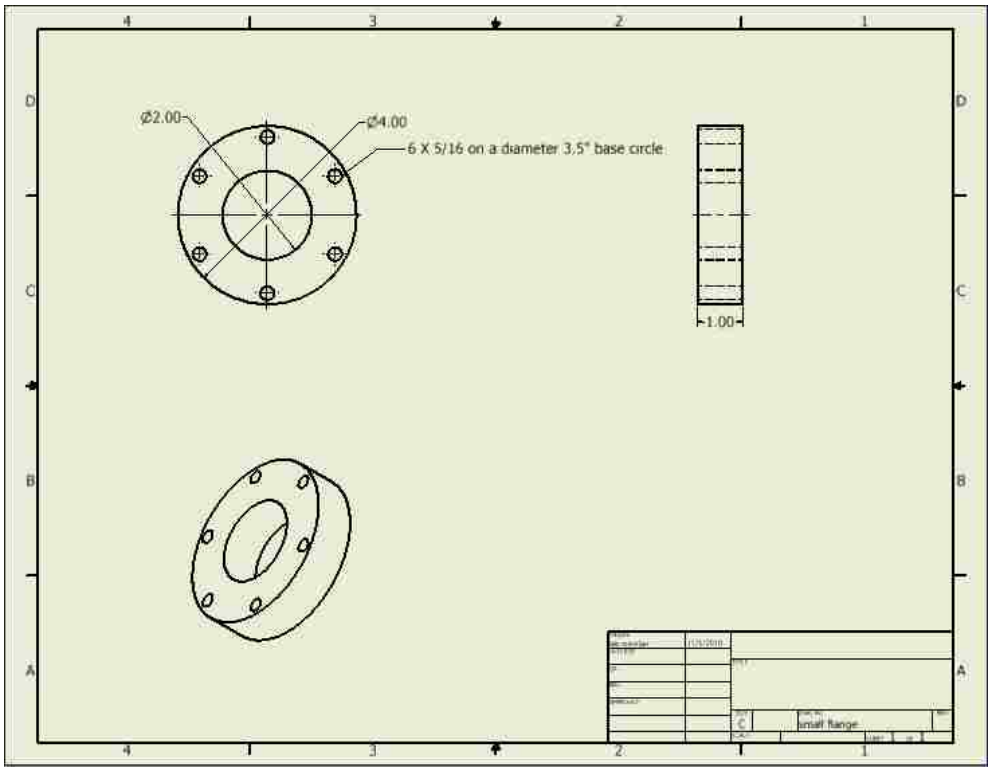

Figure A-5 Drawing of Small Flange on Exhaust Surge Tank

A new exhaust pipe with a DOC was made as described in the previous chapter. The dimension of the flange on the first cylinder was measured and recorded in Figure A-6. This could be used for future modifications.

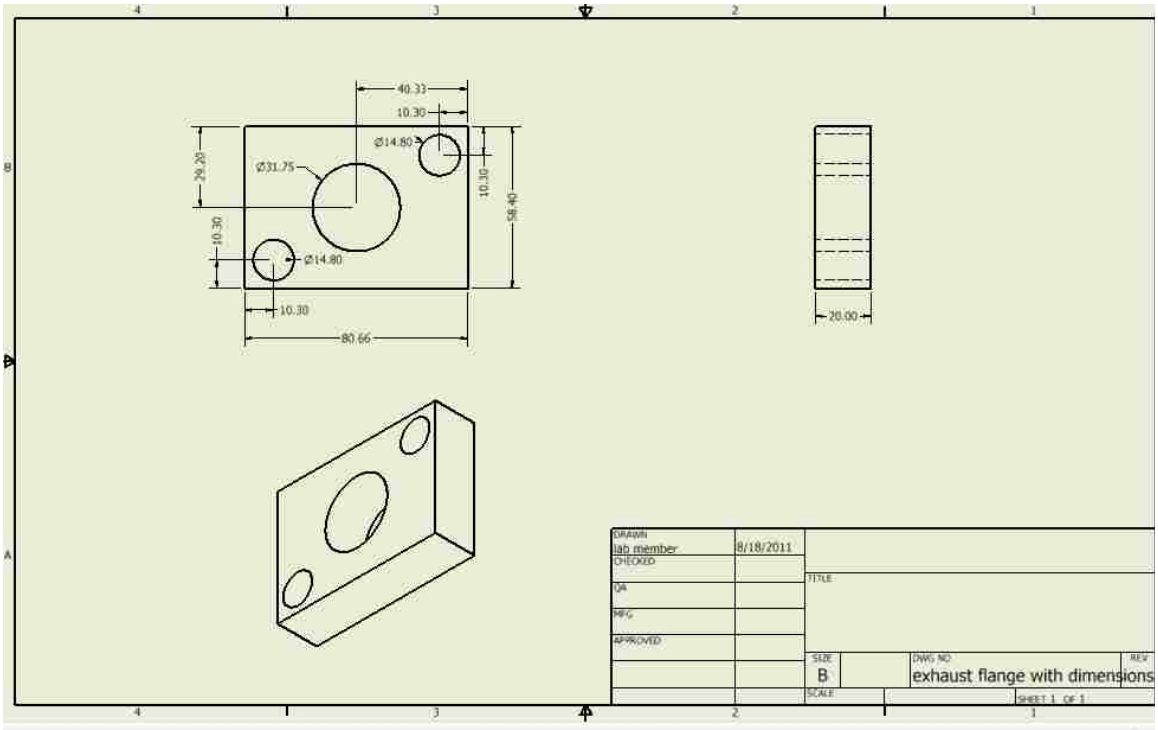

Figure A-6 Drawing of Flange on First Cylinder Exhaust

A.2 Encoder Signal Duplication

As stated in the previous chapter, an optical encoder was attached to one end of the crankshaft to provide an index and 3600 pulses outputs for each engine revolution. These signals were simultaneously shared by the injection control, on-line heat release analysis and cylinder pressure recording. A bad connection or program crash of any applications could influence the others and result in the engine out of control and serious damages.

In order to isolate the applications from each other, an encoder signal duplication box was made to avoid sharing the signal directly. In the box, two Hex inverters were employed to isolate the signal from the source. In each inverter, there were six gates embedded. Figure A-7 shows the inside view of the signal duplication box. Each signal

inputted into the box can be inverted to three sets of same signals. The index Z and clock B were reserved for the diesel fuel injection control. Clock A, -A, -B and index -Z were inputted to the box. Therefore, Three sets of A, -A, B and Z were outputted from the box and could be used for various applications. The box was tested with an encoder signal simulator and an oscilloscope. On the displayed waveform, no time delay or phase change could be observed. This box was used continuously during the engine tests and was proved to be trouble free.

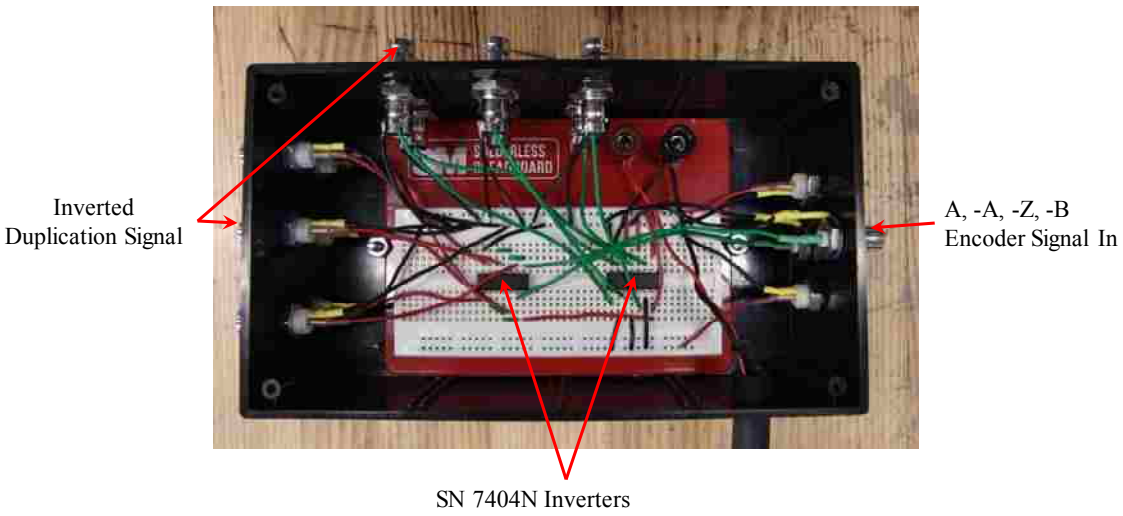

Figure A-7 Encoder Signal Duplication Box

A.3 Fuse Box

From the previous practice in the CDEL, a fuse box for each power supply was necessary to protect the sensors and actuators, and for problem diagnostics. Therefore, two fuse boxes were prepared for both 5VDC and 12VDC power supply. The photo of the 5V fuse box is shown in Figure A-8. The 5VDC power supply was split into 12 channels to supply +5VDC to 12 sensors and actuators. In each channel, an ON/OFF switch, an indicating lamp and a proper fuse were connected. A main switch was also used to turn off the entire power supply to every channel.

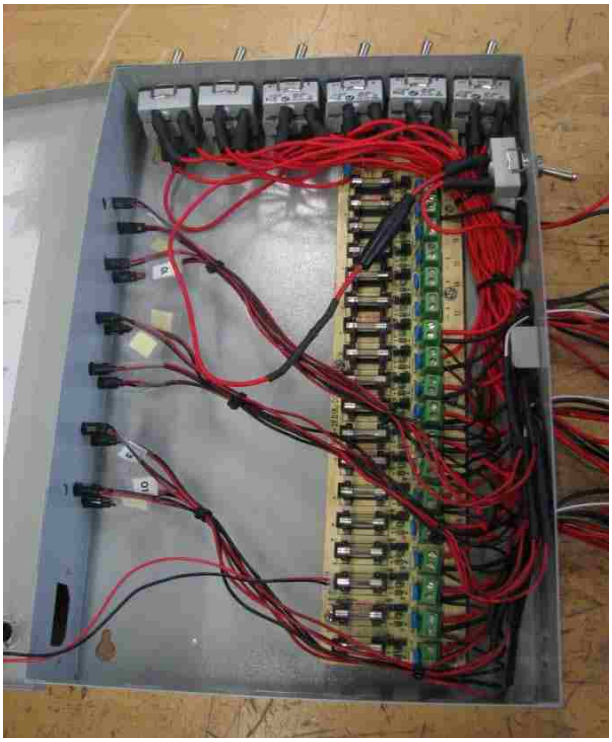

Figure A-8 Photo of Inside of 5V Fuse Box

APPENDIX B SIGNAL CABLES AND CONNECTIONS

The fuse box channel distributions, the detailed connections of each NI terminal box utilized on the Ford engine platform, all prepared cables, and the connections inside the temperature module are demonstrated in Table B-1 to Table B-4.

Table B-1 Pin Connections in NI Terminal Boxes

NI6229	Boost/EGR		NI 6220	Air/fuel flow	
AI0	68	Intake pressure	AI0	68	Roots Meter
	67			67	
AI1	33	Intake voltage feedback	CTR1, SRC	42	Fuel pulse
	32			9	
AI2	65	Exhaust pressure	CTR0 SRC	37	P0.0 in
	64			36	
AI3	30	Exhaust voltage feedback	P0.0	52	AI0 digital out
	29			53	
AO0	22	Intake regulator control			
	55				
AI5	60	Intake regulator feedback			
	59				
AO1	21	exhaust regulator control			
	54				
AI7	57	exhaust regulator feedback			
	56				
NI6220	Data record		NI6122	HRR	
	11	Z		11	Z
PFI 0	44		PFI 0	44	
	38	**B**		38	**B**
PFI 7	4		PFI 7	4	
	23	pressure		30	pressure
AI15	24			63	
			AI3	29	

Table B-2 Summary of All Prepared Cables

Series	Cable type	Label	Purpose	Wires unused	
1	Coaxial	TG 1	INJ CYL1	0	
2	Coaxial	TG 2	INJ CYL2	0	
3	Coaxial	TG 3	INJ CYL3	0	
4	Coaxial	TG 4	INJ CYL4	0	
5	Coaxial	TG 5	SEL CYL1 to	0	
11	8-wire	GT E1	Ford Encorder	0	
12	Coaxial	GT C1P	Pressure transducer from	0	Connect to amplifier
13	6-wire	GT D1	Dyno RPM		Connect to dyno controller
14	6-wire	GT D2	Dyno Torque		Connect to dyno controller
15	Coaxial	113A Ca	113A Camera 1	0	
16	Coaxial	113A Ca	113A Camera 2	0	
17	Coaxial	GT C1	115A Camera 1	0	
18	6-wire	TG 11	Monitor IPOD 4	2	Red(EV Voltage1V /-10V),Green(Effective inj monitoring), Wht(EV current1V /3A), blk(ground)
19	6-wire	TG 12	Daisy IPOD	3	crossover at computer side
20	6-wire	TG 13	Monitor IPOD 1	2	Red(EV Voltage1V /-10V),Green(Effective inj monitoring), Wht(EV current1V /3A), blk(ground)
21	6-wire	TG 14	Monitor IPOD 3	2	Red(EV Voltage1V /-10V),Green(Effective inj monitoring), Wht(EV current1V /3A), blk(ground)
22	6-wire	TG 15	Monitor IPOD 2	2	Red(EV Voltage1V /-10V),Green(Effective inj monitoring), Wht(EV current1V /3A), blk(ground)
23	6-wire	TG 16	CAM sensor	3	GRN(Signal), Blk(GND), Red(+5V)
24	6-wire	TG 17	Rail pressure		Color code in book 2
25	6-wire	TG 18	TTL to H bridge	4	Orange(+), white(-)
26	6-wire	TG 19	5V(3 sets)	0	Red(+), Black(-) to h-bridge Green(+), White(-) Orange(+), Blue(-)
27	6-wire	TG 20	Oil pressure	2	GRN(Signal), RED(+5V) WHT(V-back), BLK(GND) at sensor connector side
28	6-wire	TG 21	MAF sensor	2	GRN(GND), RED(+12V) WHT(Signal), BLK(GND)
30	6-wire	TG 23	EGR CAN	3	Usman made
33	Coaxial	TG 26	ethanol injection command	0	
43	6-wire-2 w	PR 1	Intake tank pressure	4	The black is together with white,RED(V_back)
44	6-wire-2 w	PR 2	Exhaust tank pressure	4	The black is together with white,RED(V_back)
45	6-wire-2 w	PR 3	Boost	2	(Black(output)-black, white(input)-white), (brown(+)-red, blue(-)-black)
46	6-wire-2 w	PR 4	EGR control	2	(Black(output)-black, white(input)-white), (brown(+)-red, blue(-)-black)
47	6-wire-2 w	PR 5	Fuel pressure	2	The black is together with white
48	2 wire	PR 6	Roots meter	0	Black to black, white to clear
49	2 wire	PR 7	Flow switch	0	Black to white, transparent to red
50	2 wire	PR 8	starter relay	0	

Table B-3 Thermocouples and Analogue Input Connections

Series	Cable Lable	Modual	Cable typy	Physical channel	name
1	TC1	M1	T-type	1	Ford_Coolant_Out
2	TC2	M1	T-type	2	Oil Temperature
3	TC3	M1	T-type	3	Oil Sump Temperature
4	TC4	M1	T-type	4	Intake Air Temperature
5	TC5	M1	T-type	5	Coolant_Into_Engine
6	TC6	M1	K-type	6	After EGR cooler
7	TC7	M1	K-type	7	Before EGR cooler
8	TC8	M1	K-type		
9	TC9	M1	K-type		
10	TC10	M1	K-type	10	After Exhaust tank
11	TC11	M1	K-type	11	Emission sampling temp.
12	TC12	M1	K-type	12	DOC Temp.
13	TC13	M1	K-type	13	
14	TC14	M1	K-type	14	
15	TC15	M1	K-type	15	
16	TC16	M1	K-type	16	
17	TC17	M1	K-type	17	
18	TC18	M1	K-type	18	
19	TC19	M1	K-type	19	
20	TC20	M1	K-type	20	
21	TC21	M1	K-type	21	Singal_Cyl_Exh_Temp
22	TC22	M1	K-type		
23	TC23	M1	K-type	23	3_Cyl_exh_Temp
24	TC24	M1	K-type	24	
25	TC25	M1	K-type	25	
26	TC26	M1	T-type	26	Coolant_out1_dyno
27	TC27	M1	T-type	27	Coolant_out2_dyno
28	TC28	M1	T-type	28	Coolant_IN_dyno
29	TC29	M1	T-type	29	Fuel_Return_Temp
30	TC30	M1	T-type	30	Fuel_supply_Temp
31	TC31	M1	T-type	31	air intake Temp
32	TC32	M1	T-type	0	Arturo pressure wave
33	TC33	M1	T-type	8	Arturo pressure wave
34	TC34	M1	T-type	9	3_cyl_int_Temp
35	TC35	M1	T-type	22	PFI fuel temp
36		Dev2	Voltage	AI0	Oil pressure
37		Dev2	Voltage	AI9	Fuel pressure
38		Dev2	Voltage	AI11	rpm
39		Dev2	Voltage	AI4	Torque
40		Dev2	Voltage	AI12	Fuel flow rate
41		Dev2	Voltage	AI5	Ethanol pressure

Table B-4 Channel Distributions of Fuse Boxes for +5VDC and +12CDC

Fuse box (+5V)		Fuse box (+12V)	
Channel	Power for	Channel	Power for
1	H-bridge	1	boost regulator
2	encoder copy box	2	EGR regulator
3	PFI injection power	3	Starter relay
4	beside h-bridge	4	
5	encoder power	5	
6	P-rail	6	
7	CAM	7	
8	Fuel/oil pressure sensor	8	
9	Intake/exhaust tank pressure sensor	9	
10		10	
11	Ethanol pressure	11	
12	Roots meter	12	

VITA AUCTORIS

NAME:	Tongyang Gao
PLACE OF BIRTH:	Jilin, China
YEAR OF BIRTH:	1983
EDUCATION:	B.Sc. Automotive Engineering
	Tsinghua University, Beijing, China
	2002-2006
	M.A.Sc. Candidate of Mechanical Engineering
	University of Windsor
	2009-2011